Design and Optimization of a Formula SAE Vehicle

A Major Qualifying Project

Submitted to the Faculty of

Worcester Polytechnic Institute

In partial fulfillment of the requirements for the

Degree in Bachelor of Science

In

Mechanical Engineering

By:

William Kinkead, ME

Connor Morette, ME

Adrian Pickering, ME

Zachary Sears, ME

James Waldo, ME

Date: _____

Approved By:

Professor David C. Planchard, ME Advisor

Abstract

The purpose of the Society of Automotive Engineers (SAE) Formula Major Qualifying Project (MQP) is to develop a vehicle for entry in competitions. This MQP went beyond textbook theory by designing, building and testing the performance of a real vehicle. Students worked in multidisciplinary (Mechanical, Electrical, Computer Science, Manufacturing and Aero) teams thought out the year.

Emphasis was placed on reliability, serviceability, and adjustability of critical sub-systems. Suspension, steering and drivetrain components are designed to be easily replaceable on the track with only basic tools. The engine was paired with a custom pneumatic shift transmission to allow an automatic shift mode to make fast, consistent shifts.

An aerodynamic package is designed to provide maximum downforce in the expected speed range, without creating large amounts of drag. Sensors are strategically located on the aerodynamic, suspension and drivetrain components for faster and more accurate collection of data used in tuning the vehicle. A removable steering wheel integrated drivetrain feedback, vehicle controls, and a manual paddle shift mode to provide comfortable and intuitive driver controls.

The vehicle is required to accommodate a 95th percentile model comfortably and safely in the driver's compartment. The design of the interior driver compartment and bodywork allows the driver to quickly and safely exit the vehicle in an emergency situation, while protecting them from road debris and providing an aesthetically appealing bodywork package.

Acknowledgments

This project team would like to acknowledge the following people for their assistance and support throughout this project:

Professor David Planchard

Professor Yagoobi

Professor Sullivan

Professor Hall

Barbara Furhman

Kevin Arruda

Mikhail Tan

Professor Stafford

Washburn Shops

Peter Hefti

Table of Contents

List of Figures

List of Tables

List of Equations

Introduction

The Formula SAE competition series tests the ability of students to design, manufacture and tune an open wheel racecar under a strict set of rules. For this MQP, students were provided with a chassis and were required to design and manufacture the systems necessary to compete in the 2016 FSAE competition in Brooklyn, Michigan. Students designed systems that bridged disciplines in the mechanical, manufacturing, aerodynamic, electrical, and computer science areas. Systems supplemental to the minimum rules requirements include an aerodynamic package, electronic steering wheel with paddle shift controls, pneumatic controlled transmission, sensors at strategic locations and wireless telemetry.

The drivetrain of the vehicle was centered around a Yamaha YFZ450R powertrain, which was mated to a clutch pack limited slip differential and a custom final drive assembly. An emphasis was placed on reliability and serviceability in a track environment. A Haltech Elite 1500 ECU provided precise control over engine operating parameters. The 5 speed sequential shift transmission was actuated by a custom pneumatic system to provide fast, consistent shifts in both automatic and manual modes. This transmission was controlled by a custom computing board designed by the partnered MQP, "2016 Formula SAE Vehicle Electrical Systems Design." The main computing board collected information from sensors throughout the vehicle to relay vital information to the driver through the electronic steering wheel and to a race engineer through wireless telemetry.

The driver's cell was designed to safely fit a 95th percentile model with comfortable access to vehicle controls. Various foam seat inserts were custom molded to specific drivers and swapped with ease on the track. A removable steering wheel and fitted bodywork allowed the driver to safely exit the vehicle in less than 5 seconds, should an emergency situation occur. Full car bodywork provided a functional and aesthetically appealing package that protects the driver from road debris. A diffuser equipped undertray operates at a high lift to drag coefficient and was fitted with integrated pressure sensors for design validation.

The suspension and steering components were designed to maximize driver control and vehicle feedback, as well as minimizing steering input torque. A custom steering box was designed to minimize losses through the steering shaft in a tightly packaged frame. Suspension camber and steering Ackermann were easily adjustable using only basic hand tools. Testing was performed at regional locations to tune and validate suspension, steering, drivetrain, aerodynamic and drivetrain systems.

Frame

This MQP began with a welded frame that aligned accurately with the CAD model from the previous FSAE MQP. Throughout the year, tabs were designed, manufactured and welded to this frame to accept the suspension, body and drivetrain systems designed this year. It became apparent to the team that the frame structure was not in compliance to FSAE rules. Two main issues arose with the submission of the structural equivalency spreadsheet, one with a front roll hoop support and another with the main roll hoop support. First, the front roll hoop must be triangulated within 2 inches from the top of the hoop back to the node connecting the upper side impact member to the main roll hoop. This is to transmit the forces from a front end collision throughout the frame structure and prevent a bending failure in the upper part of the front roll hoop. Second, the two members that connect the main roll hoop supports to the main roll hoop node at the upper side impact member contained a significant bend that was un-triangulated. This was initially designed to provide parallel rear suspension pickups with the frame. In the top view, the tube necked toward the centerline of the frame to reduce the size of the frame at the suspension pickups. This bend provided a weak point in the case of a rollover, allowing the frame to yield at this bend should excessive forces be applied to the main roll hoop supports.

A few solutions were proposed among the team to allow the frame to be safely and legally used in the 2016 FSAE competition, without compromising the systems already in place at the time. The issue in the front roll hoop was easily satisfied by adding a structural member from the top of the front roll hoop to the node at the main roll hoop and upper side impact member. The issue in the rear was slightly more difficult to fix without modifying existing drivetrain systems. It was eventually decided to create a node on the upper front engine support tube to properly triangulate the bent member in the rear. A structural member was welded collinear with the suspension pickup section of the bent tube, which was triangulated forward to a node in the middle of the upper side impact member. In addition to these two tubes on either side, the small diagonal cross member below the bent section was reinforced with additional diagonal pieces, completing the “x.” A CAD model of the frame after the proposed solutions were added can be seen below, with the new tubes shown in blue.

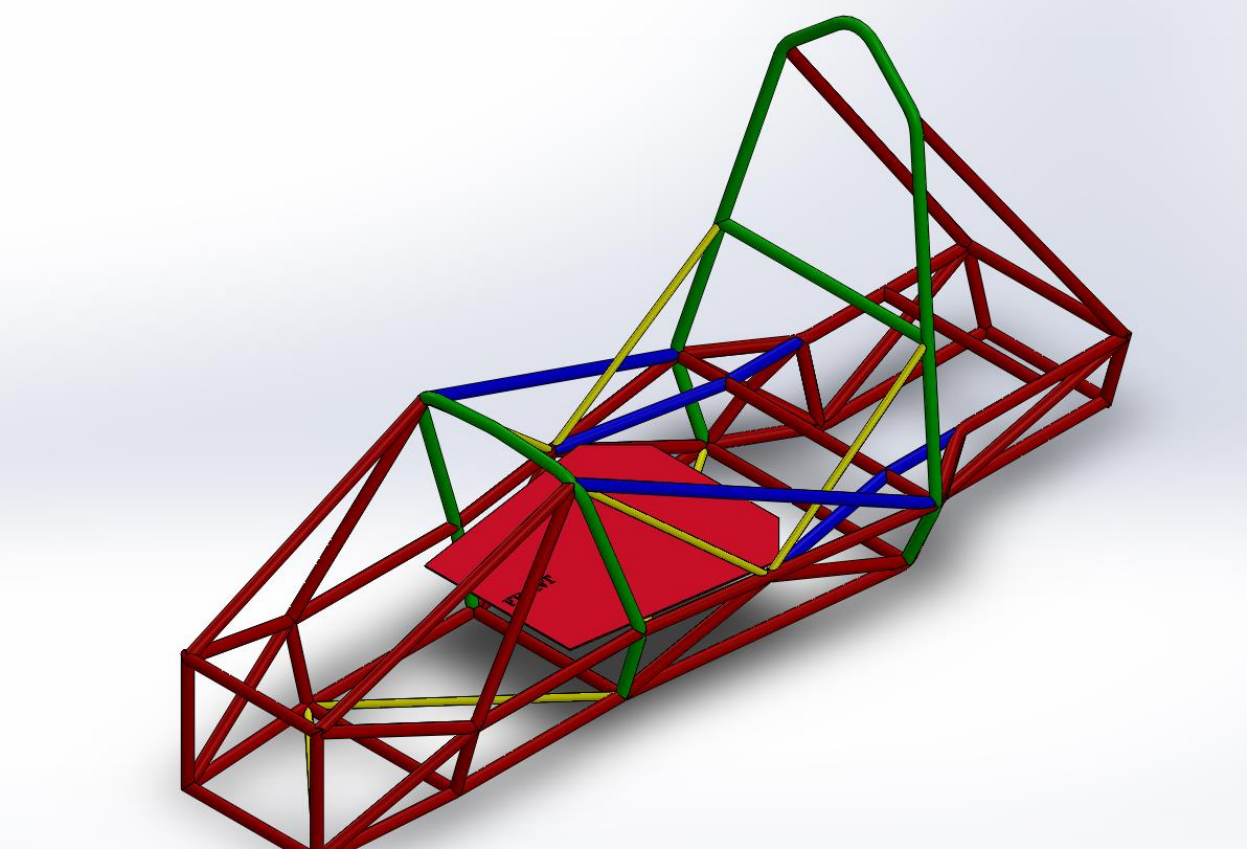

Figure 1: Frame with proposed structural member additions

These solutions were proved initially on the concept level using basic hand calculations and SolidWorks measurements. These calculations were further proven using CAD FEA, and were accepted by the responsible FSAE judge. The finite element analysis was defined by fixturing the frame at the bottom nodes of the front and main roll hoops with immovable fixtures, which fix translation but allow rotation. A load of 6000N was applied at the top of the main roll hoop in a rearward direction along the longitudinal axis as per FSAE Alternate Frame rules calculations to simulate a rollover scenario. All critical members must not exceed ultimate tensile strength of 365.4MPa or a maximum deflection of 25mm. In figure 2, the stress plot displays the resultant member stresses, with the only members reaching yield stress being the upper nodes of the main roll hoop support structure. Since this structure is made in accordance to standard FSAE structural equivalency, there is no issue. Figure 3 displays the maximum deflection under load, with the highest deflection at 15.2mm, well below the 25mm maximum deflection, resulting in a safe and legal frame.

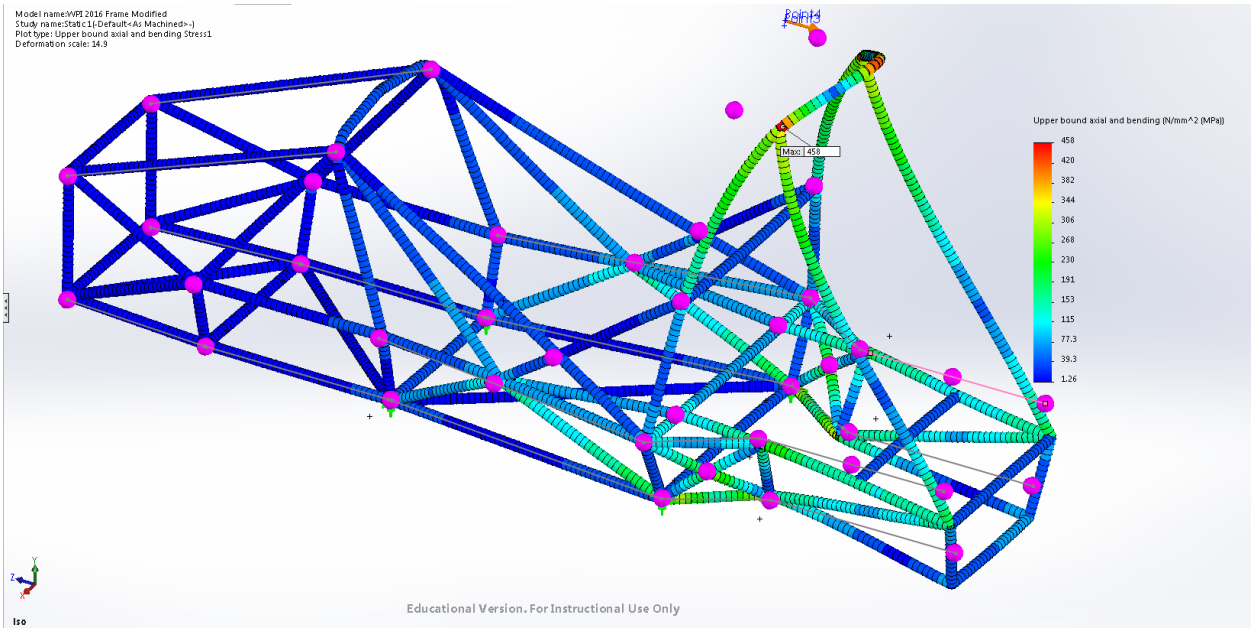

Figure 2: Frame with added structural members bending stress analysis

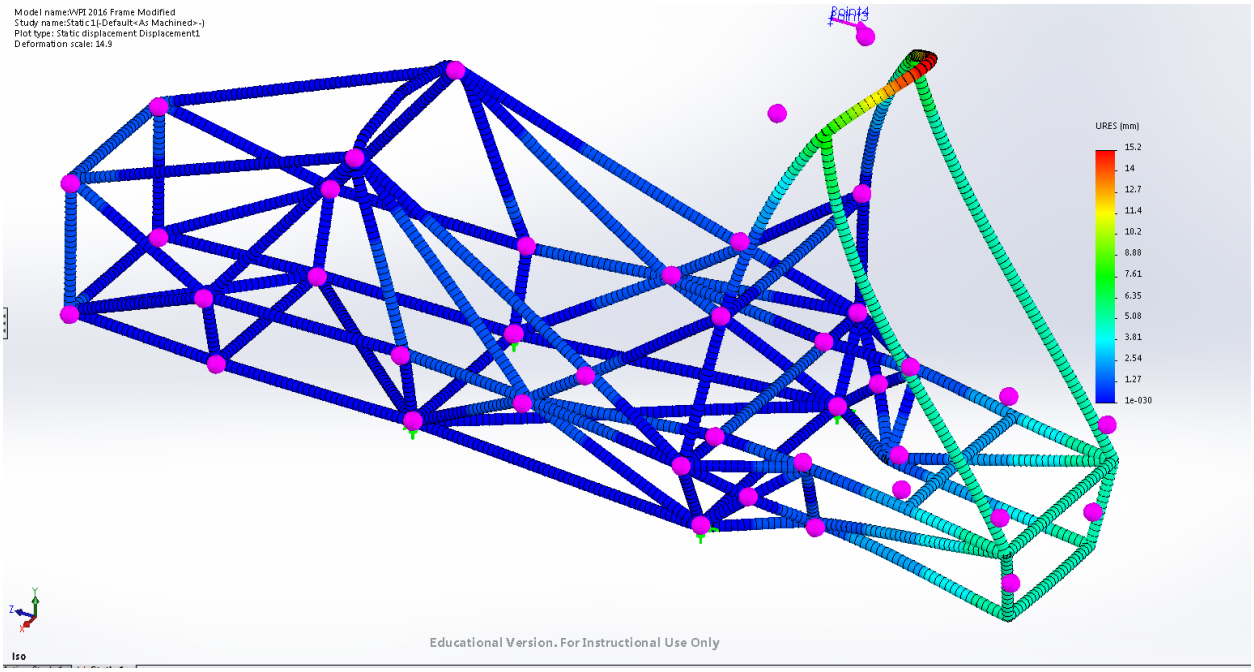

Figure 3: Frame with added structural members deflection analysis

Ergonomics

Introduction

The design of the driver compartment is crucial to the safety of the drivers during the operation of the formula car. Formula SAE rules provide standards for the size of the driver compartment opening and the driver size to ensure the safety of all drivers. The design was based on the formula SAE 95th percentile model fitting safely under the roll envelope between the front and rear roll hoop. The design relied heavily on the fit of the 95th percentile model and the formula SAE inspection templates, therefore 3D models were created to represent each template in SolidWorks to help verify the designs before manufacturing. Figure 4 below displays the 95th percentile model template created in SolidWorks with the layout dimensions displayed in inches.

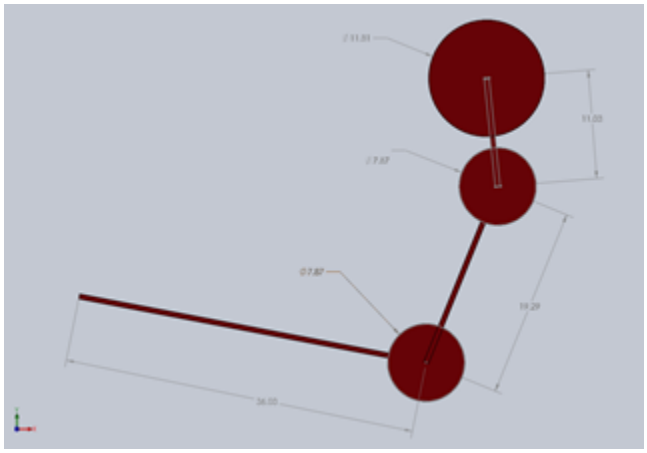

Figure 4: Formula SAE 95th Percentile Template (Top), Cockpit Opening Template (Bottom)

Seat Pan

The seat pan provided both a supportive structure for the driver to sit on in the car as well as a firewall between the driver and the engine compartment. Within the car assembly in SolidWorks, limits were set for the roll hoop envelope to clearly display the height limit of the driver's helmet. 2016 Formula SAE rule T3.10.3 states that with the driver and 95th percentile model in a normal driving configuration the helmet of the driver must be a minimum of 2 inches below the straight line drawn from the top of the rear roll hoop to the top of the front roll hoop. The 95th percentile model was then mated to the right plane of the assembly and various driver configurations were analyzed by shifting the driver model's position and recording the overall distance of the driver's head from the roll envelope to ensure a minimum distance of 2 inches were achieved. The final driver's position allowed for a distance of 2 ¼ inches from the roll envelope as an extra safety margin. A seat pan model was created to support the model in this final position. The structure of the seat closes off the driver compartment from the engine compartment due to its wide design. The final assembly of the final seat pan design is displayed in figure 5, with the 95th percentile model in SolidWorks to display its overall fit in the car.

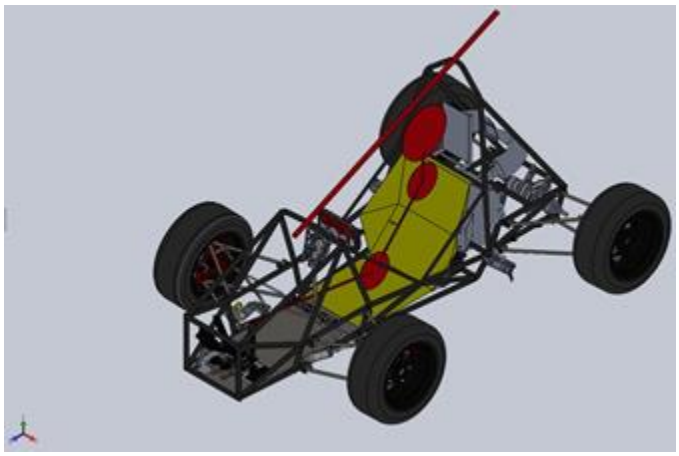

Figure 5: Final Seat Design in Car Assembly

With the seat pan design finalized in SolidWorks the dimensions were recorded and the task of manufacturing the seat pan began. Twenty gauge sheet steel was used as the base material for the seat structure due to its inexpensive cost, High yield strength and rigidity. The seat model was divided into three sections as shown by the different colors in figure 6.

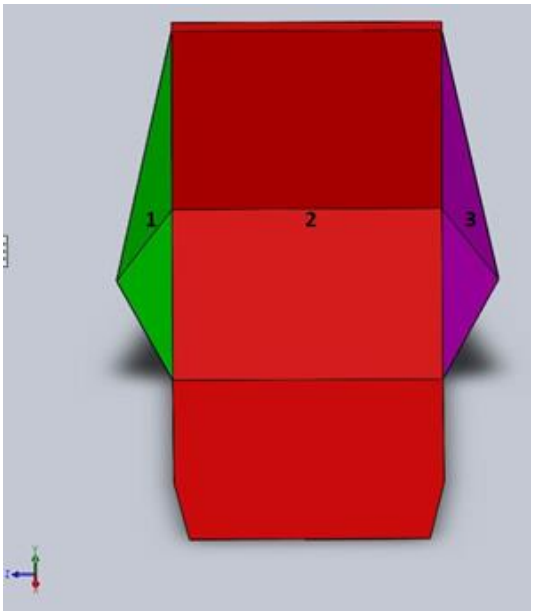

Figure 6: Sectioned Seat Pan

Each section was transferred onto a flat piece of twenty gauge sheet steel with the appropriate cut and bend lines portrayed. The parts were cut on a mechanical shear and bent into shape using a mechanical brake. On the two side pieces of the seat pan marked by the numbers 1 and 3, ½ inch tabs were included to easily join the components using a technique of plug welding to join the pieces together. A series of holes were drilled into the tabs on the side pieces of the seat and then clamped to the center section for

plug welding. The panels were fused using a TIG welder by spot welding and the seat was painted to protect the metal from corrosion. Figure 7 below displays the finished seat pan.

Figure 7: Finished Seat Pan

Due to the addition of structural tubing to the frame, as described in the frame section of this paper, the seat pan needed to be modified to fit into the modified driver's compartment. Using a hammer and an aluminum block, the metal side panels of the seat pan were re-formed until the sides of the seat were perpendicular to the back of the seat to allow the current seat pan to fit into the smaller driver's compartment.

Pedal Assembly

The pedal design and location affect the fit and feel of a driver in the car. With the seat pan fabricated, it was time to position the pedals in the car. The design was based on the setup of the average car with a manual transmission. The three pedals were arranged with the gas pedal on the right side, the brake pedal near the center and the clutch pedal on the left side of the driver compartment. To increase the strength of the mounting surface of the pedals a plate was designed as a support structure based on the width of the

driver compartment and the rough location of the pedal assembly. Figure 8 below is a representation of the pedal sub assembly in SolidWorks.

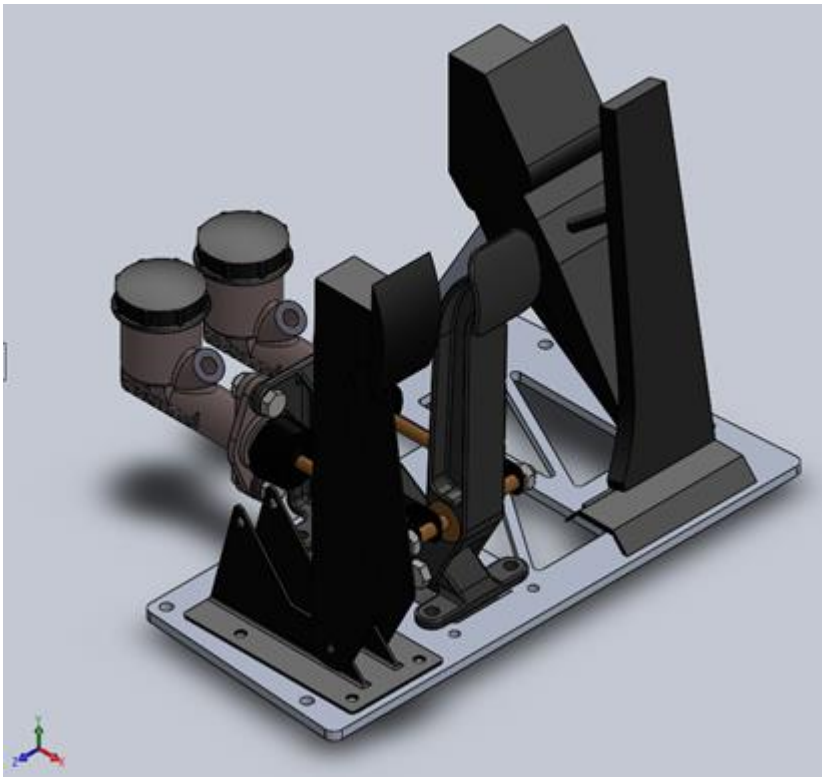

Figure 8: Pedal Assembly in SolidWorks

The pedal plate offers the operators the ability to adjust the pedals easily to their personal fit by incorporating multiple sets of mounting holes. The pedals can be shifted to incorporate a wide range of driver sizes. Weight reduction cuts were implemented to reduce the overall part weight. 6061 T6 aluminum was used for its great strength to weight properties. To verify the integrity of the pedal plate in an emergency situation a finite element analysis was performed. 300 pounds of force was applied to the brake pedal mounting holes to simulate a situation where a driver applies a large force to the brake pedal. The plate was fixed at the four mounting locations of the pedal plate to the frame. The yield strength of the aluminum was 39890 psi. The peak von Mises stress on the pedal plate was 2265 psi with an overall factor of safety of 18. This factor of safety was acceptable for the pedal assembly. Figure 9 shows the overall stress distribution along the weight saving cutouts and the low von Mises stress across the surface area of the part.

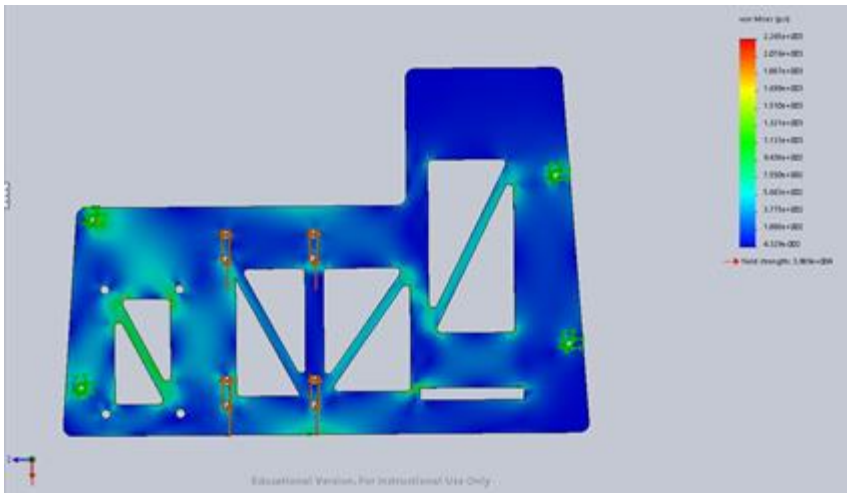

Figure 9: Pedal Plate FEA

The fabrication of the pedal plate was outsourced to a local machine shop with a water jet machine due to the complexity of the part's shape. The water jet could easily cut the part very precisely in one operation reducing the overall setup and machining time. The tolerances the machine was able to hold were +/- 0.002 which is acceptable to the standards of the Formula SAE team and to the tolerances of the pedal plate.

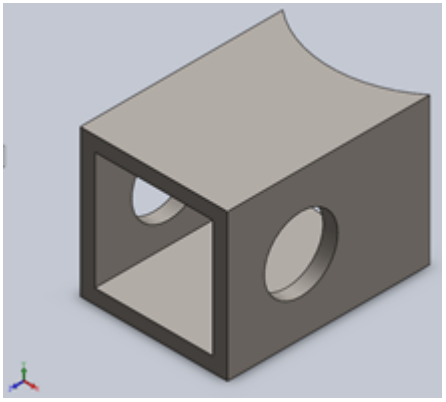

Figure 10: Pedal Mounting Tab

The pedal plate was mounted to the frame using tabs fabricated from (⅝) inch steel box tubing. Figure 10 above displays a SolidWorks model of the designed mounting tabs. The tabs were manufactured using two separate operations on a CNC milling machine. Square stock was loaded into a CNC milling machine for the drilling operation for the mounting hole. For the second operation the part was rotated 90 degrees where a ¼ inch mill created the fish mouth feature which easily joined the tab to the frame. With the pedal plate mocked up in its farthest forward position a TIG welder was used to attach the tabs to the frame in their appropriate locations aligning the mounting holes of the tab to the pedal plate. The finished pedal assembly is shown in figure 11 below with the clutch pedal installed on the left side.

Figure 11: Finished Pedal Assembly

After the installation of the pedal assembly into the car, a decision was then made to remove the clutch pedal entirely and install a hand clutch operated by a pull lever on the side of the driver. The clutch pedal installed was not able to actuate properly due to the number of bends in the pull cable and by installing a hand clutch the total distance of the cable and the number of bends decrease allowing the lever to move easily.

Head Rest

Formula SAE rules dictate that the headrest must be in the near vertical position and withstand an impact force of 200 pounds. Through the competition rules there is a constraint on the size of the headrest to be at least 6 inches by 11 inches for a non-adjustable headrest. The position of the headrest can adjust the distance between the driver's head and the roll hoop envelope between the front and rear roll hoop on the frame as dictated in figure 12.

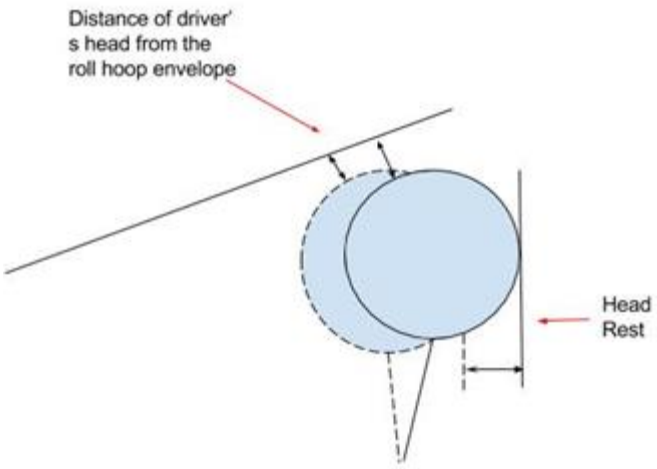

Figure 12: Head Position Relative to Roll Envelope

By shifting the headrest toward the rear section of the car the distance between the roll envelope and the driver's head increases. 2016 Formula SAE rule T3.10.3 state the top of the driver's head must be at least 2 inches below the roll envelope. With the 95th percentile model in the car in SolidWorks, there was a clearance of 2 ¼ inches between the model's head and the roll envelope as a factor of safety. The distance from the back of the seat pan to the back of the driver's head was measured and recorded to give a 1 ¼ of an inch offset from the back of the seat. From this measurement a simple wooden model was made using quarter inch plywood and attached to the car to measure the distance of each driver's head from the roll envelope. Formula SAE rule T5.6.2e states the head restraint should be no more than 1 inch away from the back of the driver's helmet, with the driver in their normal driving position. Every driver with their head in a comfortable driving position was no more than 1 inch away from the wood headrest model which allowed which allowed the headrest to be cleared for manufacture. According to rule T5.6.2b the head rest must be padded with at least 1.5 inches of energy absorbing foam. Keeping in mind the thickness of the foam padding the head rest support was shifted back 1.5 inches to a final location of 2.75 inches from the back of the seat. With the final dimensions of the headrest determined a structural design was created in SolidWorks. Using 5/8 0.095 steel tubing and 20 gauge sheet steel a 200 pound force was applied to the model. The factor of safety of the headrest is 1.5 and the overall stress was distributed evenly throughout the headrest structure as seen in the figure 13 below.

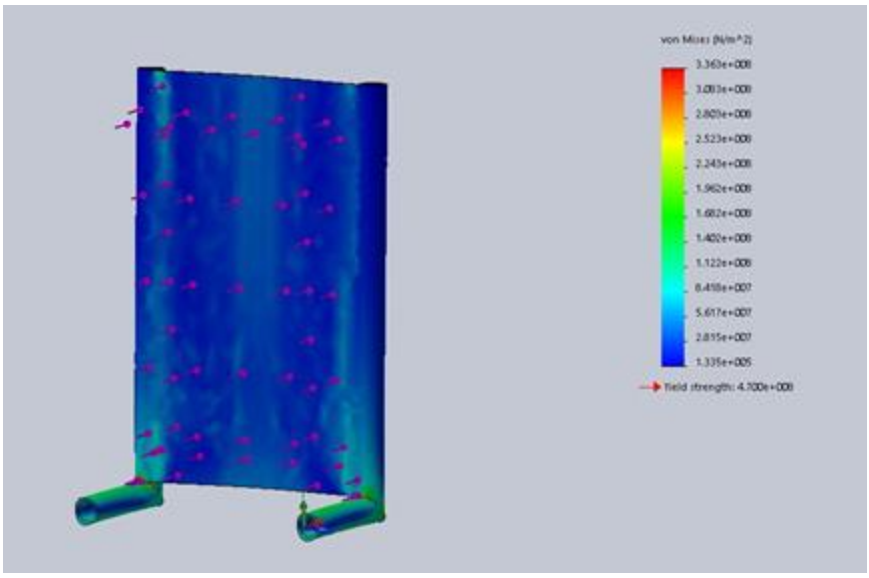

Figure 13: Head Rest FEA

With the final design of the headrest chosen the next task was to cut and notch the steel tubing to assemble the support structure of the headrest. A horizontal band saw was used to cut the tubes to length and a CNC milling machine was used to machine the notches in the ends of the tubes to allow them to fit together. The final members are welded to the upper seat support ensuring the head rest was in the near vertical position relative to the frame. The finished head rest is displayed in figure 14.

Figure 14: Finished Head Rest Assembly

Seat Insert

While the seat pan is the basis of the seat it will in not alone keep the driver cradled into the car through a high G turn. Many race teams utilize a seat insert which is formed to each driver. In a car, the driver should never have to fight the G loadings to stay in a comfortable driving position. Their seat should keep them centered in the car and allow them to concentrate less on positioning themselves in the car and more on the operation of the car. A popular solution for creating a custom seat insert is by utilizing a two part expanding foam. First, a series of bags were taped into the seat pan of the car ensuring that it was secure against all surfaces. The two part foam was mixed using a 1 quart mixing container for a total mix volume. The foam mix was poured into the bad and the driver immediately sat down onto the bag being careful not to tear the bag open. Figure 16 below displays the driver during the forming process.

Figure 16: Seat Insert Forming Setup

Figure 15: Seat Insert Foam Base

The foam was redistributed evenly around the driver. Once the foam began to expand, the driver sat in a comfortable race position until the foam set after 10 minutes. Once hardened, the foam was removed from the bag and sanded down to its final shape. Figure 15 above displays the seat insert after it was removed from the bag. Using a 3 inch rotary sander the foam was further shaped to refine the edges of the seat insert. The foam insert was sent off to an upholstery company to wrap the seat insert in a fabric for aesthetics and protection.

Suspension

Background

The suspension system of a vehicle controls the way the chassis reacts with the road surface and a sound design is critical for optimal performance, especially in racing environments. The system is comprised of sprung and unsprung masses and must react safely in a range of scenarios, including acceleration and cornering over a smooth or potentially rough track surface. While in these scenarios there are other systems that will affect the final condition of the vehicle, such as frame torsion and deflection, along with tire affects. The frame deflection will be addressed independently in order to simplify the modeling process of both the kinematics and dynamics of the system. Tire data is currently unavailable for the 2016 team and will be removed from suspension calculations other than research based assumptions. Future teams should obtain tire data and modify suspension parameters to incorporate this data.

Design Parameters

The design of this system is driven by the formula SAE 2016 rules, which determine several design parameters. According to rule T6.1.1, "The car must be equipped with a fully operational suspension system with shock absorbers, front and rear, with usable wheel travel of at least 50.8 mm (2 inches), 25.4 mm (1 inch) jounce and 25.4 mm (1 58 © 2015 SAE International. All Rights Reserved 2016 Formula SAE® Rules – May 11, 2015 inch) rebound, with driver seated. The judges reserve the right to disqualify cars which do not represent a serious attempt at an operational suspension system or which demonstrate handling inappropriate for an autocross circuit." Ground clearance must be sufficient enough to allow only the wheels to come in contact with the ground throughout the entire suspension travel. A minimum wheel diameter of 8.0 inches is required.

Based upon these basic requirements, any type of suspension linkages are permitted. The 2015 FSAE MQP team conducted an in-depth analysis to which type of suspension would be optimal for a formula SAE vehicle. This table can be seen in table 1.

		Concept 1		Concept 2		Concept 3		Concept 4	
Decision Factor	**Weight**	**Semi-Trailing Arm (Rear Only)**		**Double Wishbone**		**Unequal length wishbone (SLA)**		**MacPherson Strut**	
		Score	Value	Score	Value	Score	Value	Score	Value
Ease of Access	6	9	54	9	54	9	54	8	48
Fatigue Resistance	8	7	56	8	64	8	64	6	48
Strength of Design	7	8	56	8	56	8	56	7	49
Simplicity	9	9	81	6	54	6	54	8	72
Ease of Machining	6	7	42	6	36	6	36	8	48
Cost	7	8	56	5	35	5	35	8	56
Compatibility	8	8	64	7	56	7	56	8	64
Serviceability	6	9	54	7	42	7	42	7	42
Manufacturability	7	7	49	7	49	7	49	8	56
Performance	10	6	60	8	80	8	80	6	60
Tire Patch Control	8	5	40	7	56	9	72	5	40
Adjustability	7	1	7	7	49	7	49	6	42
Totals			**619**		**631**		**647**		**625**

Table 1: Suspension linkage design decision matrix

In their analysis, unequal length wishbone type suspension was chosen. Following research conducted using the Racecar Dynamics book by Douglas Milliken, these findings were validated as this type of suspension is simple, adjustable, and allows the vehicle to be designed using several different shock actuation methods.

A-Arm Design

Design Basics

Suspension and steering design are driven by several key factors, such as camber, kingpin inclination, castor, scrub radius, and wheel offset, and mechanical trail. Camber is the angle the wheel leans in the front view, and affects cornering dynamics by adding a trust vector inward our outward of the turn. Kingpin inclination is the angle between the two ball joints and the vertical axis in the front view, which affects camber gain with respect to steering angle and can be used to induce a non-linear camber steer. Castor is the angle of the ball joints relative to the vertical axis in the side view, which when projected to the road surface defines the mechanical trail. The scrub radius is the distance from the kingpin at the contact patch to the center of the contact patch, which defines the additional moment the wheel must overcome to be steered. In a road racing vehicle, low or moderate values (0-5 degrees) are typically set for all values angular values, with some values such as scrub radius minimized to reduce steering effort (Milliken).

Adjustment Range and Revision

Some of the original design factors that influenced the 2015 FSAE MQP design of the suspension was the Keizer 13" wheels that the team had used for years previously. For budgeting reasons, these wheels were selected to be the basis of the design of the suspension. Another key influence was the ability to test and tune the vehicle within the current work area. The front and rear track width was set as wide as possible while still being able to be able to remove the vehicle from the workspace, since previous vehicles had to be partially disassembled due to narrow doorways. Luckily due to workspace improvements, the track width could be optimized for racing scenarios, such as the autocross and endurance tracks at FSAE Michigan. The track width was increased to 1332mm in the front and 1328mm in the rear. The advantage of the track width increase is lower roll rates, a lower roll center, and increased lateral acceleration before rollover. The disadvantages include increased weight, and increased time during slalom events. The increase in weight due to the track width change was nearly negligible due to the low tubular cross section where the increase in width would be created. Increased time in slalom events was an acceptable compromise due to the high possible cornering speed and higher likelihood that the car will pass the tilt table test (the final CG will differ from the design CG, therefore only an approximation can be made)

For this design, research into typical camber ranges was conducted to determine the typical road vehicle camber, sports vehicles, race vehicles, and formula 1 vehicles. Since a formula SAE vehicle is closest to a formula 1 vehicle, those figures would be driving the design, with adjustability to be moved to values that a normal sport or race vehicle might have.

Positive camber is not beneficial in any location throughout the suspension travel, therefore the range for adjustment was set to contain only values of zero camber or negative camber. A general extreme for camber was set to -5 degrees as a good compromise for all potential testing and tuning options.

A-Arms design for manufacture

The layout sketches for the A-Arms were converted to solid parts using weldments in a similar fashion to the main section of the frame. The team worked with VR3 Engineering, commonly known as Cartesian. Cartesian recommended that hollow nodes not be used in the design due to the weakness of this type of joint, which is where both tubes are notched with the same priority, and an open section is left. The proper way to notch tubes for the strongest configuration is to leave one tube untrimmed with the mating tube being notched to fit together. If both tubes meet at another tube or component, they are trimmed as noted above with respect to each other, and then the pair is notched to the third component. The designs were updated and sent to Cartesian, who provided a fast turnaround with accurate parts.

A-Arm welding process

The A-Arms were made by using a MIG welder to fuse the members together for ease of use since MIG welding is a quicker process compared to TIG welding. A test weld was completed using scrap tubing and upon inspection the welds were acceptable. Threaded rod was used to set the distance of the A-Arm pivot points. This method both accurately set the width of the A-Arm pivots as well as ensured the pivot holes were cylindrical to each other. Figure 17 below displays the threaded rod used to set the width of the A-Arms.

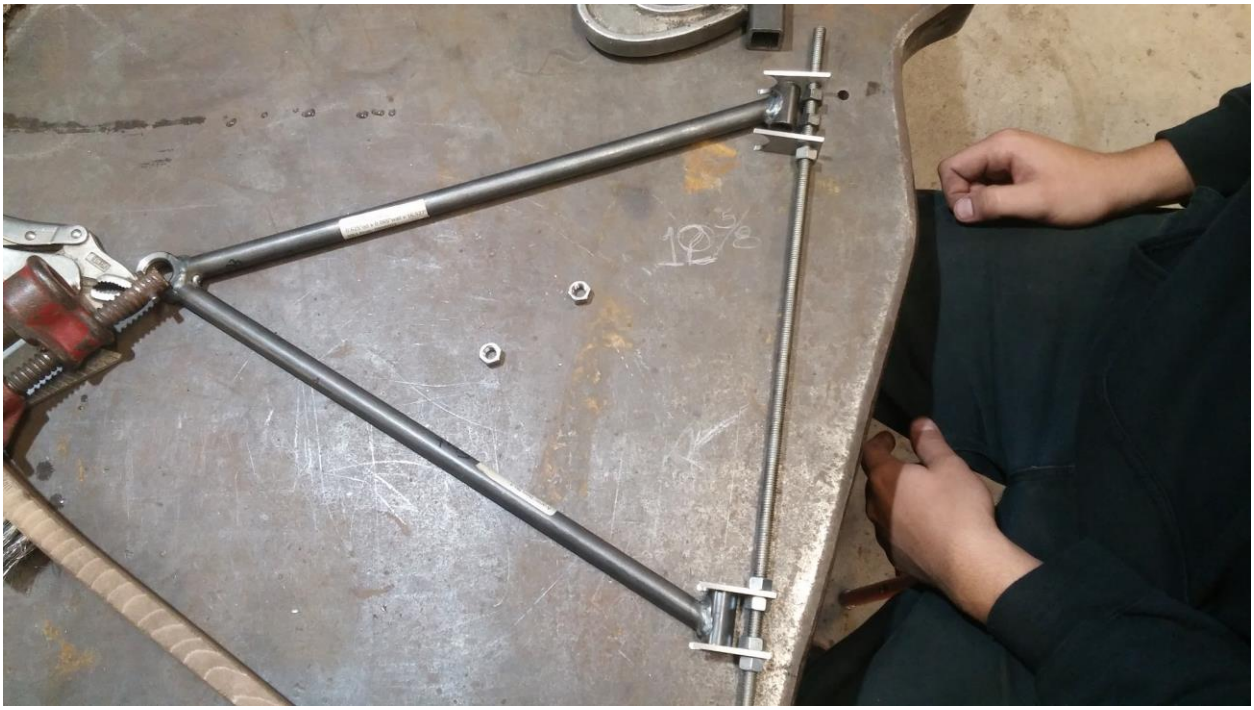

Figure 17: Threaded Rod A-Arm Jig

To set the position of the other A-Arm tubes off the pivots the parts were laid out on a flat steel surface. Steel shims were used to properly elevate each component and a protractor was used to set the angle of each tube. Weights were added onto the components to hold them in their final orientation. Figures 18 and 19 display the setup of the A-Arms and figure 20 displays the finished A-Arm.

Figure 18: A-Arm Jig

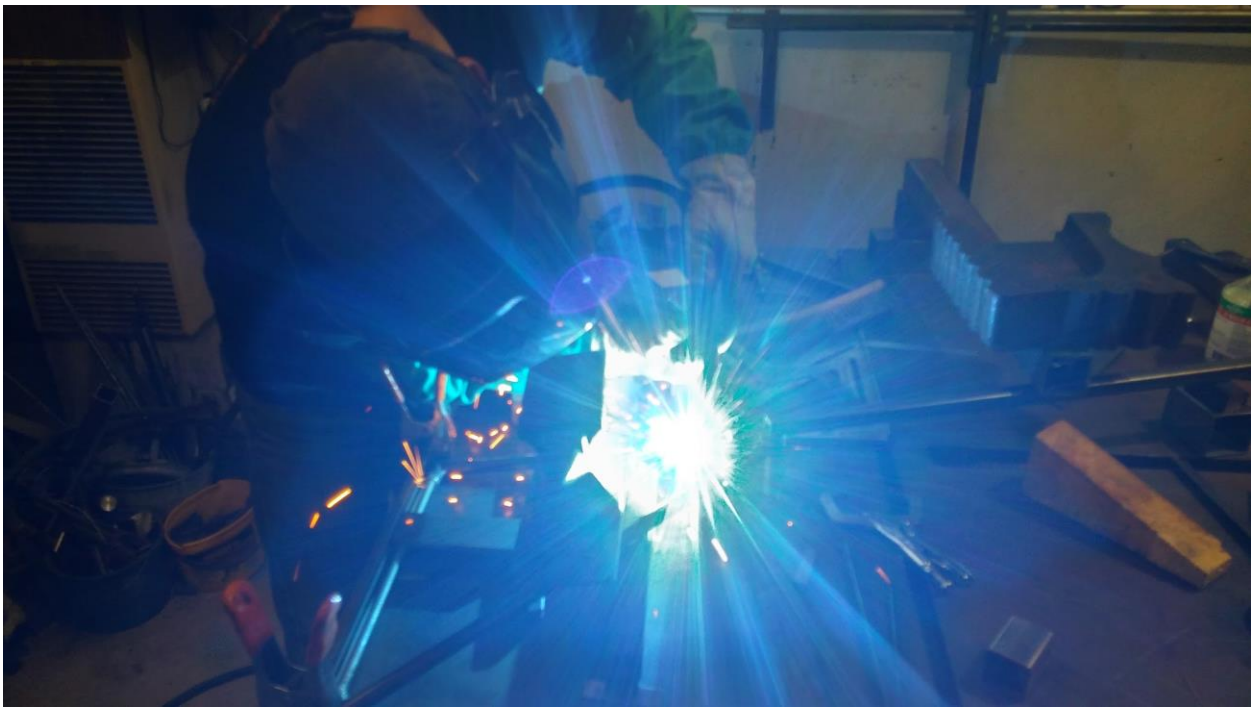

Figure 19: A-Arm Welding Process

Figure 20: Finished A-Arm

To properly assemble the A-Arms to the upright's two bushings were needed to ensure a tight fit between the components. Using a CNC lathe, aluminum bushings were created to fit in the ball joint fittings of the A-Arms. The bushings were pressed into the top and bottom sides of the ball joint and the distance between the two outer surfaces of the installed bushings match the width of the upright mounting location as a tolerance fit. The inner diameter of the bushings was undersized and reamed out with a ¼" under reamer to fit the shoulder bolt. Figure 21 below displays the finished A-Arm bushing sets.

Figure 21: Finished A-Arm Ball Joint Bushing

Tab Design

Based upon the determined range of 0-5 degrees of negative camber, the tab geometry could be determined. Several different tab types were considered including box tube type, solid billet tabs, slotted solid plate stock tabs with camber plates, and solid tabs with the adjustment in the A-Arm using rod ends. The last option was eliminated first due to the danger of exposing a rod end to bending loads, along with the difficulty of the suspension setup since discrete locations could not be set on the threads of the rod ends. One of the main goals of the competition is to have a low vehicle weight, which eliminated the solid billet tabs although they were the strongest design. With the final camber setting undetermined during the design phase, adjustability was the driving factor since the camber could be validated with on-track testing. The box tube style tab was eliminated due to the lack of readily available box tubes to fit the various shapes and lengths of tabs needed, along with the inability to easily integrate a reliable camber adjustment method. This left the plate stock style tabs with camber adjustment plates for the final design. This allowed slots to be created in the tab with a plate with a single centered or offset hole to locate the control arm. These tabs also offered a lightweight and easily manufacturable solution, with the only potential issue of stress concentration along welded areas due to local heat treating. This issue was solved by a heat treating process which was done on the frame and control arms. While these tabs are strong enough for the FSAE competition, it is recommended that gussets be welded in between tabs in each set to stiffen the tab pairs to eliminate the possibility of paralleling.

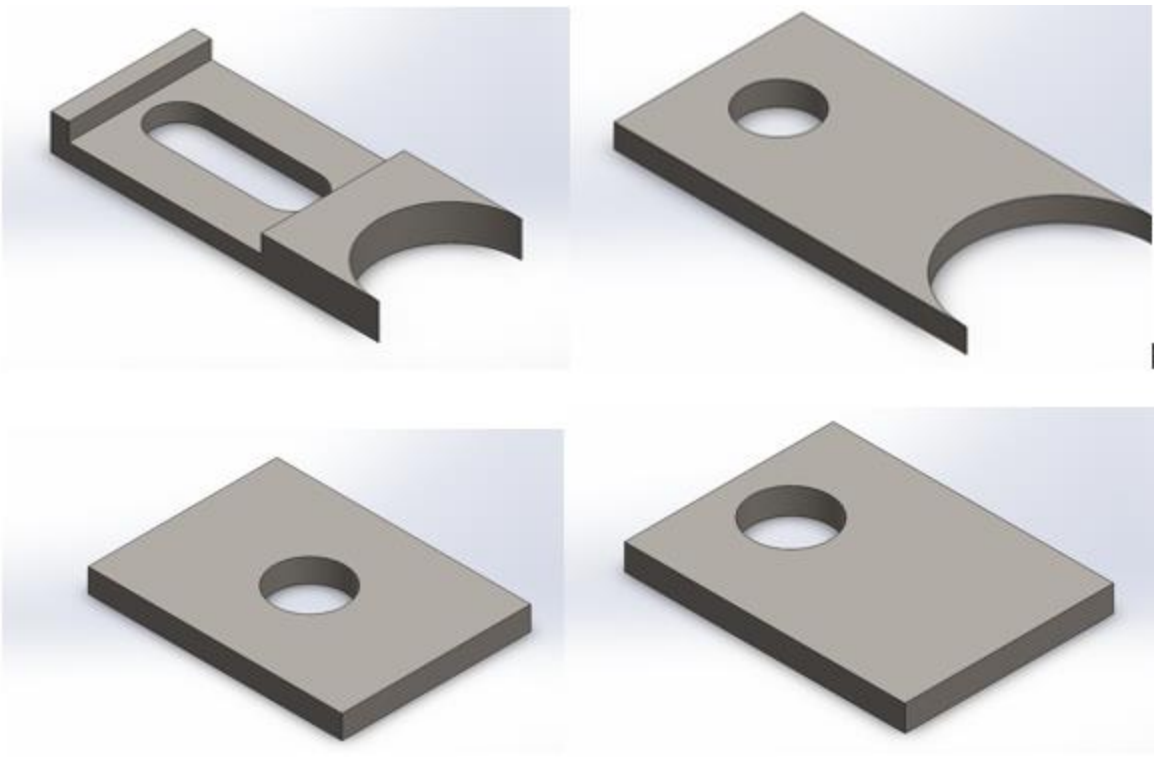

Figure 22: Tab and insert design. Top left: Upper tab; Top right: Lower tab; Lower left: neutral insert; Lower Right: extreme insert

Using the frame geometry, the A-Arm geometry, and the determined wheelbase the tab dimensions could be determined. The spacing was set to allow at least 0.25" from the frame tube to the A-Arm to allow for weld beads and prevent any potential collision in the highest camber setting. Table 2 below was created to explore all possibilities and camber settings.

Front Tabs					Rear Tabs			
Top Position 0.75 Slot	Bottom Position 0.5 Spacing	Resultant KPI	Resultant Static Camber		Top Position	Bottom Position	Resultant KPI	Resultant Static Camber
Out	Inside	-1.63	0.37		Out	Inside	1.39	0.39
Neutral	Inside	-4	-2		Neutral	Inside	-1	-2
Inside	Inside	-6.36	-4.36		Inside	Inside	-3.38	-4.38
Out	Outside	-4.79	-2.79		Out	Outside	-1.79	-2.79
Neutral	Outside	-7.14	-5.14		Neutral	Outside	-4.17	-5.17
Inside	Outside	-9.5	-7.5		Inside	Outside	-6.53	-7.53
					Rear Upright with +1 Degree of Camber using Front Tabs			
	Tabs	Inserts per Tab	Total Inserts	Total Parts	Out	Inside	-1	0
Top Front	8	2	16	24	Neutral	Inside	-3.38	-2.38
Lower Front	8	0	0	8	Inside	Inside	-5.75	-4.75
Top Rear	8	2	16	24				
Lower Rear	8	0	0	8				
Totals	32	4	32	64				

Table 2: Tab camber adjustment table

Each of the settings was set at ride height with the top position referring to the position of the A-Arm in the slot on the upper tab. Initially, a slot was simulated on the upper tab with two locations on the lower tab. This was to create an overlapping range of camber values and was simulated for both the front and rear tabs. In order to simplify the design, it was determined that the second order of adjustability was not necessary and would complicate the design. Following this process, the front and rear tabs to be made to slightly different dimensions, resulting in unique sets of tabs from front to rear. In order to potentially simplify the machining process, a calculation was done to determine the camber if the front tabs were used in the rear suspension. The resulting camber was slightly too high, although the camber could be easily adjusted by setting a stock 1 degree of positive camber in the rear uprights.

Tab Manufacturing

The tabs and inserts were machined out of hardened steel due to the process used to make the stock. They were then used to mount the body and other parts onto the frame. Due to the steel being hardened it caused some trouble with drilling the holes however some HSS drills worked in this process. Two different types of flat inserts and tabs sets were made so in order for maximum production due to needing many of them, softjaws were created that ran the insert paired with its tab in the same program. Figure 23 displays the machining setup for the suspension tabs.

Softjaws

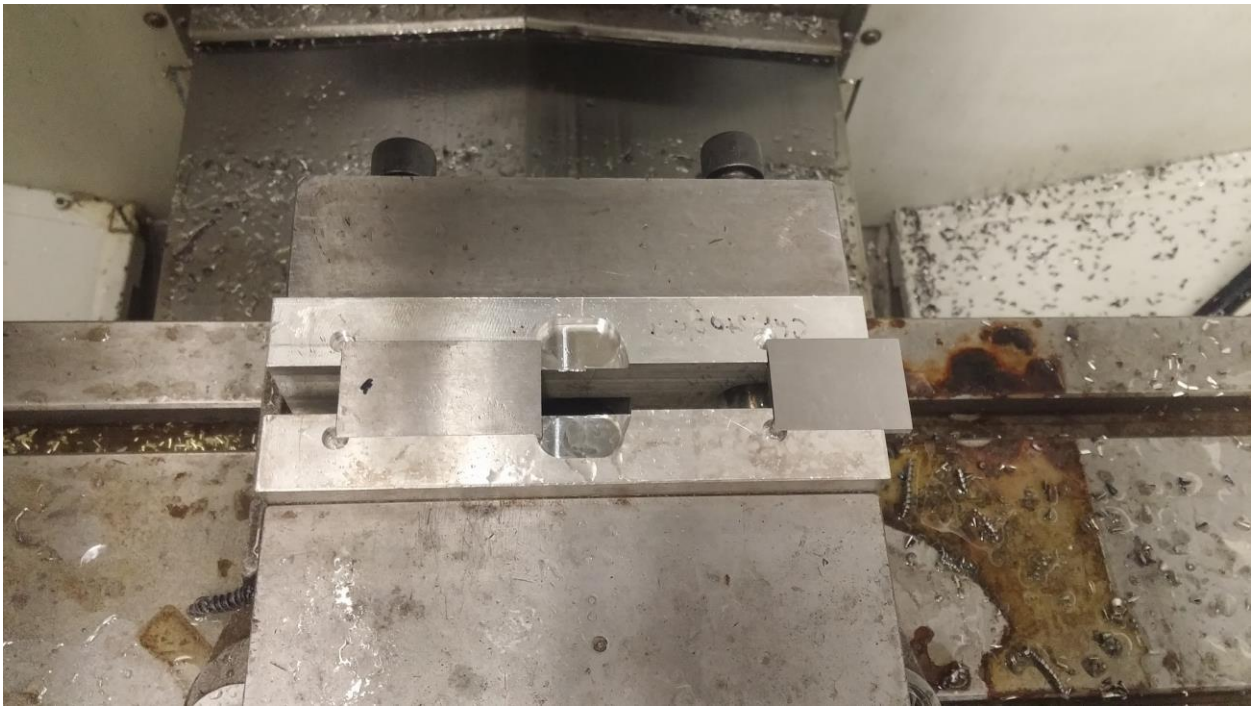

Figure 23: Tab and insert manufacturing using machined softjaws

Tabs and Inserts

Figure 24: Machined upper tab with neutral insert

Finished Parts and Fitting

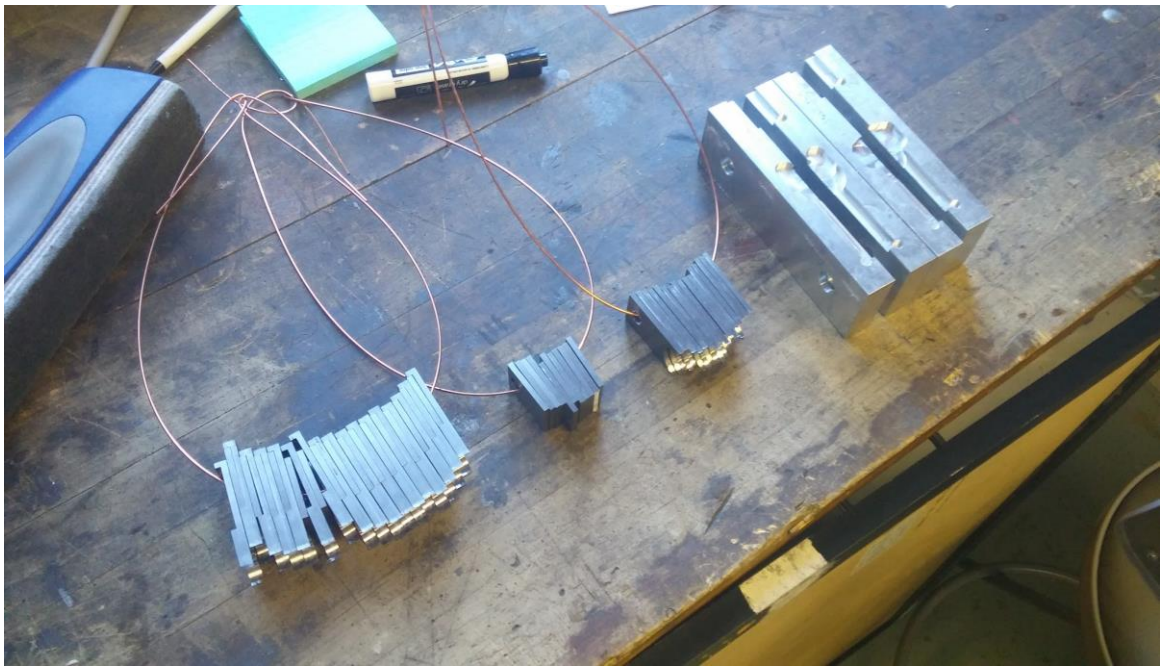

Figure 25: Machined tabs and inserts with dual softjaw sets

Welding

A threaded rod was utilized to set and hold the location of the tabs based on a set distance from each other. With the tabs secured to the threaded rod the assembly was secured to the frame using C clamps and angle iron steel as a supporting structure as seen in figure 26 below. The location of the tab assembly was set using a known distance from the front tab to the rear and front tubes of the frame. MIG welding was used to join the tabs to the frame and the threaded rod was removed after the components cooled to ensure the parts wont warp during the cooling process. Figures 27 and 28 further show the jigging and welding process for the tabs.

Figure 26: Suspension Tab Jig

Figure 27: Suspension Tab Jigging Process

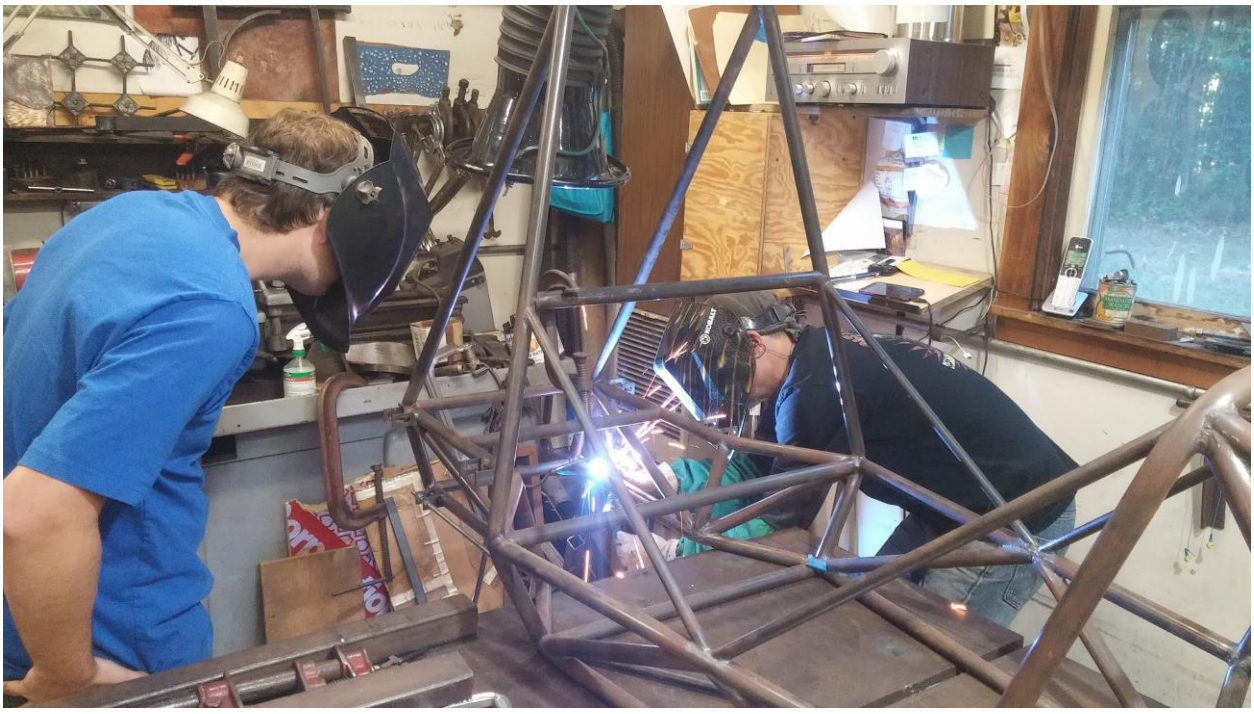

Figure 28: Suspension Tab Welding Process

Rocker Design

Rocker conceptual design

The pullrod suspension system must utilize rockers as a key part of the design because the shocks only work in compression. To convert the tension to compression, a rocker must be used. The design intent behind these components is to have a strong and reliable part which is lightweight and can interface with position sensors.

Different designs were investigated and due to packaging constraints and optimizing for the lowest center of gravity possible, the designs were limited to rockers that acted as a class 1 lever. For ease of calculation, the angle between the ground point, pullrod node, and shock node was set to 90 degrees. Two design methods were found, a type that used two similar plates which were spaced apart using spacers and bushings and a billet type rocker which is machined from one solid piece of stock. A design decision matrix as seen in table 3 was used to justify each design.

		Plate Type		Billet Type	
Decision Factor	Weight	Score	Value	Score	Value
Strength	10	6	60	10	100
Manufacturability	8	10	80	7	56
Weight	9	5	45	8	72
Assembly	6	3	18	9	54
Totals			203		382

Table 3: Rocker type design decision matrix

Although the first type would be considerably easier to manufacture, the billet type rockers would be much stronger due to continuous stress distribution and would be potentially lighter due to the lack of sub-assembly hardware.

Figure 29: Basic rocker layout [Front]

Figure 30: Basic rocker layout [Rear]

Tab design

In order to meet the packaging requirements for the rockers and shocks, the tabs needed to be able to be notched to fit the tubes at not only in the normal direction as seen in the rear, but at compound angles. Since the tabs won't be aligned with the tubes, a plate steel tab will not be acceptable due to the low contact area. While billet tabs could be manufactured, they would be heavy in comparison to the other tab types. Box tube style tabs have the larger section and moment of inertia of the billet tabs, but a considerably lower weight. Since there is no adjustment needed, these tabs were chosen as they were also low cost and easy to manufacture.

Before the geometric conditions for the rockers were determined, an analysis of the degrees of freedom (DOF) was conducted to ensure the system would not bind or lock up during movement.

The above equation shows that if the rocker is constrained with a pin joint to the frame, the system will have 3 DOF, with 2 of which are idle degrees of freedom and can be ignored as limited rotation of the pullrod and shock are not important to this analysis or the performance of the suspension system. This leaves the system with 1 DOF, the proper degrees of freedom for a linkage system which will not lock up.

Prior to creating geometry and selecting material, the worst case loading scenario was calculated. While using a pin joint on the rocker supplies the system with only 1 effective degree of freedom, as the suspension moves up or down, the rocker is side-loaded on the pullrod node. At low loads this is a negligible force, but at high loads it must be taken into account. The worst case scenario would be a 3g bump which could be seen if the vehicle hit a bump or pothole at a high speed. The worst case will be taken at the full jounce position, since this is where the load on the rocker/shock assembly is the highest, and the side-loading angle is also at its maximum. The side-load angle is 5 degrees at this location with the force of 500lbs located at 45 degrees from the initial pullrod position.

Transmission angle analysis

The motion ratio of a vehicle refers to the ratio of amount of shock travel to wheel travel. In a direct acting suspension system this is a linear or nearly linear function since the angle change of the pullrod with respect to the control arm through the entire travel is minimal. On rocker systems, the rocker rotates through a non-negligible range to move the wheel and compress the shock. In order to determine the angle of rotation to set the rockers in this system, an analysis of the rotation of the transmission angles of the pullrod to rocker and rocker to shock was conducted.

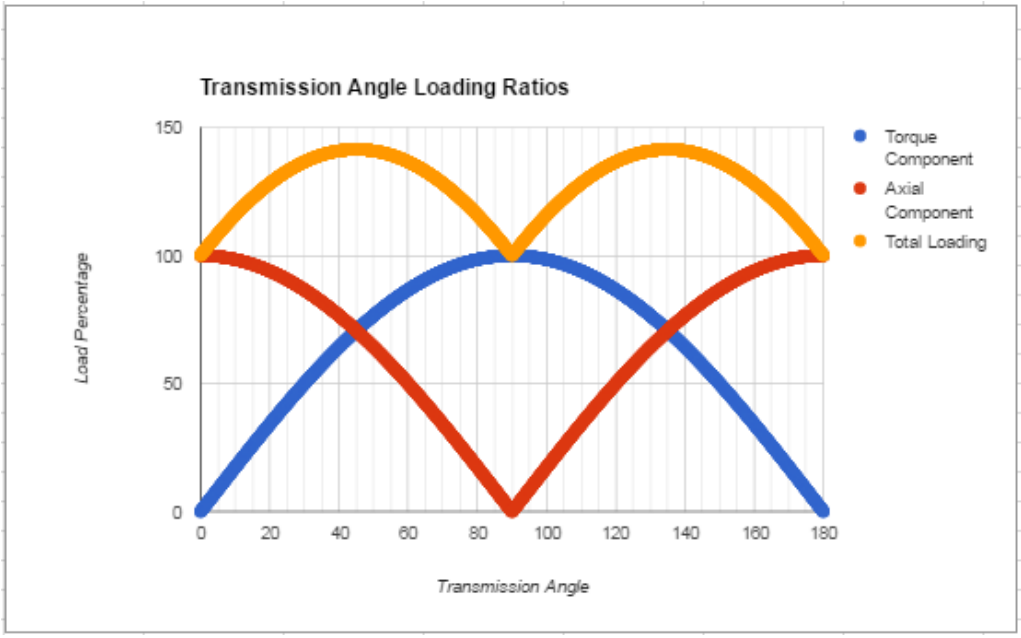

Figure 31: Transmission angle loading ratio graph

The above graph shows the ratio between the axial and normal/torque component with respect to the transmission angle. The coordinate system is set up in such a way that with a transmission of 90 degrees between the applied force and output link, the force is creating a pure normal force to the output link, therefore the torque is equal to the force X the output link length. At 0 and 180 degrees, the force is collinear with the output link, which results in a torque of zero with all load being applied axially. The total load is also graphed, which is just a sum of the normal and axial loads, and can be used to represent the worst case scenario where the output link is experiencing the highest net load, which is seen at 45 and 135 degrees.

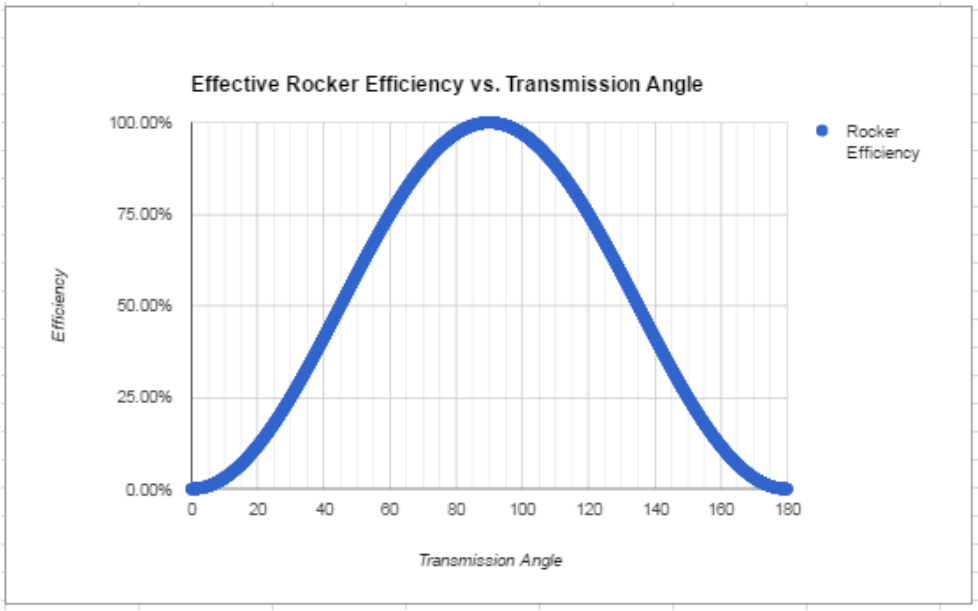

Figure 32: Transmission angle efficiency graph

Using the previous transmission angle loading ratio graph, the above graph can be created. This chart displays the effect of the efficiency change which is experienced during rocker travel as the transmission angle changes. Efficiency in this case is determined by the percentage of force being transmitted to pure torque, for example the case when both transmission angles are 90 degrees, the efficiency is 100%, whereas when both transmission angles are 180 degrees, the efficiency is 0%. The transmission angles are also set to be the same with the input and output links to simplify the solution. If a large angular displacement was needed for the rocker (over 90 degrees total travel) then the input and output transmission angles would need to be exactly 90 degrees out of phase in order to create a linear transmission angle efficiency of 50%. While this would solve the problem of changing efficiency, it would result in higher net loads experienced by the entire system along with creating challenging packaging issues. Due to the total displacement of the shocks that were selected and the necessary wheel travel to meet FSAE rules, a small rocker travel could be used.

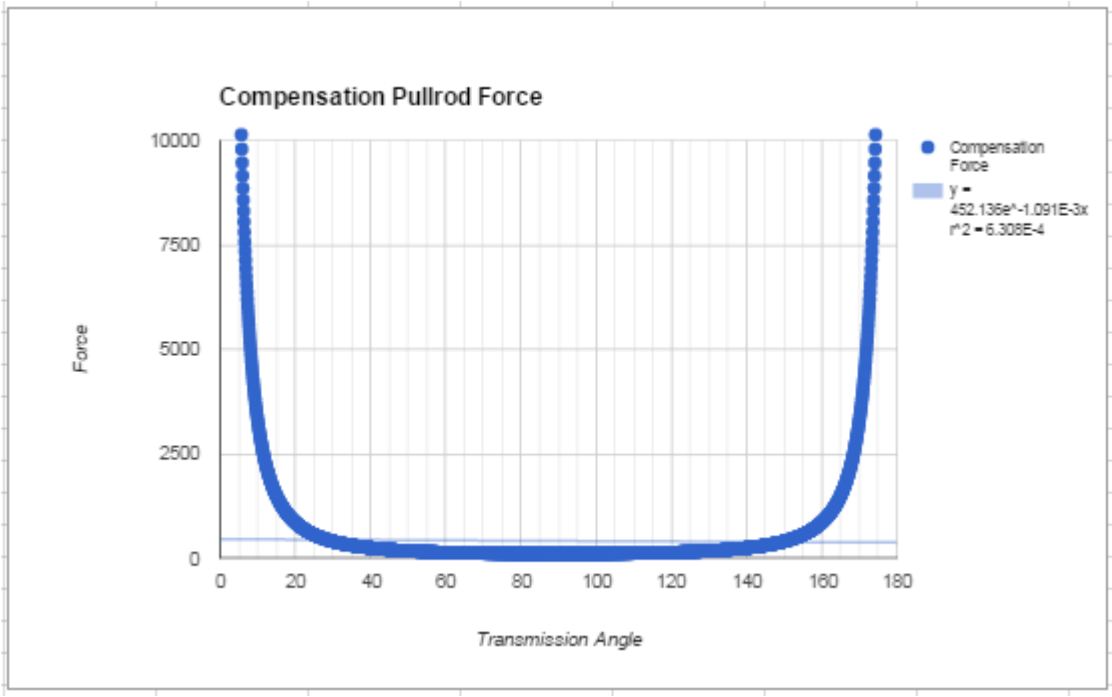

Figure 33: Input force to constant output torque for changing transmission angles graph

Next, as a logic check for the previous graphs, the above graph was calculated. This represents a defined output torque with the resulting needed force on the output link at differing transmission angles (this takes into account both transmission angles on the rocker). As can be seen, in the range of 45-135 degrees, the curve is mostly flat since the efficiency is high, but as angles farther from 90 degrees are reached, the required force increases exponentially since the transmission angle efficiency approaches zero in those areas. At 0 and 180 degrees, the pullrod required force is infinite because of a zero rocker transmission angle efficiency, which proves that for a rocker system high transmission angles must be avoided at all costs. After reviewing the efficiency graph and compensation pullrod force graph, at total travel is set to the 45-135 degree range.

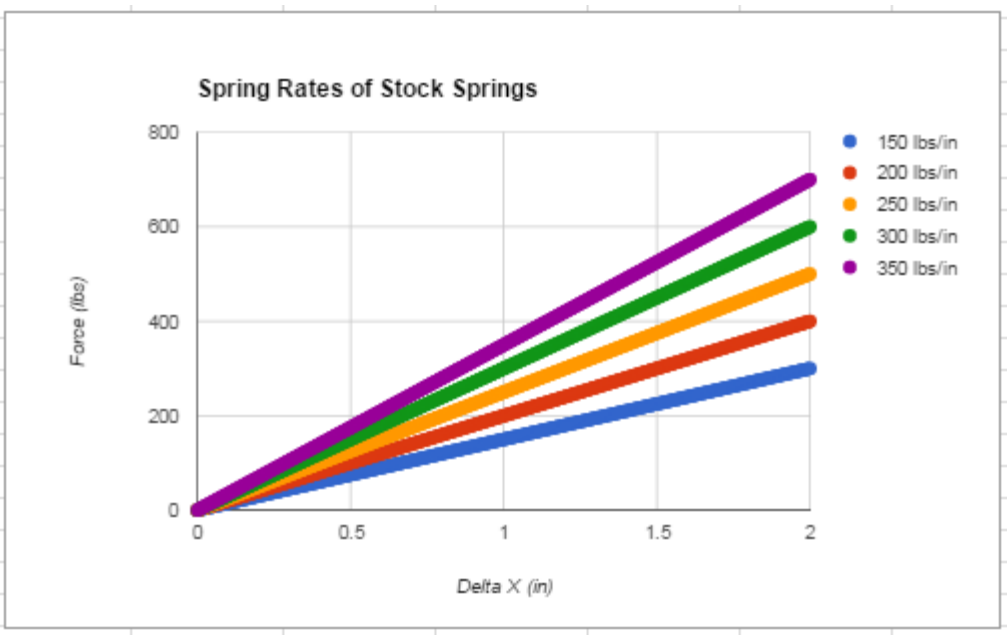

Figure 34: Linear spring graph

The next graph was created as a basis for the final shock travel graph. This graph simply plots 5 different widely available springs using their spring constants to graph force with respect to displacement. These linear graphs will be combined with the efficiency graphs to determine how much force will need to be applied to the pullrod node of the rocker to obtain a certain shock displacement.

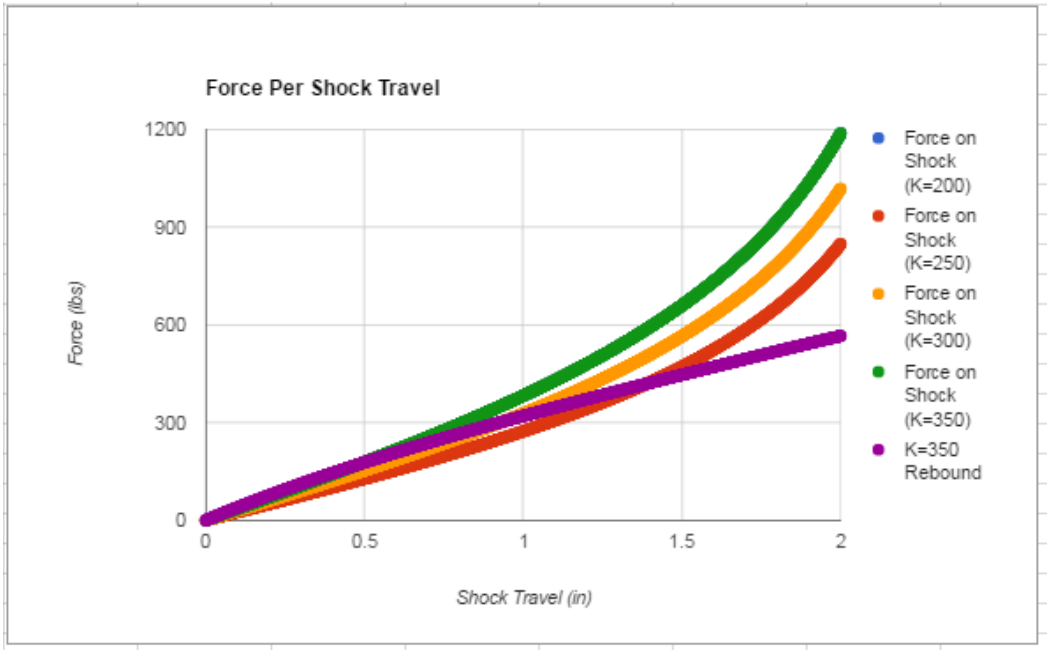

Figure 35: Non-linear shock loading graph

Initially the results were graphed by setting the transmission angles of the rockers to 90 degrees at the full rebound position. This would mean at 45 degrees, the suspension would reach full jounce. As can be seen above, this situation results in a nearly linear graph which begins to exponentially increase as the shock reaches full jounce. While this will provide a stiffer ride than a typical consumer vehicle might require, for a racecar situation this was found to be ideal because the wheel and roll rates increase exponentially, roll center migration is highly reduced at high loads, and the potential to bottom the shock out and cause permanent damage are highly reduced.

Next, the transmission angle was set to 90 degrees at neutral travel/ ride height. This would mean that at full rebound and full jounce the rocker would be located at 22.5 degrees from its initial 90 degree transmission angle, at 67.5 degrees and 112.5 degrees. Since the efficiency change at these locations is relatively low, this graph results in the flattest of the three curves. This setup could be best suited for reducing the total potential suspension loads and for the use of a linear motion ratio and wheel rate approximation with a rocker system since phasing the transmission angles is not geometrically feasible in this specific system.

Lastly, the transmission angle was set to 90 degrees at full jounce. The resultant transmission angle at full rebound is 45 degrees. This causes the rate of change of the force/displacement curve to decrease over the total travel. Since the total travel must be at least 1" of rebound and 1" of jounce from ride height per FSAE rules and 1.25" each direction per the design constraints for this system to avoid tolerancing issues, this type of system is not recommended. This is due to the fact that the neutral position will have to be reached by a 150lb driver being seated in the vehicle. This would mean that very soft springs will have to be used, and since the rate of force/displacement decreases after the neutral position, the shocks will bottom out after a load of less than 150 lbs, which for a 600lb car with driver is equal to a 1g bump which is completely unacceptable and unsafe. In figure 35, this scenario is graphed in purple, with the initial scenario of the optimal transmission angle at full rebound being graphed in green. In both cases, the same springrate is used, and this chart shows the benefit of the initial case through the non-linearly increasing force/deflection graph.

The motion ratio changes throughout the range of suspension travel. This change is due to three significant angle changes in the pull rod system, pull rod to A-Arm, pull rod to rocker, and rocker to shock. In reality, the motion ratio is a 3D geometric system with many angles to consider. In order to simplify the motion ratio calculation at full bump and droop, two 2D sketches were constructed in SolidWorks for both the front and rear suspensions, one in the front plane using the dimensions of the upper A-Arm, pull rod and rocker pickup and one in the plane of the rocker using the dimensions of the rocker and shock.

First, the relevant members in the front suspension were sketched in the front plane using their position at full bump, which was measured using the 3D sketch in the full vehicle model. A second set of members was overlaid using the same dimensions, but with the wheel position 1mm above the full bump position. Relevant degrees of freedom were fixed in the appropriate ways, such as the lower end of the pull rod fixed along the path of the pull rod in the front plane. In reality this end of the pull rod will also move a small factor in the top and right planes, however this amount only affects the motion ration by a small fraction compared to the motion in the front plane. The distance the pull rod moves the rocker during this

1mm droop movement was then measured in the sketch to be 0.365mm, and transferred to the second sketch.

The sketch in the plane of the rocker was fixed using the dimensions and rotational position of the rocker in addition to the angle of the shock to the rocker at the full bump position. Like the front plane sketch, a secondary set of members was also sketched, in the theoretical position after a 1mm wheel movement. The pull rod measurement found using the first sketch was then used to set the distance between the rocker-pull rod pickup point between the two set of members, shown below. This allowed for a simple measurement of the two rocker-shock pickup points between the two set of members, which moved from 188.965mm to 189.736mm. This estimated shock travel, found from 189.736mm-188.965mm=0.771mm, was then divided by the 1mm wheel movement to show the motion ratio at full bump to be 0.77:1. This calculation method was then repeated for the front suspension geometry at full droop and found to be 0.694:1, and again for both maximum rear suspension positions (0.840:1-0.995:1). Knowing the motion ratio at neutral suspension position, the designed system provided a progressive motion ratio though suspension travel, which is very desirable in a racing situation. These four maxima calculations provided the motion ratios at full bump and full droop for all four wheels, and could be repeated through each point through the suspension travel to provide the complete motion ratio function.

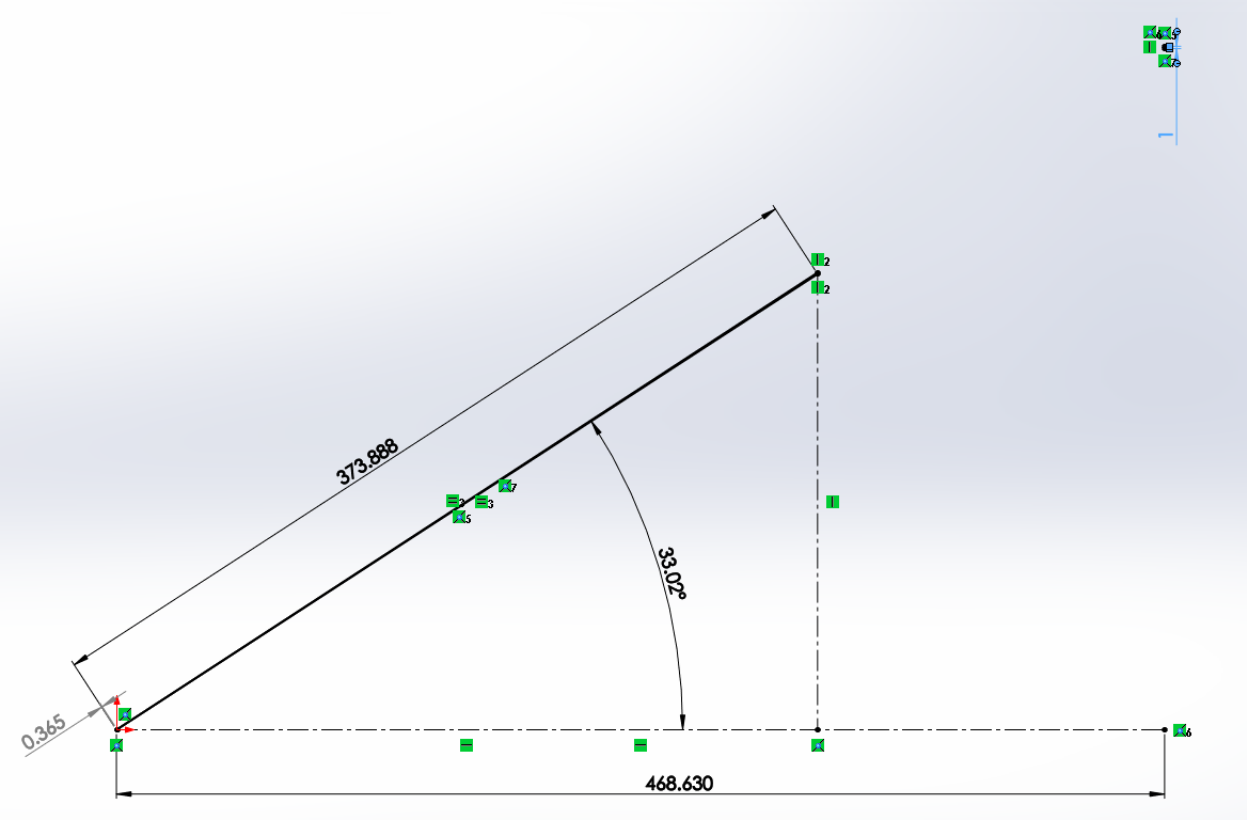

Figure 36: Front Suspension Pull Rod Geometry in the Front Plane (Full Bump)

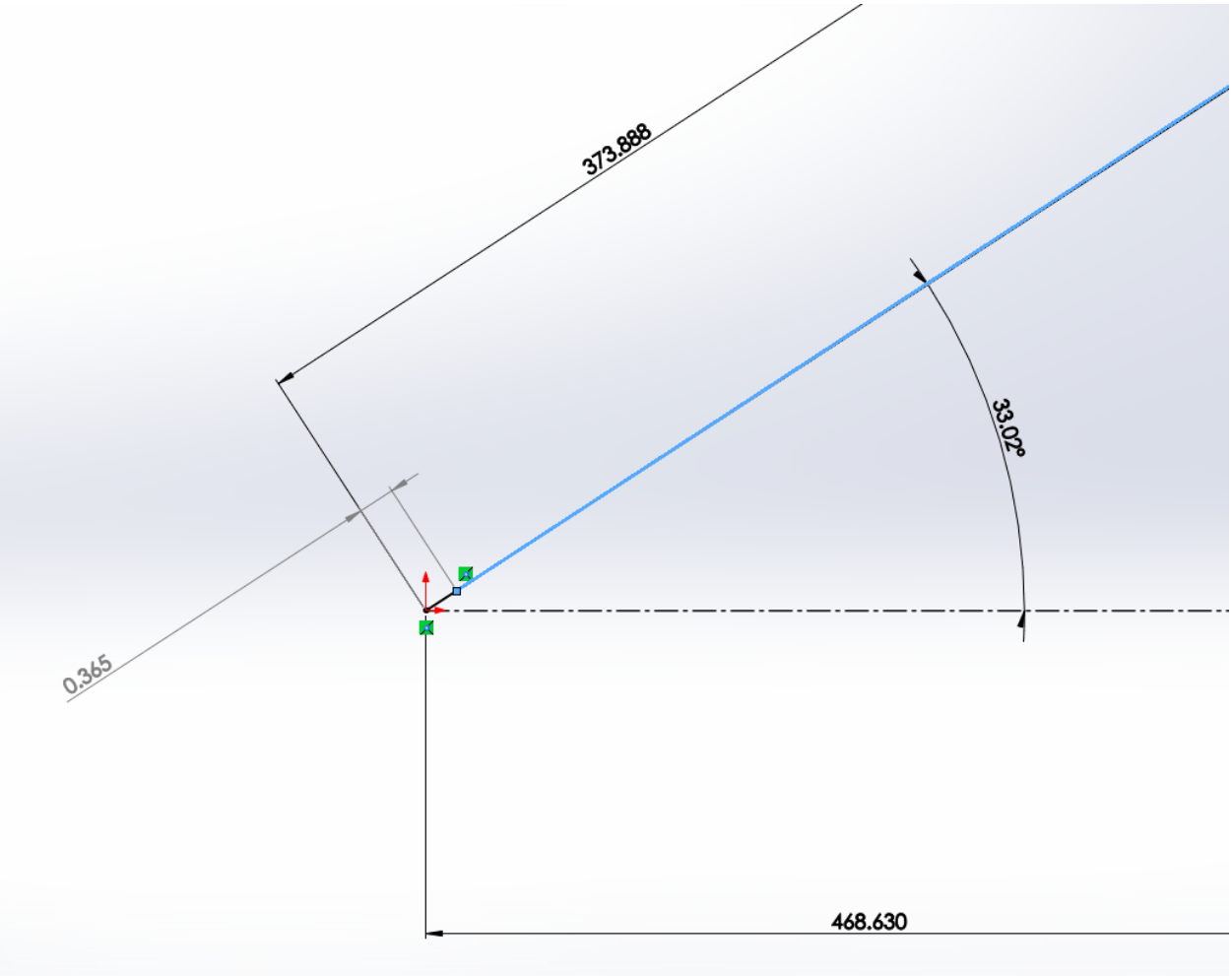

Figure 37: Close Up of Front Rocker-Pull Rod Pickup Location in the Front Plane (Full Bump)

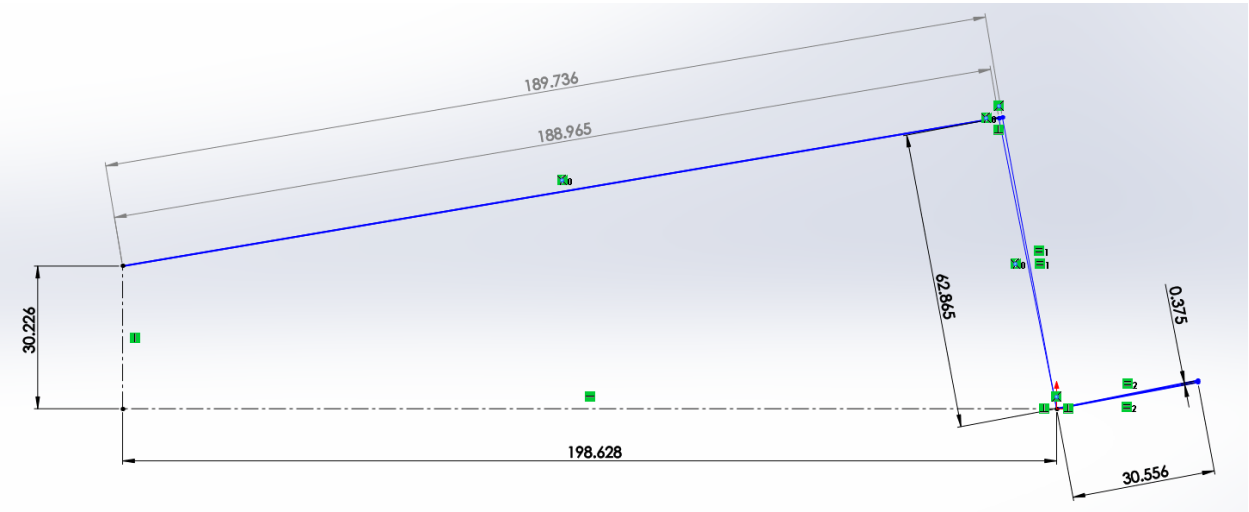

Figure 38: Front Suspension Rocker Geometry

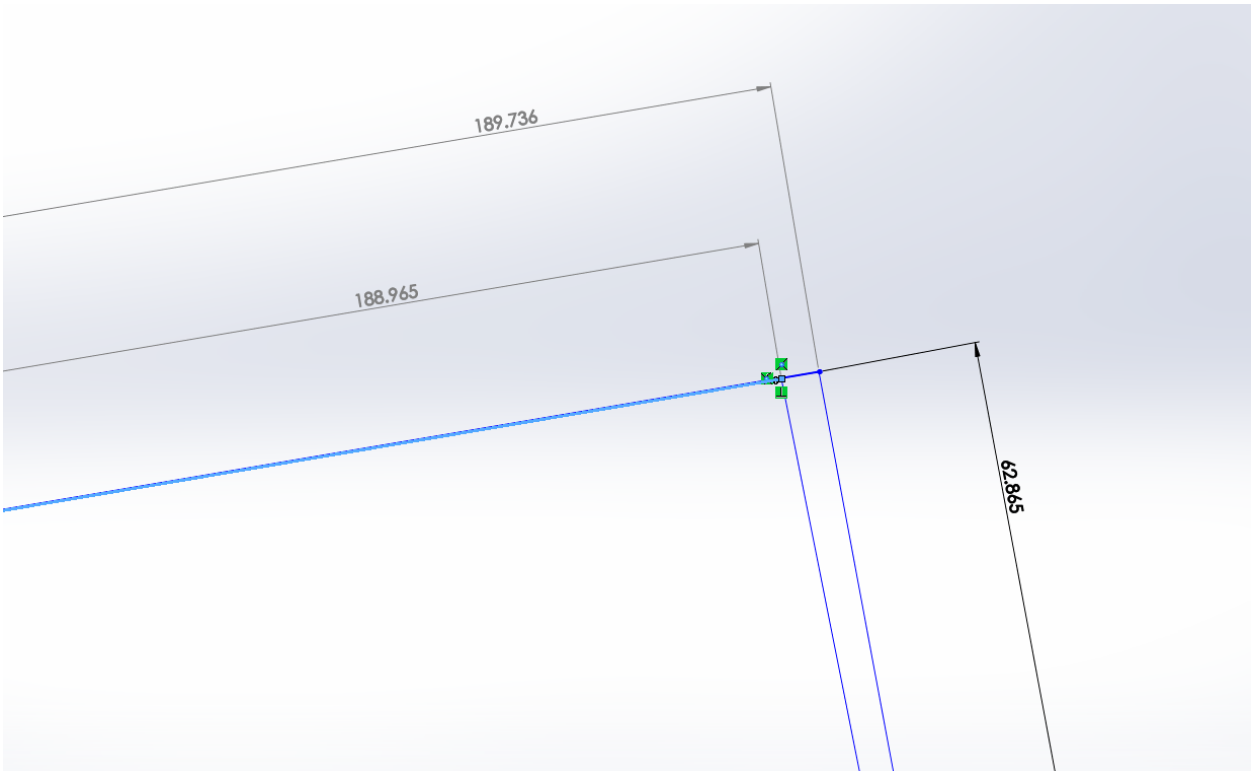

Figure 39: Close Up of Front Rocker-Shock Pickup Location in the Rocker Plane (Full Bump)

Initial shock geometry

After the tab and A-Arm geometry was inserted into the model following the creation of layout sketches, the shock and rocker geometry could be determined. In order to simplify the geometric setup, the entire system was modeled at the neutral position and then alternate positions were created at the system extremes. With the A-Arm geometry and frame geometry fully defined, the extreme positions were set to 1.25" of rebound and 1.25" of jounce. From here, the rocker plane was set to be aligned with the pullrod and shock at neutral travel. The shock tabs were set to achieve as close to a 90 degree transmission angle as possible at full rebound. Finally, the rocker arm lengths were set equal to the similar arm lengths in the other permutations of the suspension travel in order for the system to be fully defined. This method of solving the rocker geometry means that the rocker can be easily fully defined based upon the travel and packaging and the geometry or requirements can be changed and the model will automatically update.

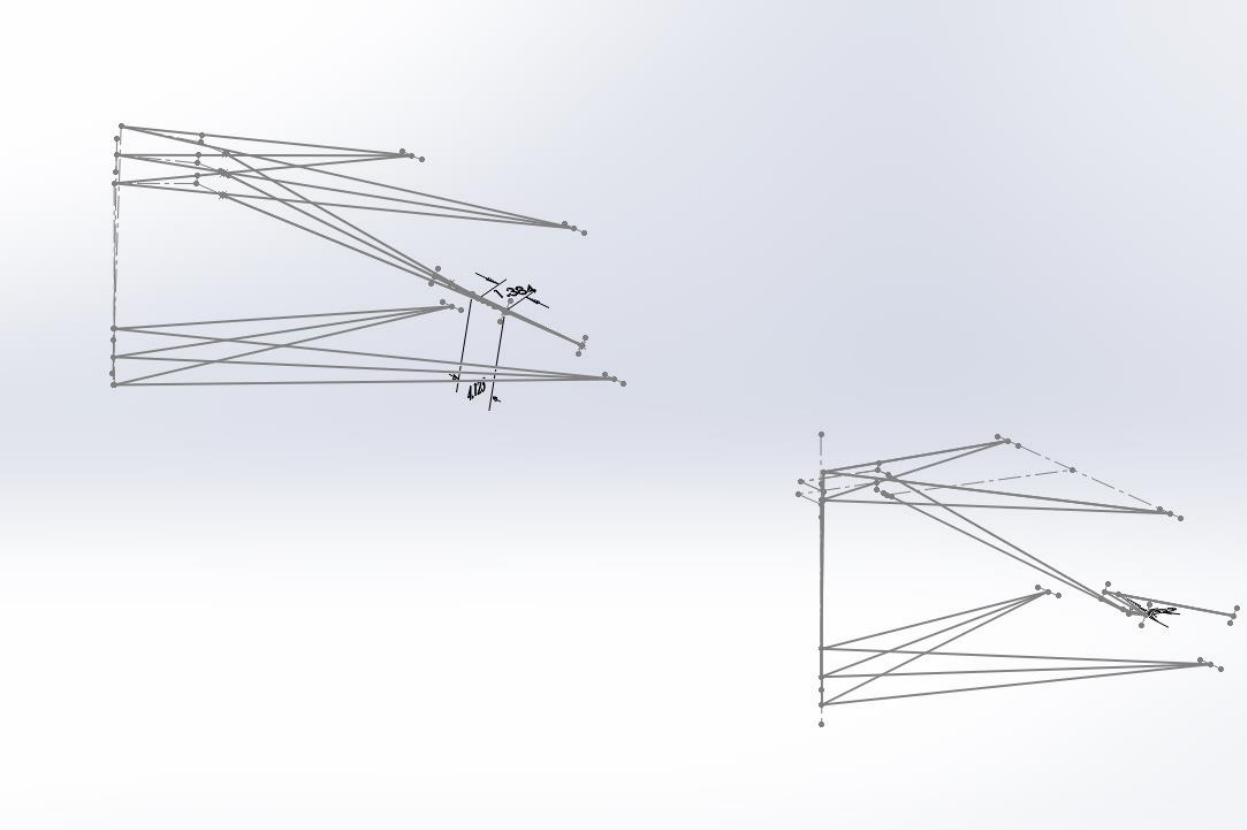

Figure 40: 3D Solidworks layout sketch of suspension geometry

From the initial geometry of the 3-D SolidWorks sketch, the basic SolidWorks were created in order to begin the solid modeling process. This can be seen in figure 40.

Revision 1

After the basic geometry was defined for the rocker arm lengths, the shape and size could be designed based upon the desired design intent. Several factors drove the design, including safety, manufacturability, and low mass. In order to achieve low mass while being strong and easily manufacturable, 6061-T6 was chosen. A factor of safety of at least 2 was set, while a higher FOS would be preferable if the part was adequately lightweighted. The part needed to not collide with the shocks in all location and needed to allow travel of the pullrods and shocks throughout the travel. The rockers were then lightweighted using the technique of offsetting the perimeter and holes and making an extruded cut partially through the part. Ribs were added, every corner was given a fillet with the radius of 0.3" since a 0.25" endmill would be used and full engagement would greatly lower surface finish quality. The remaining pockets were extruded through the part. Sharp corners were avoided at all costs since they would create a stress concentration, causing premature failure of the part.

A worst case scenario analysis was conducted on the front and rear rockers, with a load of 500lbs loaded at the pullrod node with an angle of 45 degrees from vertical and a side load angle of 5 degrees. A factor of safety of 2.8 (figure 42) was achieved for the front rockers, with the rear rockers resulting in a factor of

safety of 3.2 as seen in figure 44. In both the front and rear rocker analyses, the stress was concentrated in the diagonal compression members as seen in figures 41 and 43. Both analyses resulted in a safe design that was lightweight and ready for manufacture.

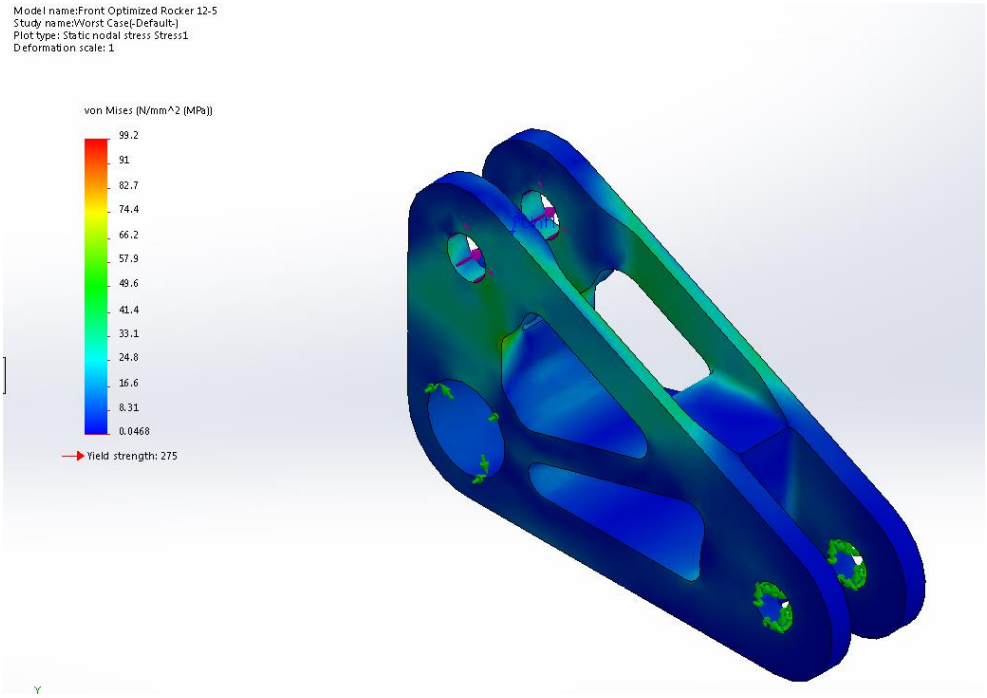

Figure 41: Revision 1 Front Rocker Stress Analysis

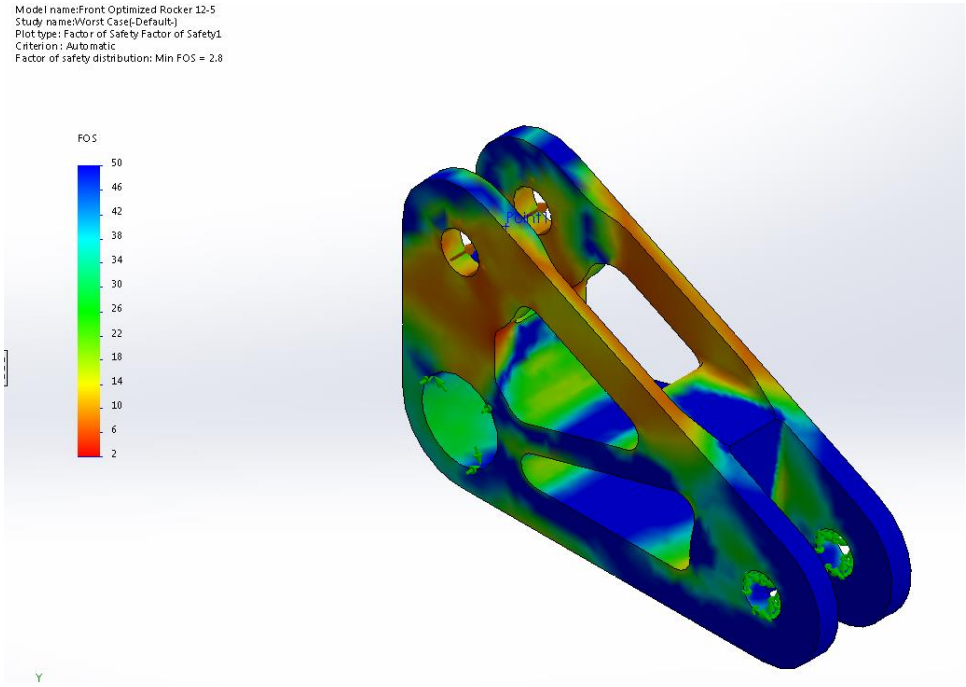

Figure 42: Revision 1 Front Rocker Factor of Safety Analysis

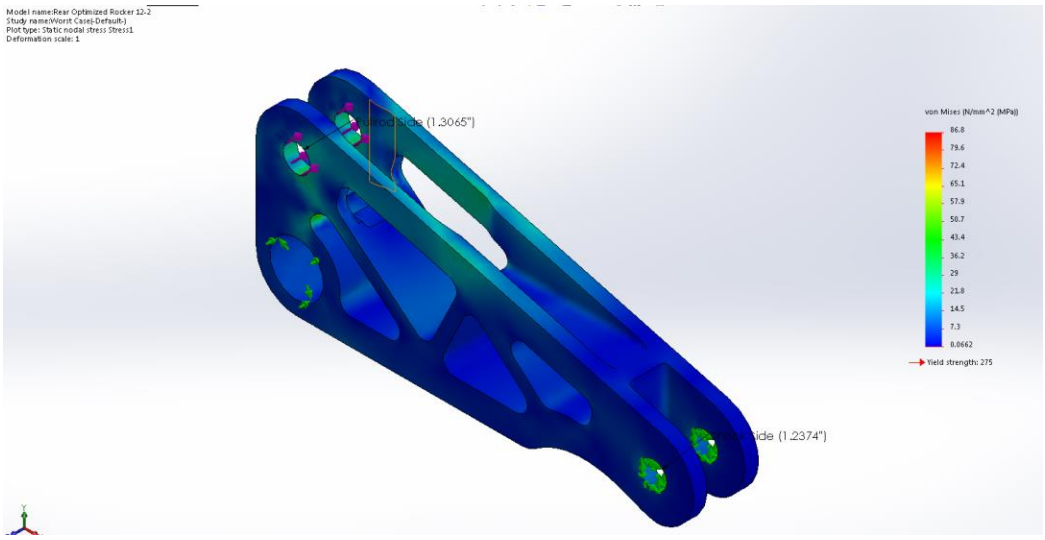

Figure 43: Revision 1 Rear Rocker Stress Analysis

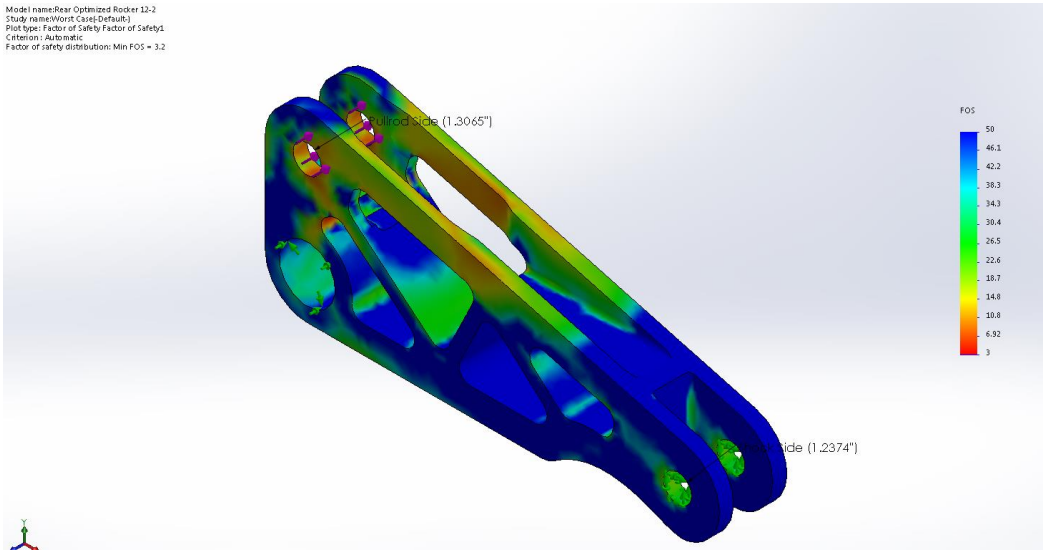

Figure 44: Revision 1 Rear Rocker Factor of Safety Analysis

The front and rear rockers were then organized into an assembly to save material during the machining process. The spacing between the parts was set to 0.45" to allow for a 0.375" endmill to not have to complete a slotting operation. A sacrificial plate was created to allow the rocker stock to be bolted to. The large billet for the rockers was initially squared and drilled to the proper hole spacing for the pullrod and shock nodes. The billet was then bolted to the sacrificial plate and a profit milling operation was used to remove material around the rockers and inside the lightweighting pockets. Finishing operations were completed on each part to create the slots for which the pullrods and shocks fit into

After machining, the rockers were found to fit well with the brass bushings, while the fitment with the brass washers was unacceptably tight as rotation was restricted. The top brass washer was deemed ineffective, since only the lower washer was necessary to prevent the rocker from wearing against the steel tab. Upon full assembly, there was a clearance problem with the shocks, and additional machining

needed to be completed. Even with the additional machining, the system still locked up since the slots that were made for clearance for the pullrod were not wide enough to allow for the extremes of suspension travel. This issue was amplified by the design change that occurred in the pullrod design, since originally the pullrods were to have a tapped tube which was modified to a welded left or right hand thread nut due to the lack of available properly sized tubing. The welded nuts were wider than the original tubes, causing the collision and limited travel. At this stage the design was revisited since additional machining was not an option due to the part having an unacceptably low FOS following machining, as very thin aluminum walls would be created, and if failure occurred in these parts, a catastrophic crash could occur.

Figure 45: Revision 1 Rocker Initial Manufacturing

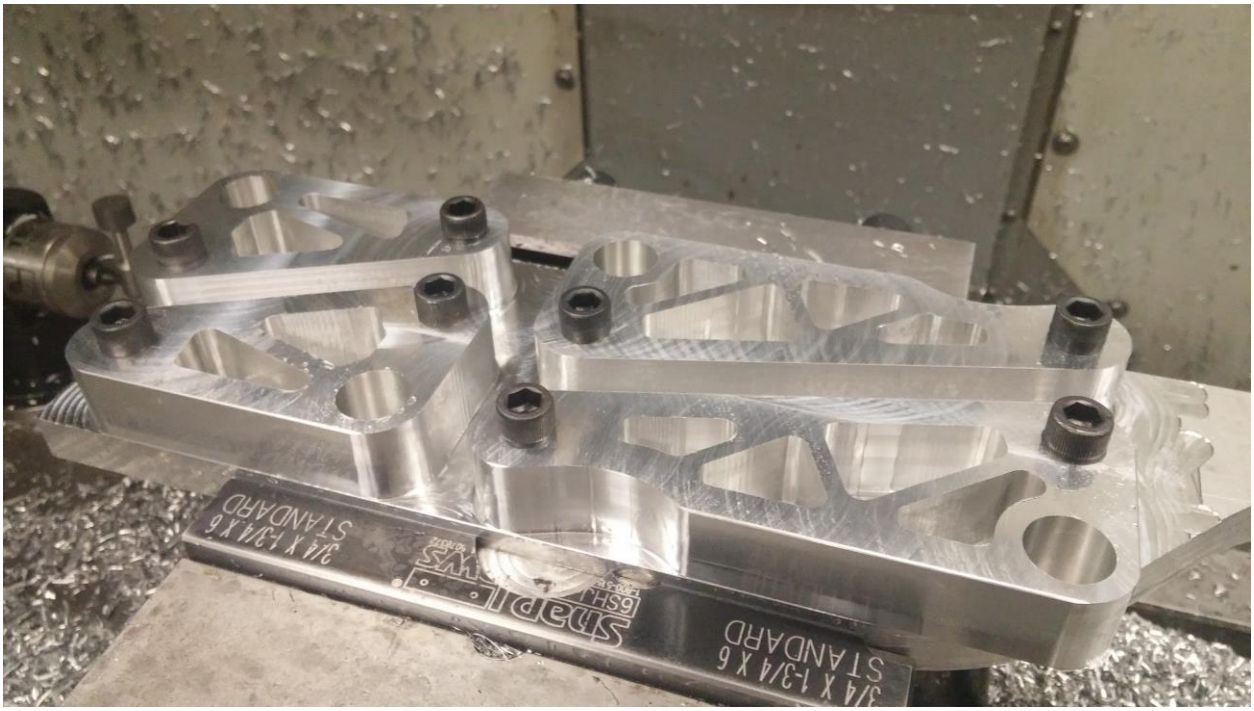

Figure 46: Revision 1 Rocker Manufacturing

Figure 47: Machined Revision 1 Rockers

Revision 2

Following an unsuccessful first revision, a second revision of the rockers needed to be made. Changes that needed to be made were drastically increasing clearances around the pullrods and shocks to allow for tolerances in welding and the extremes of suspension position. To allow for potential future changes, the wall thickness on the width of the parts was increased, which in turn increases FOS in the designed state. The material was also changed from 6061-T6 to 7075-T6 due to nearly double yield strength. This material was not originally used due to the high material cost, but material was donated to eliminate the cost for each rocker. Fillets and chamfers were also added to the external profile, along with external lightweighting. 2-D contouring operations and several 3D mold Z-level finishing operations were needed to machine the new features.

Following design changes, a worst case scenario loading was considered and analyzed using finite element analysis. By strengthening the highest loaded members and upgrading the material to 7075-T6, the factor of safety of the front rockers increased to 7.1, with the rear rockers increasing to 6.1. The stress and factor of safety plots can be seen in figures 48 and 49.

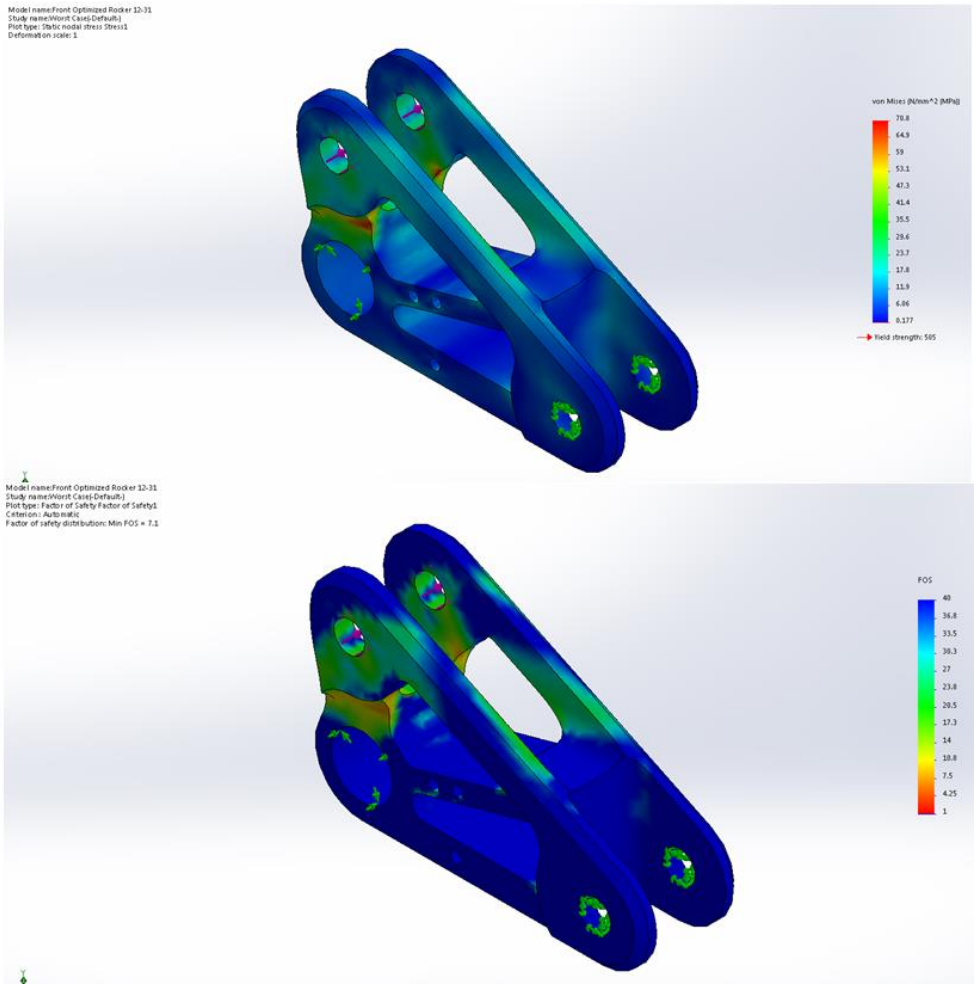

Figure 48: Revision 2 Front Rocker Stress and Factor of Safety Analysis

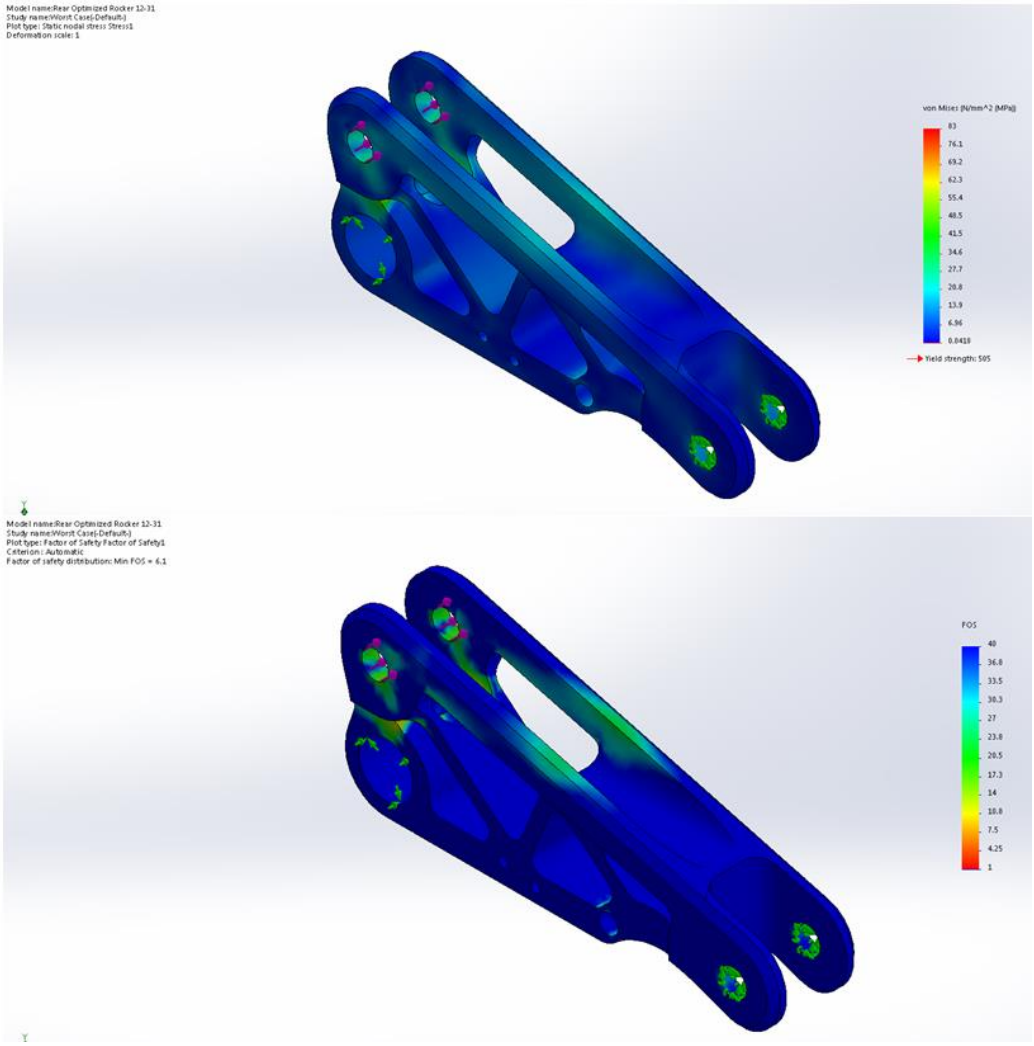

Figure 49: Revision 2 Rear Rocker Stress and Factor of Safety Analysis

The machining operations were similar to the initial rockers (squaring the billet, drilling, internal and external profit milling type pocketing), except a finish pass was added to all surfaces to improve the surface finish of the parts.

Following machining of the rockers, several bushings needed to be machined to remove translating of the shocks and pullrod ends. During the assembly phase, all components were found to fit properly following minor finish sanding and filing. The system was then tested without springs using just the shock absorber, rockers, pullrods, and upper A-Arm. All parts moved through the range of motion without issue. Once the wheel assemblies were installed, the springs were installed and the system was run through the range of motion. As in the prior test, there was adequate range of motion with no collisions and all systems performed as predicted.

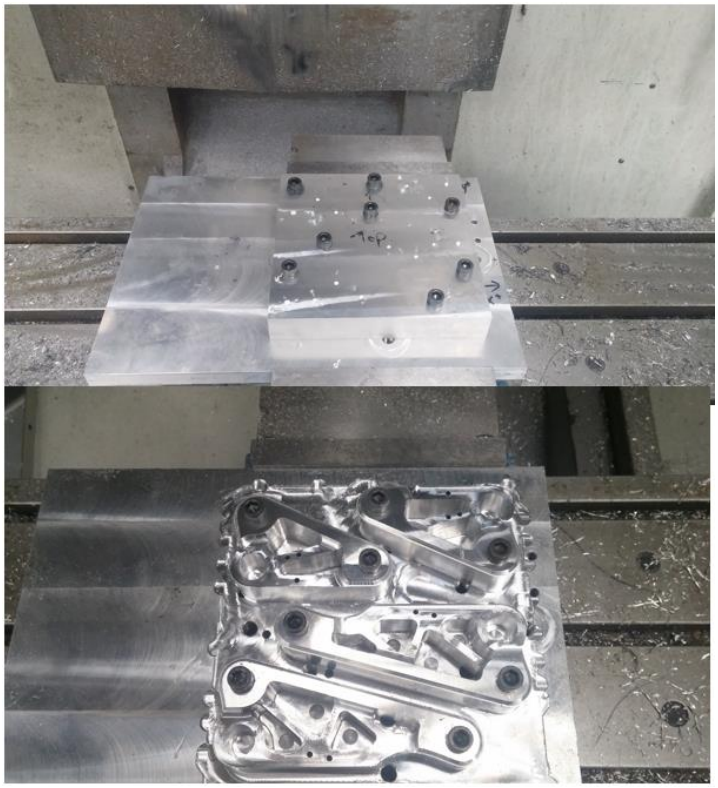

Figure 50: Revision 2 Rocker Manufacturing

Figure 51: Upper: Manufactured Revision 2 Rockers; Lower: Revision 1 & 2 Rocker Comparison

Upright Design

Kinematic Design and Structure

The initial conditions of the suspension system were the driving factors of the kinematic design on the upright. The design needed to be strong yet lightweight, allow 1.25" of jounce and rebound and full range of motion of the steering rack, and not allow any of the systems to bind or collide in any suspension position and steering position.

Initially, the upright height was defined by the wheels and A-Arm angles at ride height. The king-pin inclination was determined, although the stock camber would be too extreme at this resultant camber. The set KPI was -4 degrees, and the desired camber was -2 degrees. To achieve this, +2 degrees of camber was integrated into the upright.

The wheel bearings were the next driving factor in the upright design. The upright had to capture the wheel bearing and be strong enough to not yield under worst case loadings. The wheel bearings that were selected were BMW E46 OEM wheel bearings and a 0.002" press fit was set. To avoid large axial loads during the press fit process, the uprights were evenly heating around the bearing surface using a propane blowtorch to slightly expand the bearing hole. A slot was machined into the upright to hold a large internal snapring. The other face of the bearing was captured by a shoulder machined into the upright.

The uprights also needed to integrate the specified brake components. In the front, Wilwood Dynalite calipers were used, with Wilwood PS-1 calipers specified for the rear. The front calipers were significantly larger due to the much larger brake forces, and introduced packaging issues. Since the hub design defined the rotor location on the rotational axis of the hub, the caliper was therefore defined in that direction as well. The caliper then needed to be located radially, and vertically. Using the rotor model, each caliper was located a specified radius from the rotation center to allow maximum braking torque while not allowing any interference. A clearance of at least 0.1" was specified by the design team to account for manufacturing tolerances and heat expansion. Once the radial locations were determined, the vertical location was determined based upon the lowest CG location with the best packaging options. The packaging options were weighted higher than CG location due to the very limited locations for mounting, and the ease of mounting and service if they were in the upper section of the wheel. After a location was determined, the calipers were checked for collision and clearance from all other components of the system, such as the wheel, rotor, and hub. A minimum clearance was set to 0.1" to account for unknown wheel casting tolerances and machining tolerances.

As explained in the steering section, the maximum steering angle was set to 33 degrees for the inside wheel, with 26 degrees for the outside wheel at full lock of the steering rack. The moment arm length and location are also explained in the steering section of this paper. In the rear, toe bars were added to fix the rotation of the uprights.

Sensor integration was the final design parameter of the uprights. Both the wheel speed sensors and the wheel board assembly with brake temperature sensor needed to be integrated. The brake sensor was an

aftermarket part, and was aligned with the deadaxle plates in the front, and the CV adapters in the rear maintaining a distance of 0.15 inches radially from the steel teeth of each part. The brake temperature sensors that are integrated into the wheel boards were mounted on the front facing flat surface of each upright. Two holes were drilled and tapped to allow for a 3D printed case to be mounted and aligned to allow for a correct field of view for the brake temperature sensor.

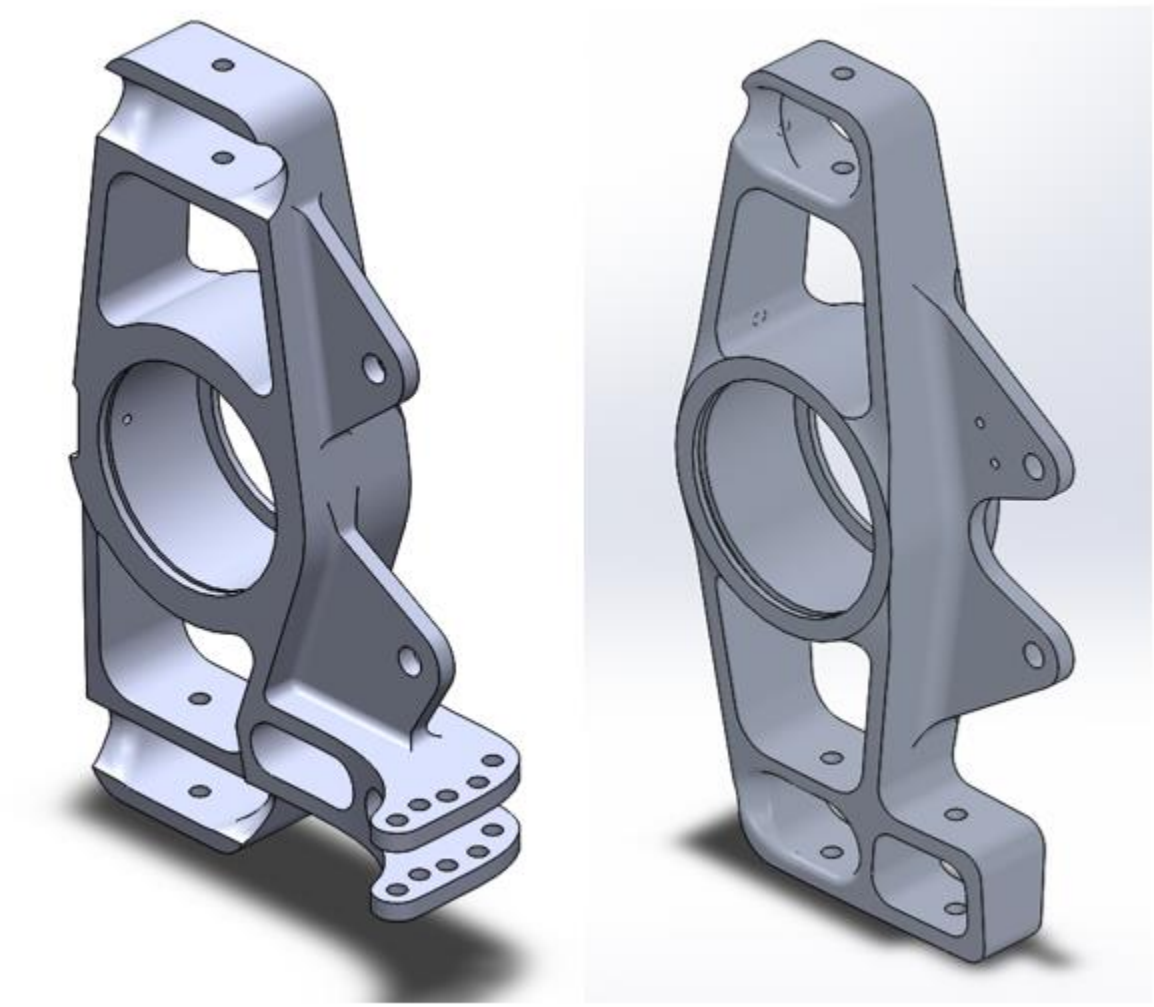

Figure 52: Front and Rear Uprights

Full wheel assembly

Following the initial design phase, the front and rear wheel assemblies were created in SolidWorks to determine proper fit and alignment of all subsequent parts. Cross sections were utilized to ensure proper fitment of all parts. Once these assemblies were consulted by the design team, modifications were made for rotating and nonrotating part clearances. At this stage, it was ensured that the parts could be easily assembled, and wrench clearance was ensured with each specific fastener type being modeled and inserted. Following this stage, the upright designs were modified to improve manufacturability.

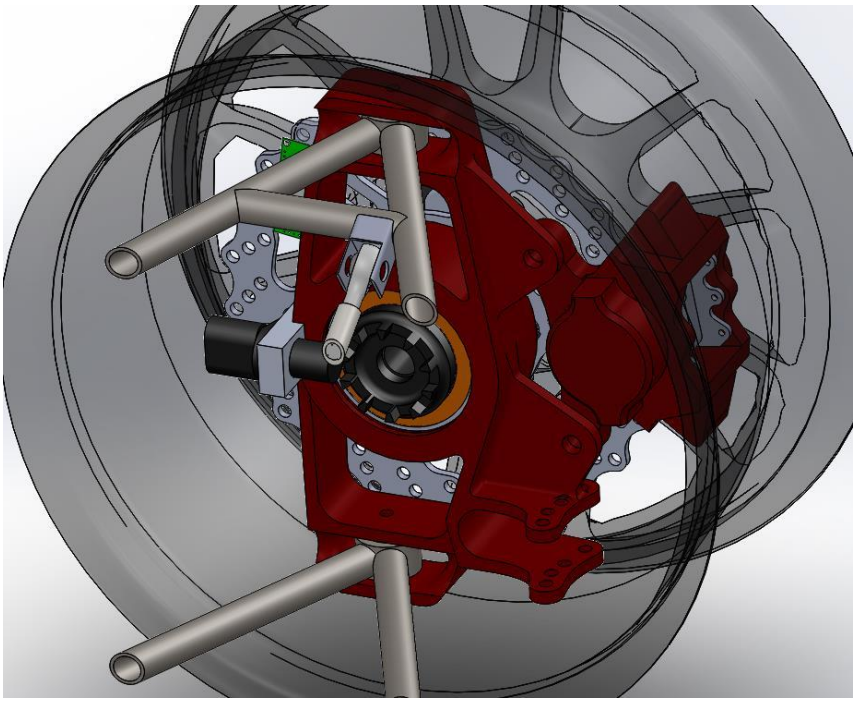

Figure 53: Initial Front Wheel Assembly

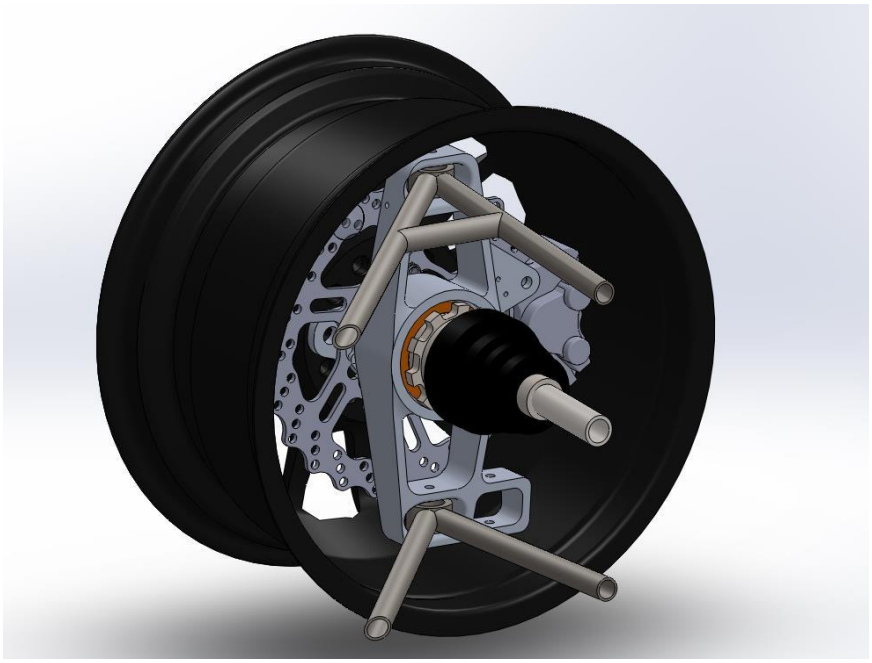

Figure 54: Initial Rear Wheel Assembly

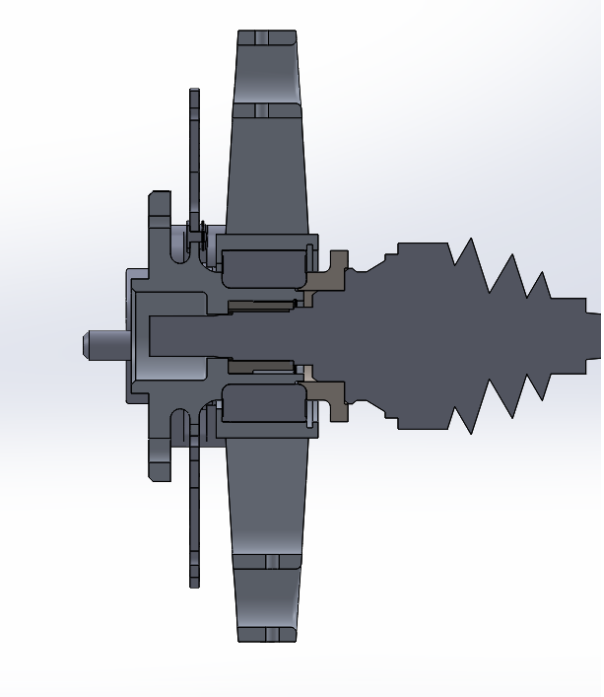

Figure 55: Rear Wheel Assembly Cross Section

FEA and material

Before taking the parts through the initial stress and deflection calculations, a material needed to be considered. Only aluminum alloys were considered due to the low weight, ease of manufacturability, and low cost. Following research, 7075-T6 aluminum, a very strong aircraft grade aluminum was preferred, although the material needed for the billet stock would be greatly out of the project budget. Other alloys were researched, and 6061-T6 proved to be just as light, while retaining an acceptable strength, with a significantly lower cost. This material was selected for manufacturing. Peterson Steel in Worcester, MA generously donated all billet stock for the front and rear uprights, along with the front and rear hubs.

In order to set up the stress analysis for the uprights, the worst case loading situations needed to be determined. A situation was simulated for the front uprights with full lockup of the brake system, which translated into a torque of 350ft-lb applied to the caliper mounting surfaces. A vertical load of about 3g, or 400lbf total was applied to the upper and lower mounts where the upright interfaces with the A-Arm spherical joints. A fixture was set to the bearing surface of the upright. The front uprights also experienced a load of 200lbf total to the tie rod pickup point at neutral steer.

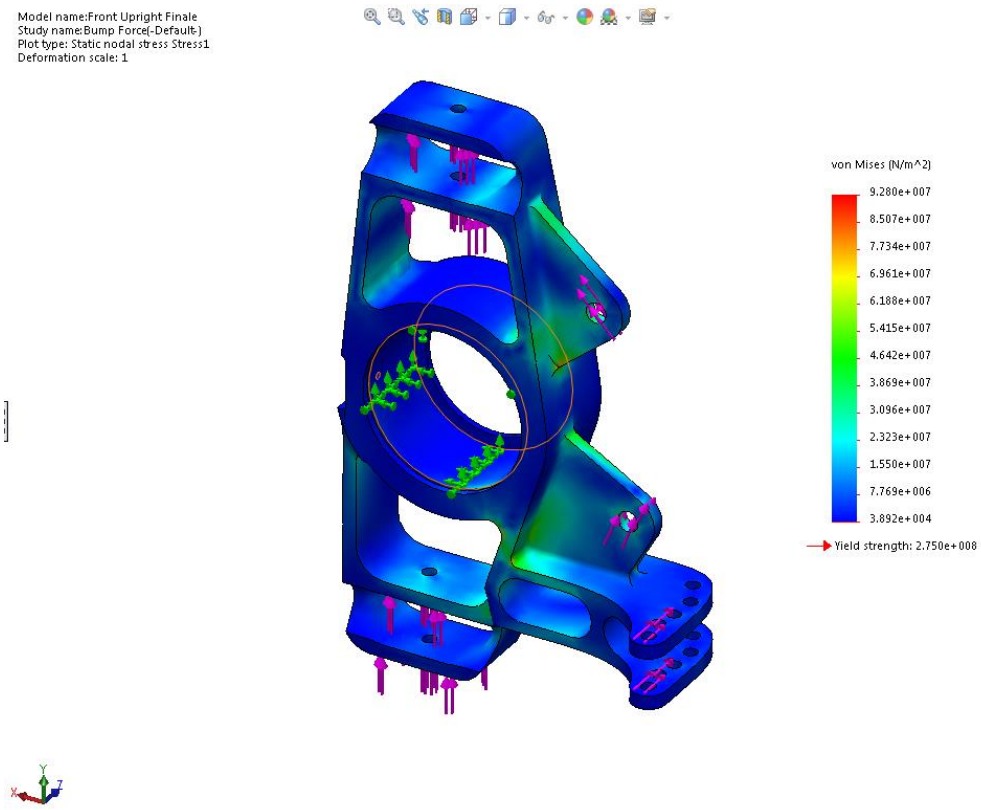

Figure 56: Front Upright Stress Analysis

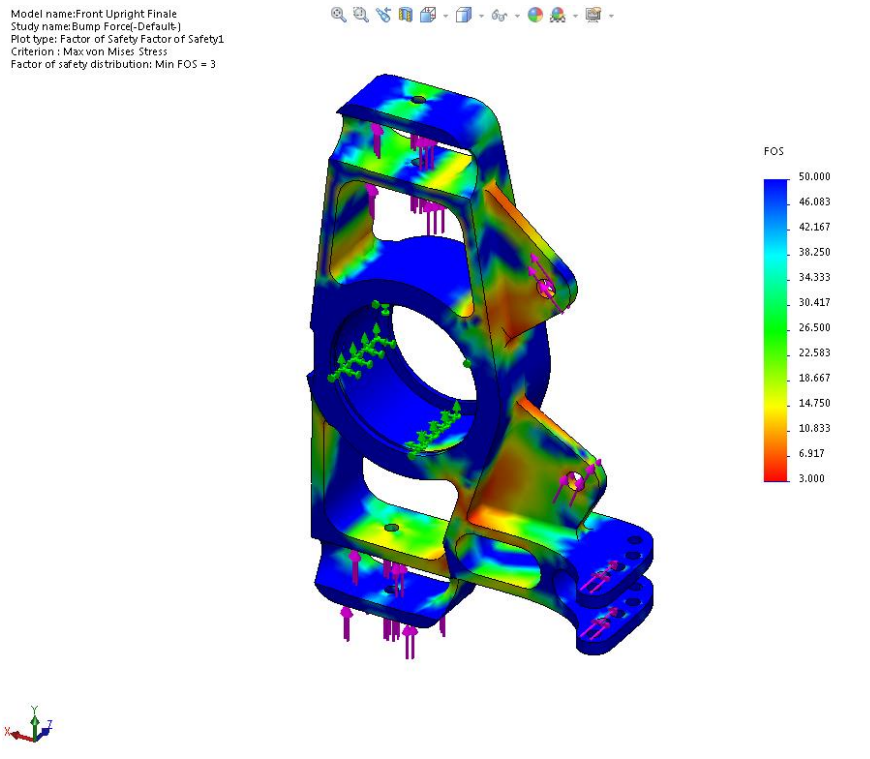

Figure 57: Front Upright Factor of Safety

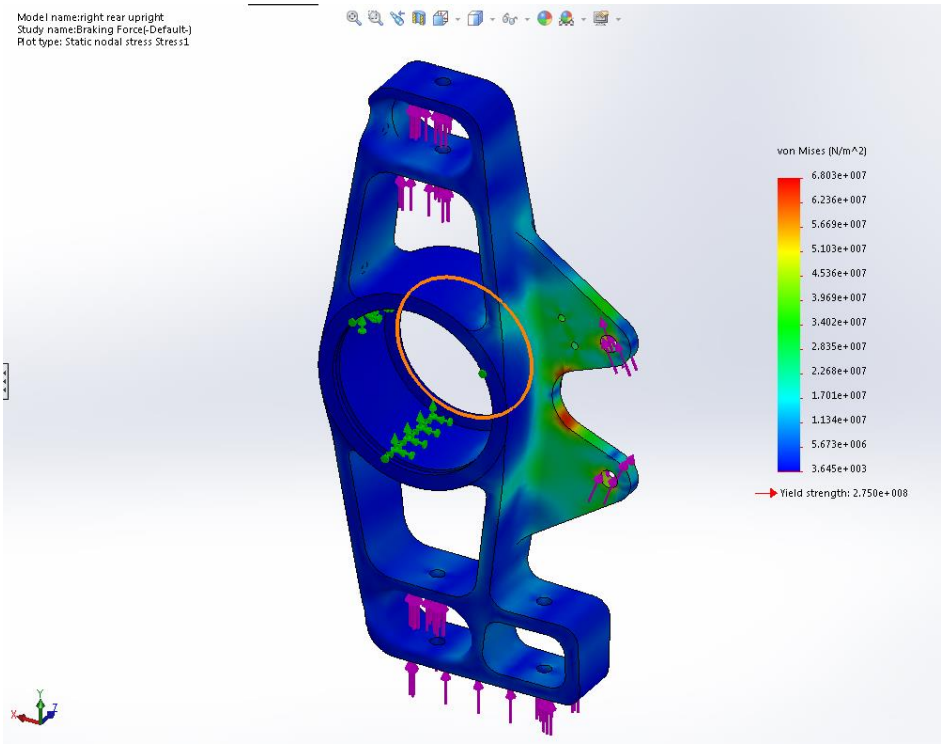

Figure 58: Rear Upright Stress Analysis

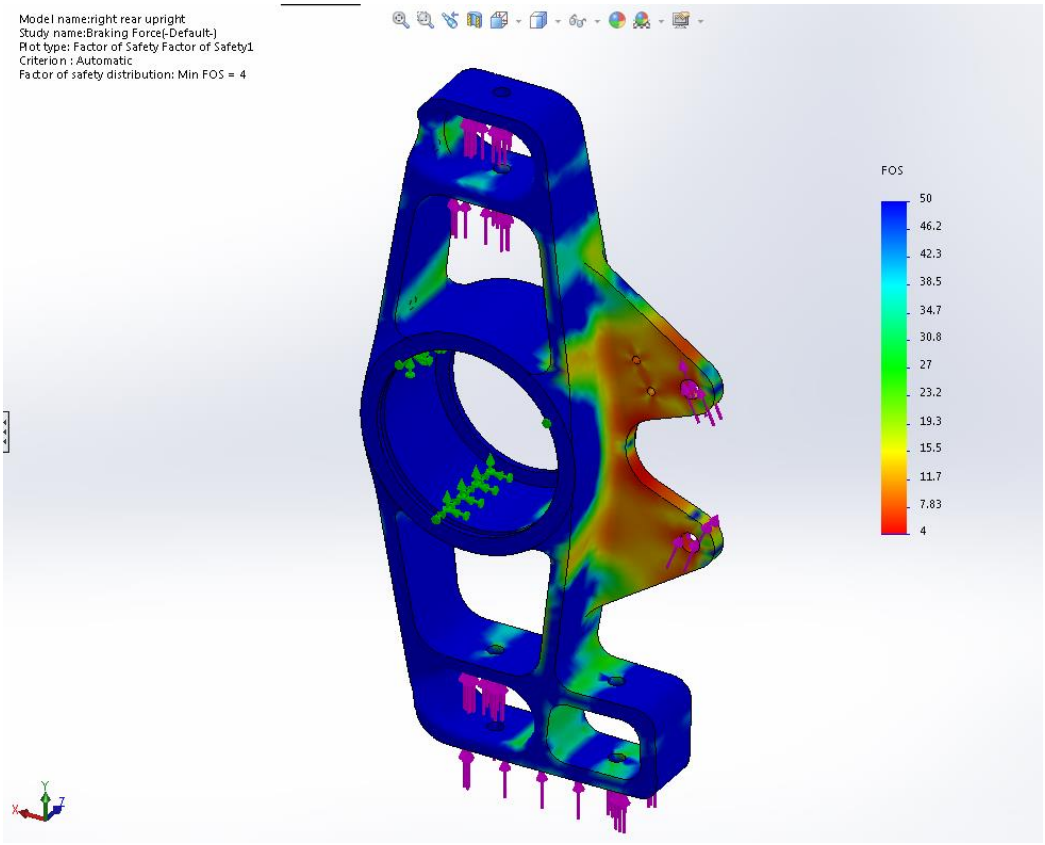

Figure 59: Rear Upright Factor of Safety

Following both finite element analyses, the models were examined for failure points and stress concentrations. Due to large fillets being used on all load bearing components, the stress was not causing any localized stress concentration, and the minimum factor of safety was found to be 3 for the front uprights with the rear uprights having a factor of safety of 4. An ideal factor of safety of 3-5 was determined prior to the design phase, so further lightweighting was not necessary as it would yield little return, therefore the models were cleared for manufacture.

Rear Upright Manufacturing

Figure 60: Right Rear Upright

The first upright that was done was the right back rear, which served as a test in a sense for seeing how much the tools could be pushed and different ways to possibly fixture the part. Originally the plan was to strap the upright stock to the table, which was 12x8x3 ft block of aluminum. This would have been very tedious and troublesome as it would require retract settings not to be optimized to make sure machine straps did not get hit and possibly multiple re-fixturings. Instead a vice that had just over 8 feet of travel was used. Some of the other issues with fixturing however were that the part had very little flat surfaces due to the desire to save weight. Due to this, soft jaws had to be made for one side of the upright in order to fixture it as seen below.

Figure 61: Softjaws for Rear Uprights

The problem with these particular soft jaws were that the jaws themselves were not made to the actual shape of the bottom surface. To ensure the part came out right the team carefully trammed in the top surface of the part. The part required 4 operations, 2 in order to machine the features and 2 to machine the holes on the sides. Another problem with the design itself of this upright were that internal corner radii on the part itself caused too much of the tool to be engaged at once causing it to break.

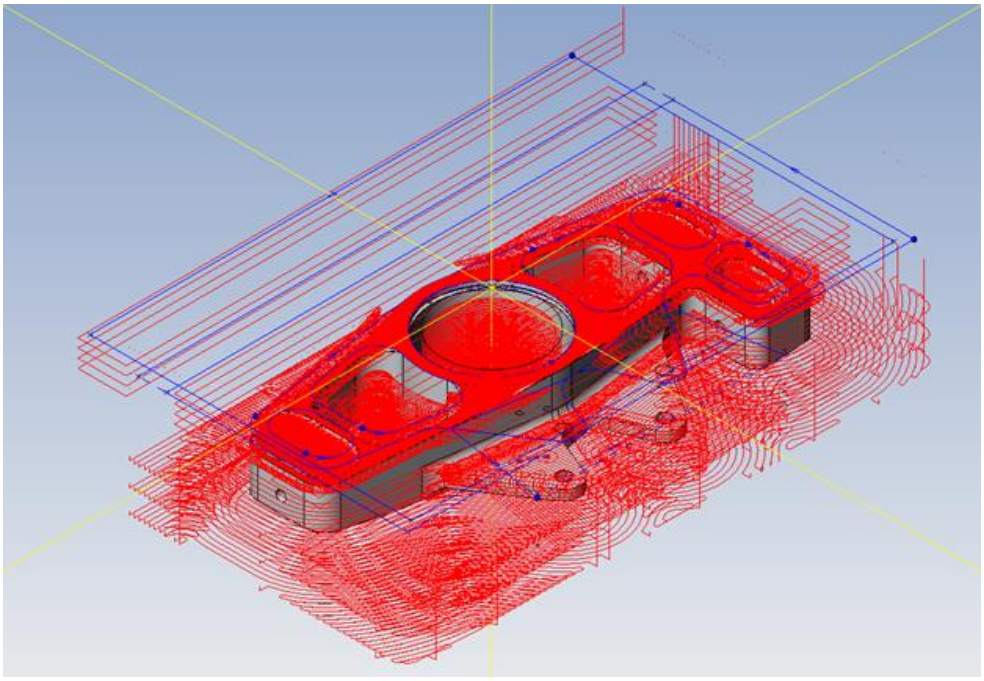

Figure 62: 3rd operation of Left Rear Upright

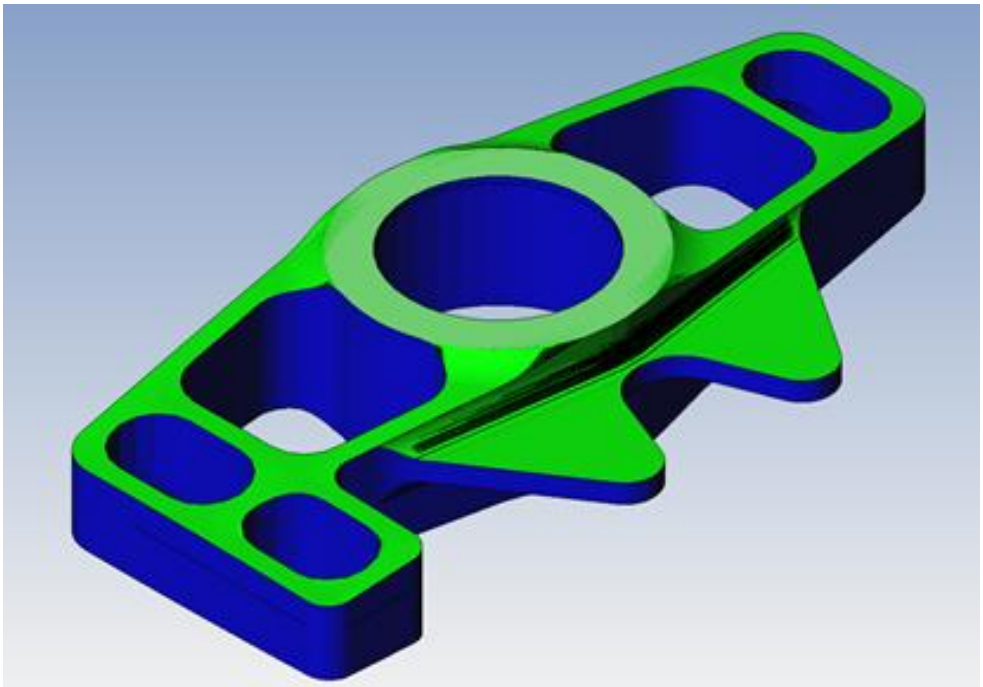

Figure 63: Completed simulation of rear upright

For the left rear upright the same softjaws were used again simply flipped around, and mirrored operations from the first. This time however the retract optimization in the mold roughing operation was adjusted to remain within the operation as opposed retracting to the full clearance of an inch above the part. The simulation ran fine on both the CAM and the controller however when the program was run, it made a feed move, or what looked to be a feed move, that took a decent bit of the material out of the part. The reason this happened is unknown as the NC code itself was even reviewed and no apparent issues appeared there. One theory is that parameters might have not been as specific as needed for simulating accurately or perhaps dogleg rapid was not on. What dogleg rapid does is it simulates the actual rapid move the machine will make. Aside from minor tweaks in depths of cut and step overs to try to speed the process due to the part having a total run time of over 2 hours not much was changed in this upright.

For both these uprights there was a considerable amount of deflection from the extended reduced shank ½ EM that was used. Due to this finish passes were used where dimensions were critical in order to ensure the correct dimension. Even with this however the large bore was not at the correct dimension needed for the bearings so additional passes were run with cutter compensation on to get the optimal size to press the bearings in. To speed up the process a shorter ½ EM was used that had longer flutes (1.5in) in order to have a larger depth of cut and step over wherever the machining time could be decreased. This tool could use the full flute length for the depth of cut while having a 25% step over and feeds increased by 15% roughly from the catalog suggestion.

Front Upright Manufacturing

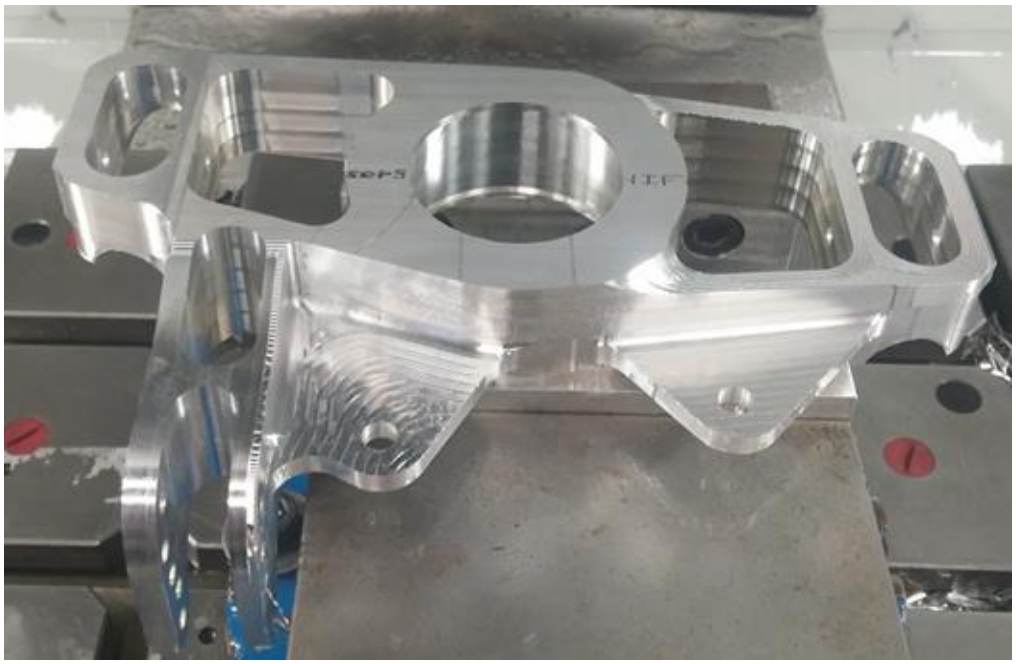

Figure 64: Front Left Upright

The front uprights were unique in design to the previous uprights which caused for some slight complications. The stock height itself was now equal to the block height making the orientation in the CAM slightly difficult to get as it had to be adjusted to visually it appeared in the right spot within a

roughly .001 which was roughly the tolerance of most features. Due to the extra features the run times would be quite large. A feed mill was used on this part in order to attempt to speed the process up as well as attempt to do the depth with less deflection as the tool had a larger diameter than the ½ extended endmill that was previously used. Issues occurred however where the machine was being data starved. The machine itself can only read so many lines at a certain rate which in this case were more than the machine could handle so it caused the tool to pause every constantly instead of feeding the 200 fpm that it was programed too. It also gave a very poor finish in certain areas even after the finish pass was done.

For the left rear upright, the ½ extended endmill was used however during the facing operation with a 3 in facemill it ended up crashing causing it to take extra material off. This was due to dogleg rapid not being on for the simulation in esprit so it did not show the accurate rapid motion. Since retract optimization was left to "within operation" it caused the tool to not move up enough before making the rapid move. After this was fixed the machining of the upright went smoothly.

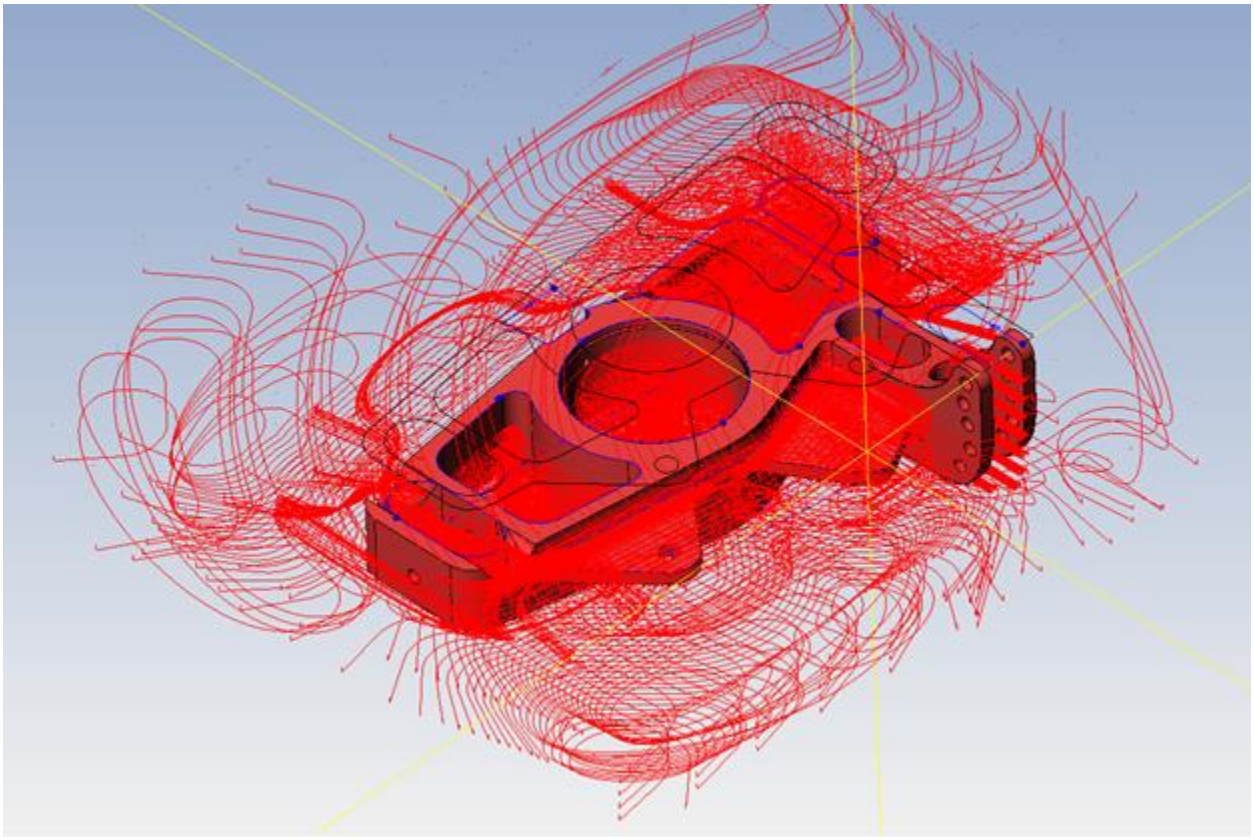

Figure 65: Tool path for Front Upright

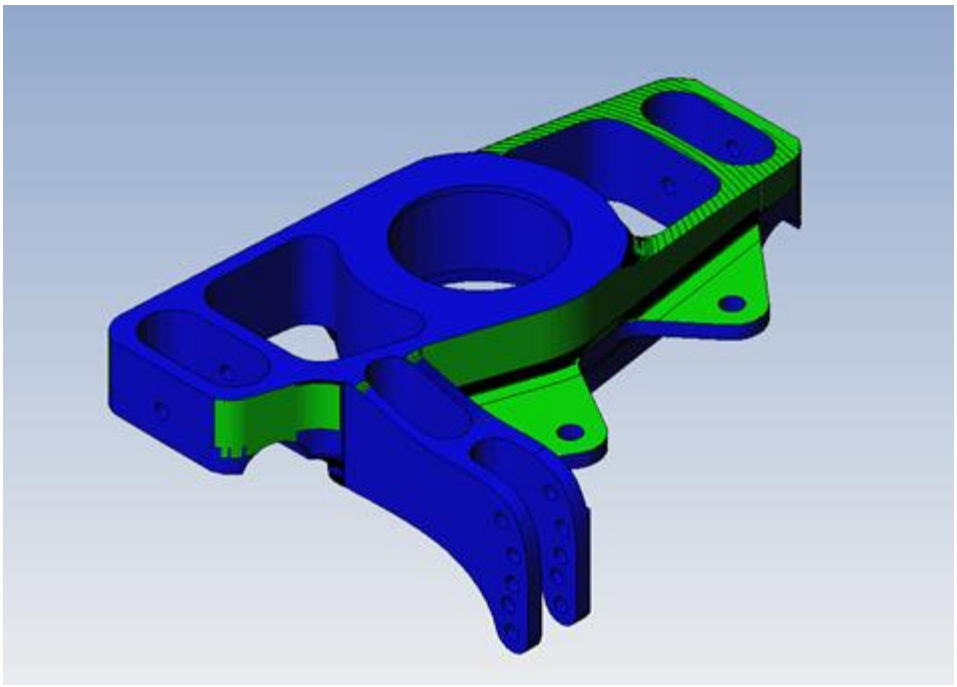

Figure 66: Simulation of Front Upright

Hub Design

General

The design intent behind the front and rear hubs is to safely transfer the torque from the axles to the wheels, slow the vehicle in a 1.5g braking scenario, and not yield under a 3g bump scenario, while remaining lightweight and optimizing packaging. Each hub will contain several important features, including mounting tabs for wheel studs, a mounting ring for the wheel to transmit radial load, a bearing surface to transmit radial and axial load to the wheel bearings, and mounting tabs for the floating rotors. The front hubs will be pressed into the wheel bearings and held into the bearings with a shoulder on the outer side and a deadaxle plate which will hold the hub to the inner race of the bearing with a deadaxle threading into the hub with a locknut used on the outside. The rear hub will be pressed into the wheel bearings and be held in with a shoulder on the outer side and a CV adapter plate on the inside, which will be pressed onto the outer CV joint of the axle. The rear hubs will also need to mate with the drive axles in order to transmit torque to the wheels.

Packaging driven for optimization

The design of the front and rear hubs were based around the wheels and upright design. The length of the hubs was minimized in order to reduce weight and limit the moment on the wheel bearings which can cause excessive wear. Having a small effective spindle length also improves steering input force, which was one of the core design intent areas, since previous SAE vehicles have been noted as very difficult to steer.

The spindle length was minimized in this design by setting a clearance of 0.1" from the caliper to any location on the wheel to account for machining and casting tolerances as noted in the upright section. By defining the axial location of the caliper, the rotor location could therefore be defined relative to the upright. The length of the spindle was then defined by the mounting surface of the wheel, which was offset from the centerline of the wheel by 22mm. As noted in the steering section, the scrub radius was minimized to 11mm by setting a clearance of at least 0.1 inches on the rotating components of the hub (rotors and buttons) along with setting a spacing of 20mm between the rotor centerline to the mounting surface of the wheel studs to allow for proper installation of the wheel studs.

With the basic geometric conditions specified for the hubs, the initial solid geometry was created. Fillets were added to all corners of load bearing areas to reduce the concentration of stress in those areas. A tapped hole was centered on the rotation axis of the front hubs for the deadaxle to mate to, with a spline cut centered on the rotation axis of the rear hubs to mate with the drive axles.

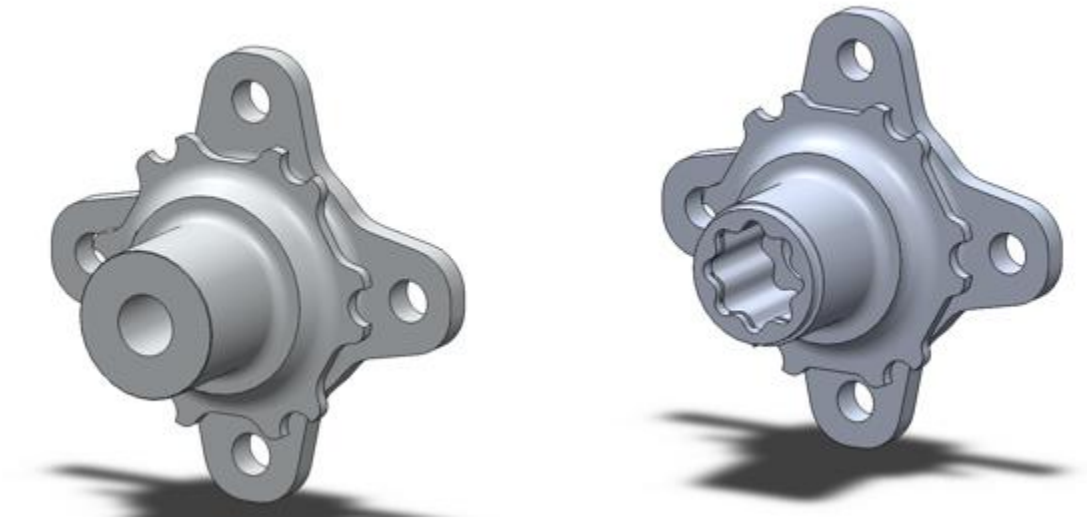

Figure 67: Front and Rear Hubs

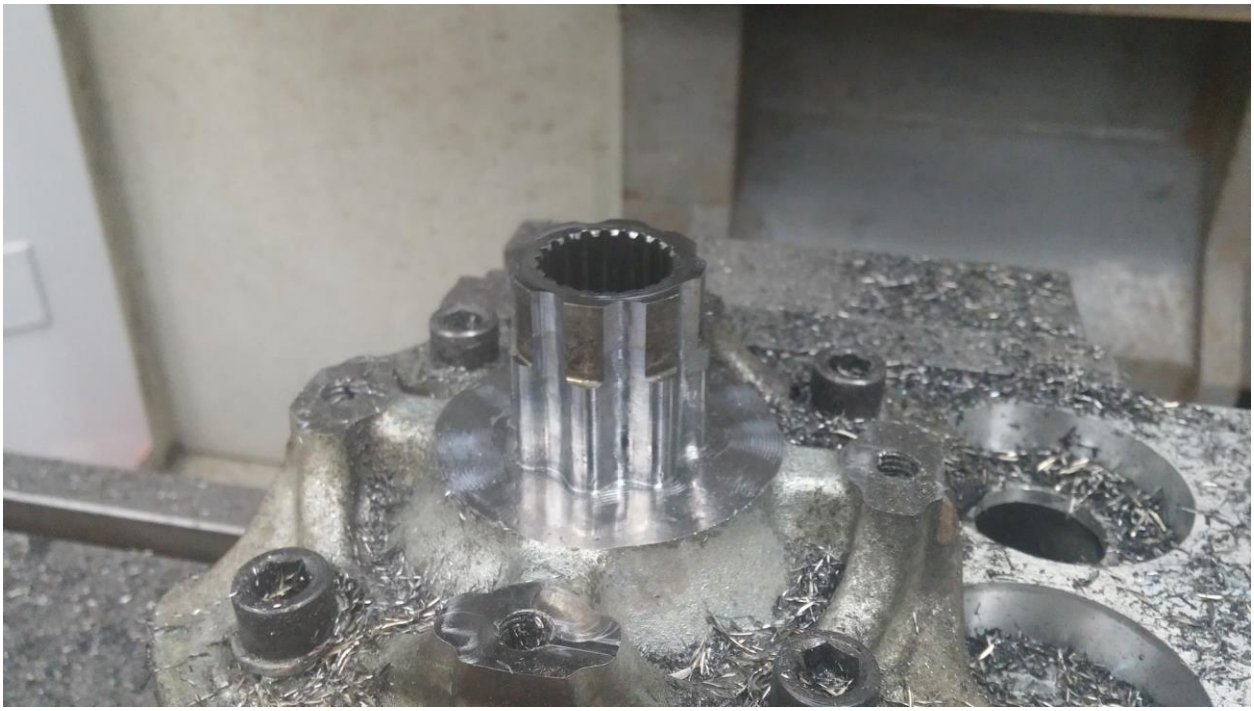

Figure 68: Manufactured Spline Insert for Rear Hub

Design for Manufacture

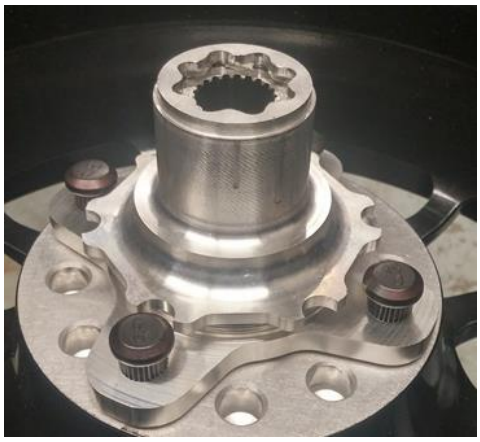

Figure 69: Rear Hub

Originally the hubs were designed with a hex shape in them with sharp corners however this was not manufacturable. The design you see above was then made in order to allow for easy machining as well as effectively drive the axle. Both the front and rear hubs were done using the ST30 (lathe) as well as the VM2 (mill). The operation on the lathe for both the front and rear hubs were the same as they had the same outer shape coming. The jaws of the ST30 had to be machined out to 5 inches diametrically in order to hold the stock. One difficulty with the part was a deep groove that had to be made. In order to do

this the cutoff tool was used for the length and made the filleted shape through a series of groove operations and contour operations while being conservative as to not pull the insert out of the holder. Below is what the parts looked like after the lathe operation as well as the toolpaths used.

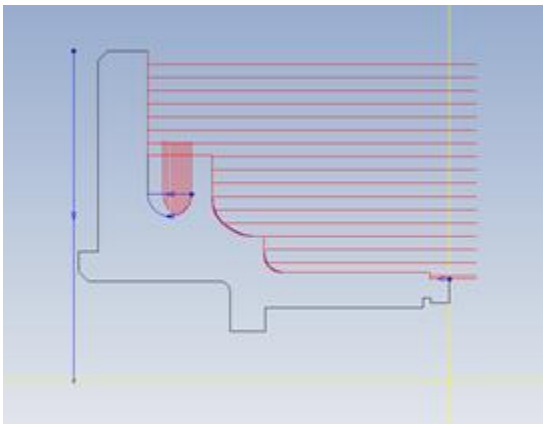

Figure 70: Lathe Tool Path for Hub

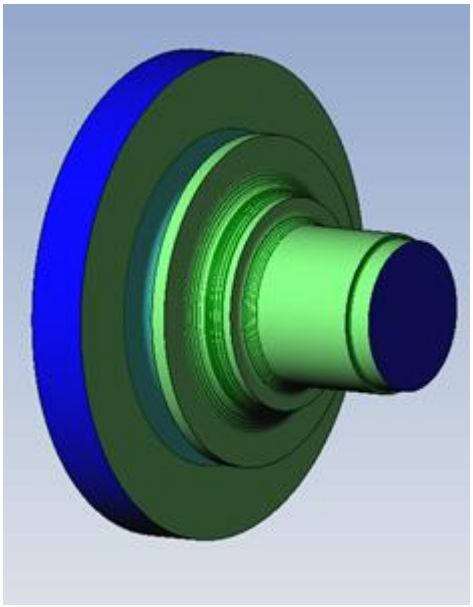

Figure 71: Lathe Operation for Rear and Front Hubs

From there the parts were put in the mill to finish the operations. For this operation a simple V-block was sufficient enough for the clamping force in the vice for the cylindrical side, then for the other side softjaws were made. The only difference between the two uprights was the rear had the star-like shape in it with the snap ring which you see in Figure 5, while the front upright had a simple hole there instead as seen below.

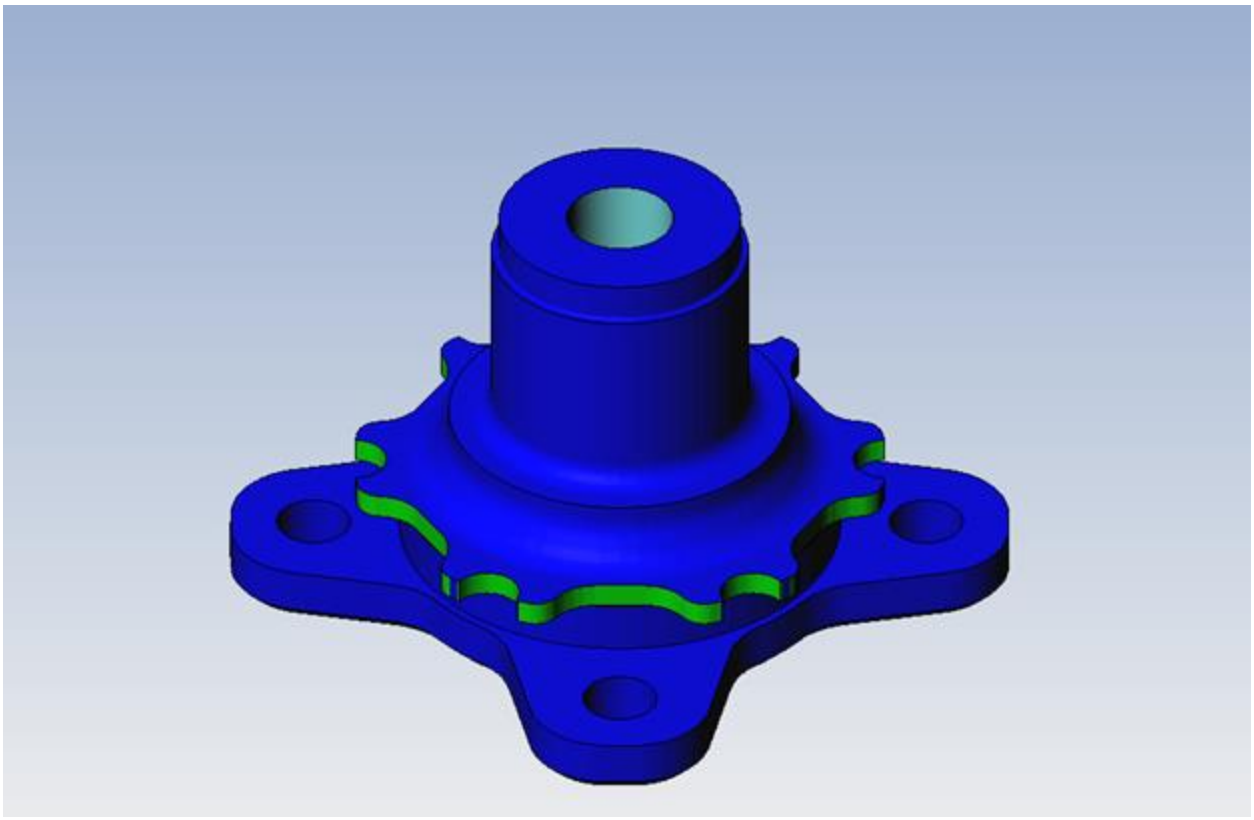

Figure 72: Simulation for front hub

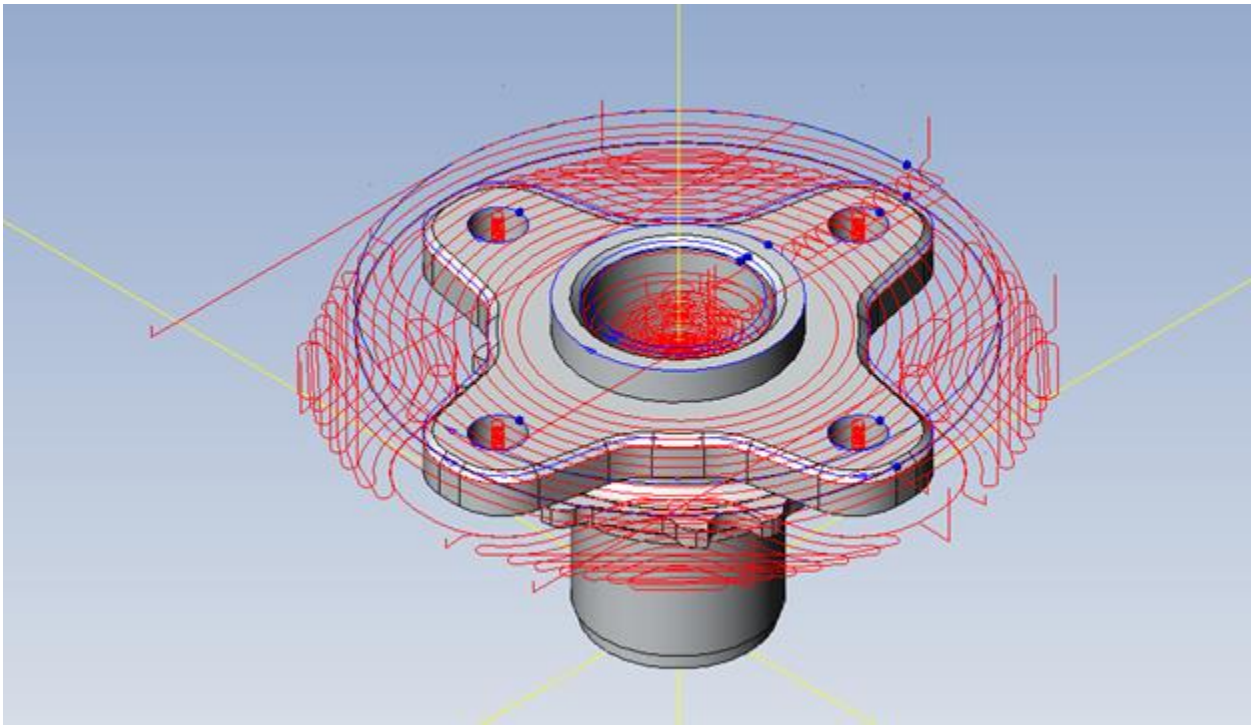

Figure 73: Tool Path for first mill operation

FEA for worst case

To simulate a worst case scenario the following parameters were used:

Actual Force/Scenario	Simulated Forces
Full braking (maximum torque on hubs)	7800 lbf.in on wheel stud holes
3g Bump Scenario	450 lbf on mounting ring aligned vertically
Wheel Bearing	Bearing Support Fixture on bearing surface
Wheel Bearing Edge	Fixed axial motion of hub
Rotor Buttons transmitting braking torque	Fixed geometry on rotor mounts

Table 4: Hub Finite Element Analysis Setup Table

The material was set to the preferred material of 6061-T6, the mesh was refined by using a curvature based solid body mesh to allow accurate modeling of the numerous curved surfaces on each part.

Front Hub FEA

An FEA analysis was completed on SolidWorks to analyze the stress concentrations on the front hub design. Using aluminum with a yield strength of 275MPa the peak Von Mises stress only reached 79.9MPa. The overall factor of safety of the component was 2.5. Figures 74, 75, 76, 77 display the FEA data of the front hubs and the even stress distribution across the part.

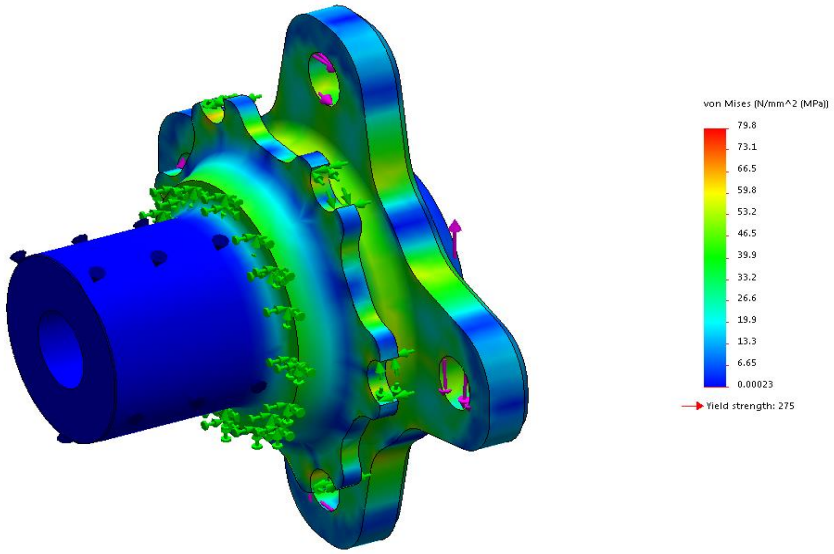

Figure 74: Front Hub Von Mises Stress

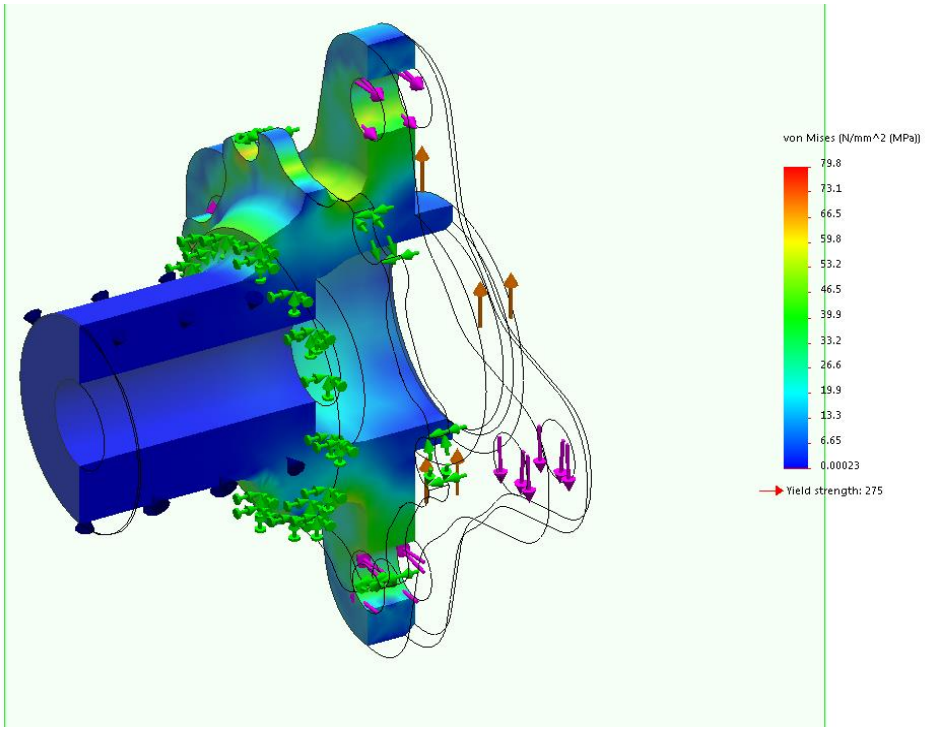

Figure 75: Front Hub Von Mises Stress Section View

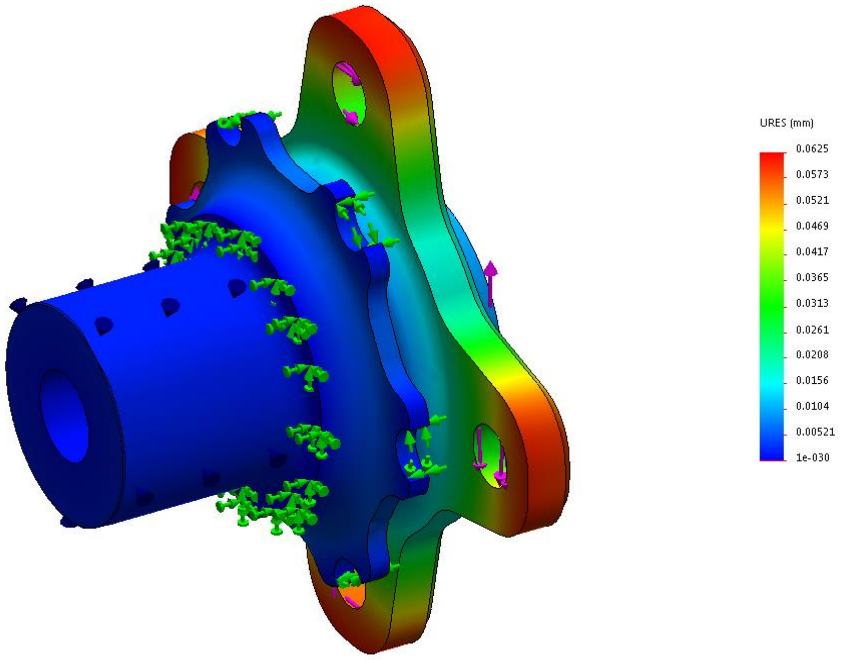

Figure 76: Front Hub Deflection

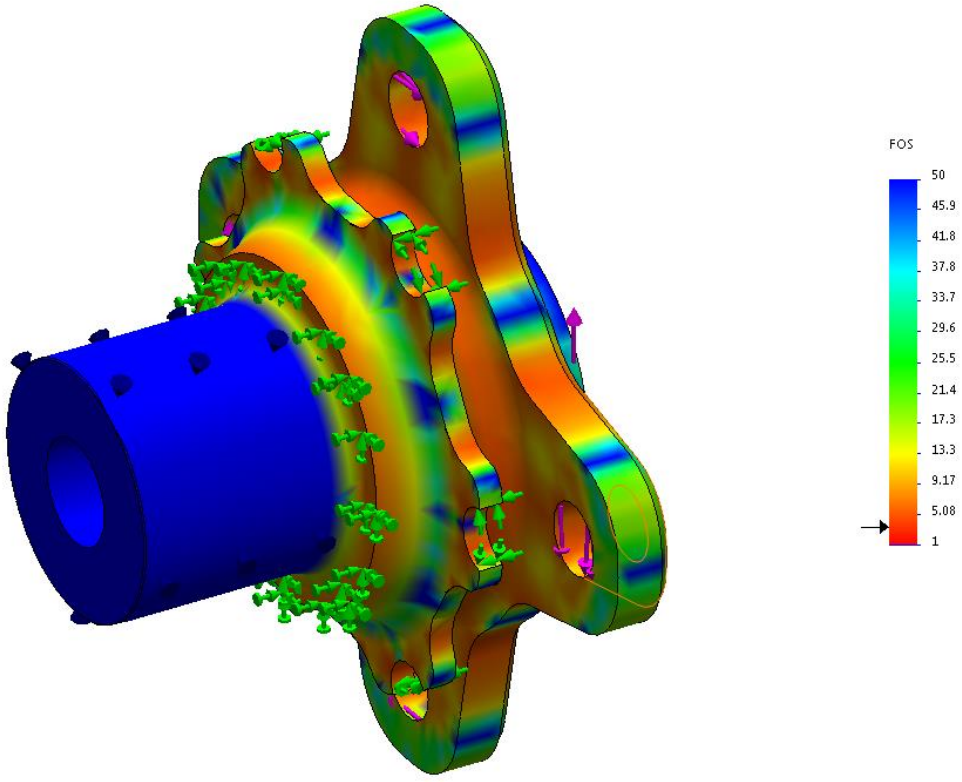

Figure 77: Front Hub Factor of Safety

Rear Hub FEA

An FEA analysis was completed on the design of the rear hubs. This component transmits the torque from the axles to the tires and is put under the highest loading conditions. Using an aluminum with a yield strength of 275 MPA the peak Von Mises stress only reached 84.3MPa. The factor of safety of the rear hubs were 1.5 and the stresses were evenly distributed across the part as seen in figures 78, 79, 80, and 81 below.

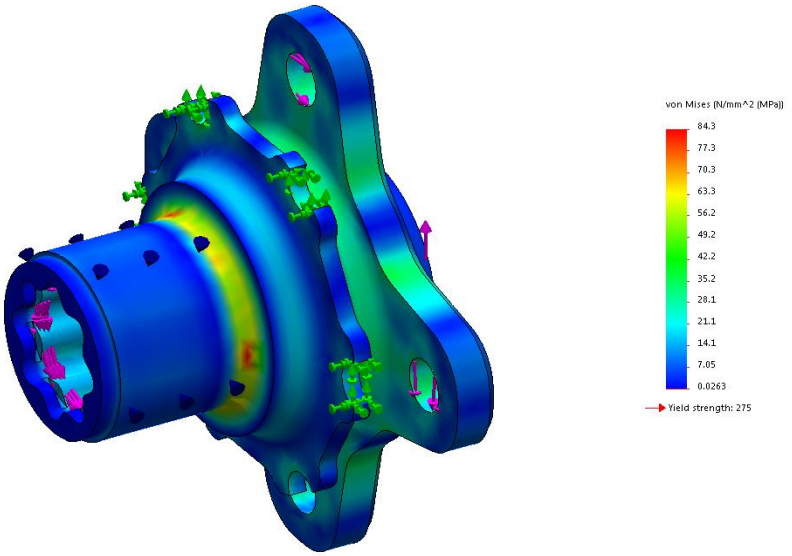

Figure 78: Rear Hub Von Mises Stress

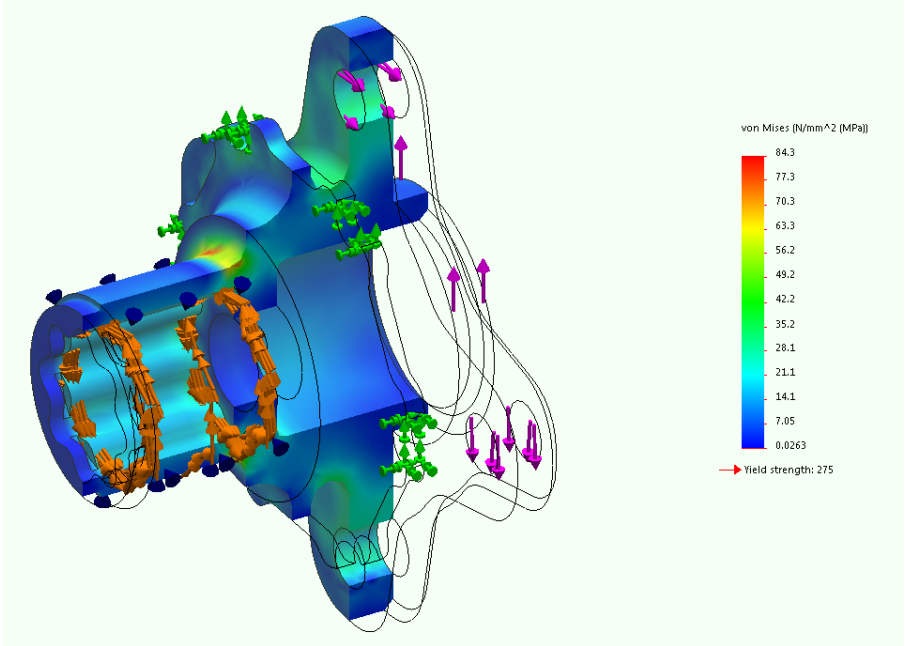

Figure 79: Rear Hub Von Mises Section View

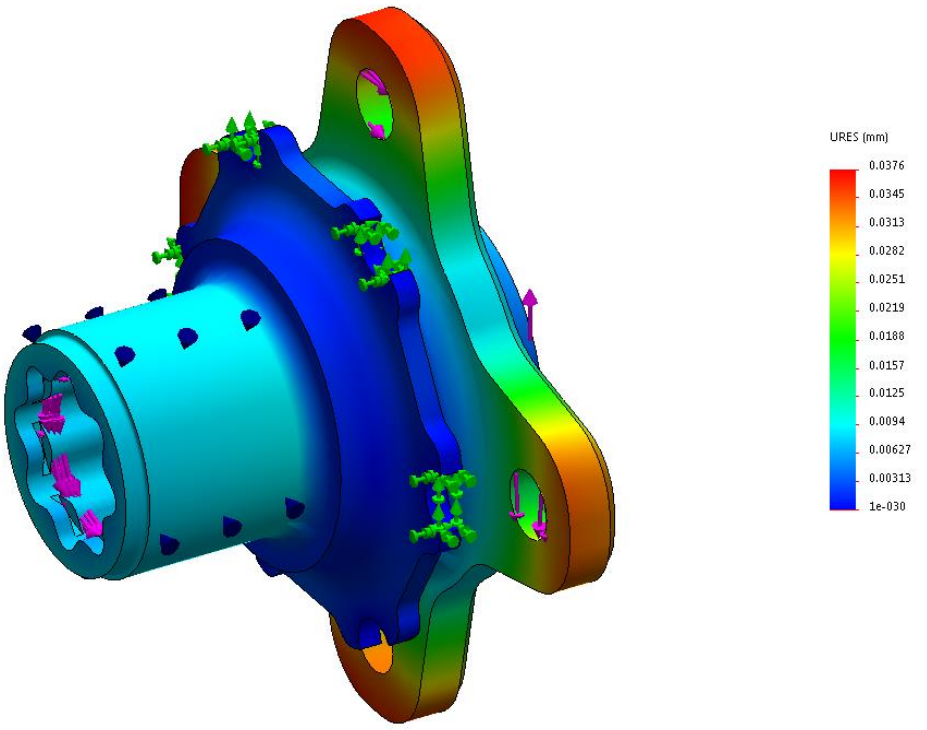

Figure 80: Rear Hub Deflection

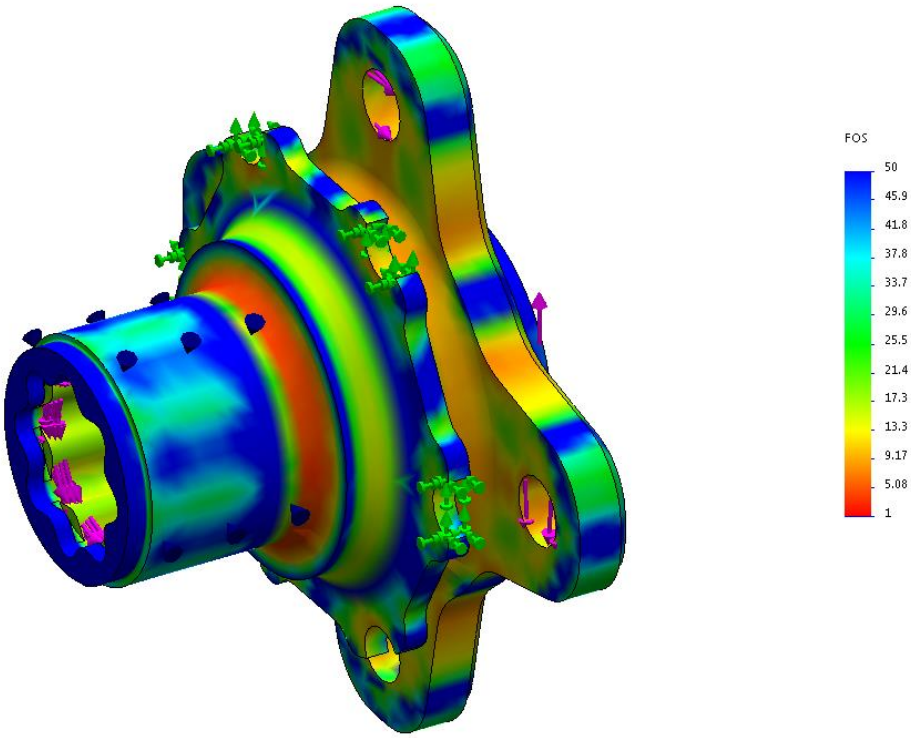

Figure 81: Rear Hub Factor of Safety

Steering

Design Parameters

To design a proper steering system for a formula SAE vehicle, several design parameters needed to be determined following the design intent. The overarching design intent for this system was to provide the driver with a system that did not require excessive steering input force or excessive wheel rotation, proper wheel feedback, and adequate wheel steering angle to allow the driver to navigate the tightest corners on the autocross course.

The minimum radius of the outside of the hairpin corner of the autocross track was stated to be 14.75ft. The corner will also be a maximum of 135 degrees. The corner was initially modeled, with the proper trackwidth of the vehicle. A best line was plotted on the corner model sketch for which the fastest time and lowest radius corner could be obtained, resulting in a radius of 16.5ft. Due to the lack of professional drivers, the system needed to be able to facilitate an average driver during this course. A minimum turning radius of 15ft was set as a goal.

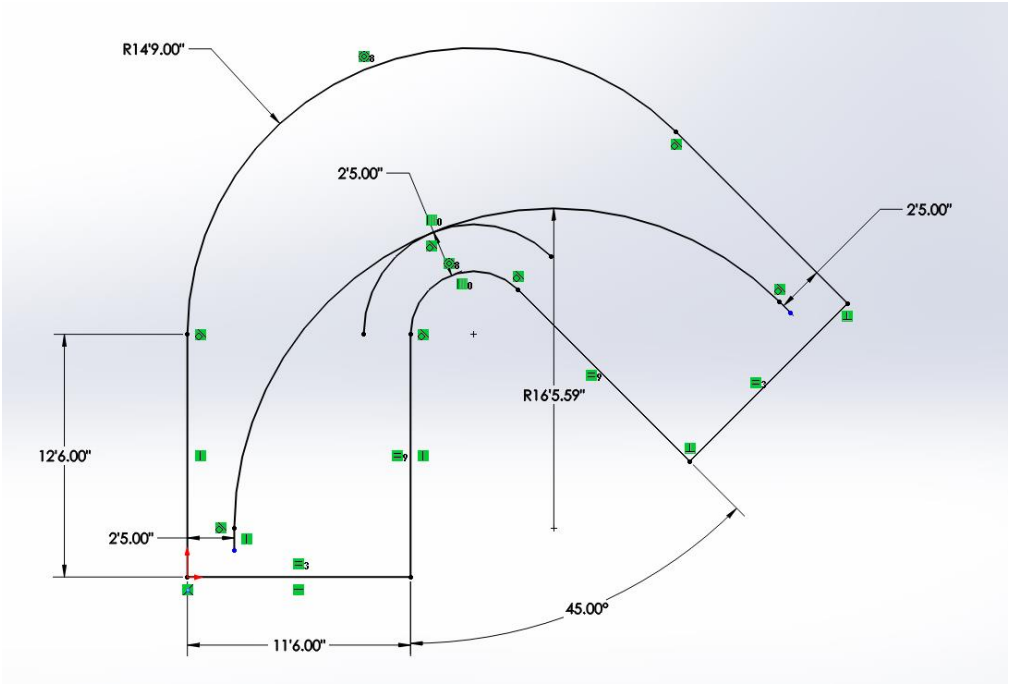

Figure 82: Turning Radius Sketch with Fastest Line

The wheels assemblies were checked in the assembly to determine the maximum wheel angles before collision. This was checked at neutral suspension travel and at both extremes. Using a clearance of at least 0.1”, a maximum wheel angle of 26 degrees was set for the inside wheel, with 33 degrees was set for the outside wheel.

By changing the Ackermann settings of the car the overall turning radius of the car can be adjusted. The steering radius was calculated based on the ideal Ackermann position of 100%. Since the two front wheels turn at different angles based on the Ackermann setting on the uprights the average steering angle $cos\delta$ first needed to be determined for the Ackermann setting. The average steering angle was calculated using equation 1 below using the inner and outer tire turning angles.

Equation 1: Average Steering Angle

$$cot\delta = \frac{cot\delta_i + cot\delta_o}{2}$$

$$\delta_i = inner\ wheel\ turning\ angle$$

$$\delta_o = outer\ wheel\ turning\ angle$$

With the average steering angle calculated the overall turning radius of the steering setup the overall turning radius was calculated using the CG distance from the rear axle and the wheelbase distance both in inches. Equation 2 below displays the overall relation used to calculate the turning radius in feet.

Equation 2: Turning Radius

$$R_{car} = \frac{\sqrt{{CG_{axle}}^2 + l^2 * cot^2\delta}}{12}$$

$$CG_{axle} = CG\ distance\ to\ rear\ axle$$

$$l = wheel\ base\ distance$$

$$cot\delta = average\ steering\ angle$$

The car had a wheelbase of 59 inches and the distance from the CG location to the rear axle was 29.5 inches. The steering angles of the Ackermann setup were 35.12 degrees for the inner tire of the turn and 24.47 degrees for the outer tire of the turn. These values gave a turning radius of 14.5 feet which are reasonable for the expected hairpin turns of the Formula SAE autocross track.

As seen above, the wheel angles of 26 degrees on the outside and 33 degrees on the inside will be satisfactory to achieve a turning radius of 14 feet. The next step in the design process was to determine the method for transmitting the steering force and how the system would be packaged. Once this was determined, the system could be optimized to allow for the minimum steering force over a given steering angle.

Design

Geometric Constraints and Packaging

In a vehicle, a wheel using a standard upright design with a rack and pinion, the wheel assembly can be steered by attaching the steering rack to the upright in one of the four quadrants of the upright.

Since a low center of gravity is a driving factor in this system design, the upper quadrants were not considered since the steering arm, tie rods, and steering rack would have to be located at an elevated position, therefore raising the center of gravity. If the front lower quadrant was used, the steering shaft would have to be longer which would increase the overall system weight. The rear lower quadrant would allow for a more compact, lightweight packaging. The rear lower quadrant was selected for this reason, since a light compact design was aligned with the overall vehicle design intent.

Optimization for low steering effort on the autocross and endurance track

With a specified turning radius and wheel angles, the system could be optimized for a low steering effort. The reason behind this design was to prevent driver fatigue, which with previous WPI FSAE vehicles proved to be a serious problem with autocross and especially with endurance events. While the lowest steering effort possible would be ideal, a compromise would have to be determined since a low steering effort also gave a slow steering response and therefore a large steering wheel angle at full lock. To allow for a fast steering response with a reasonable steering wheel angle, the full lock position was set to 120 to 160 degrees from neutral steer. This compromise allowed for the uprights to incorporate the necessary moment arm to achieve the maximum wheel angle based upon the selected steering rack.

System Goals and Final Specifications

Suspension Parameters	Units	Front			Rear		
Tire Size, Compound and Make		20.5X7.0-13 R25B			20.5X7.0-13 R25B		
Wheels (width, construction)		7X13 Cast Aluminum 1 Piece Wheel; 22mm Offset			7X13 Cast Aluminum 1 Piece Wheel; 22mm Offset		
Suspension Type		Unequal length double A-Arm suspension, pullrod actuated with position sensing and camber adjustment			Unequal length double A-Arm suspension, pullrod actuated with position sensing and camber adjustment		
Suspension design travel	mm	Jounce (col D): / Rebound (col E):	31.75	31.75	Jounce (col G): / Rebound (col H):	31.75	31.75
Wheel rate (chassis to wheel center)	N/mm	34.0			25.0		
Roll rate (chassis to wheel center)	Nm/deg	1.15			0.72		
Sprung mass natural frequency	Hz	3			2.5		
Jounce Damping	% critical	85	at __ mm/sec:	3063	80	at __ mm/sec:	2580
Rebound Damping	% critical	70	at __ mm/sec:	2523	70	at __ mm/sec:	2257
Motion ratio	_.__:1	.694-.773	Type:	Progressive	.840-.955	Type:	Progressive
Ride Camber (Rate of Camber Change)	deg/m	32.41			30.59		
Roll Camber	deg/deg	0.58			0.61		
Static Toe (- out, + in)	deg	1			0		
Static camber	deg	-2			-1		
Static camber adjustment method		Camber plates, Min: +0.37; Max: -4.36			Camber plates, Min: 0; Max: -4.75		
Anti dive / Anti Squat	%	0			0		
Roll center height above ground, static	mm	74.7			69.6		
Roll center position at 1g lateral acc	mm	Height (col D): / Lateral (col E):	74.3	-25.2	Height (col G): / Lateral (col H):	68.8	-31.8
Front Caster, Trail, and Scrub Radius		Caster (deg):	5.28	Kin Trail (mm):	39.67	Scrub Rad (mm)	11.21
Front Kingpin Axis		Inclination (deg):	-4	Offset (mm):	0.014		
Static Ackermann	%	75	Adjustable?	Yes			
Suspension Adjustment Methods		Ackermann is adjustable using 5 pickup locations on the upright, from 90% to Parallel steer					
Steer Ratio, C-Factor, Steer Arm Length		Steer Ratio (x:1)	5.25	c-factor (mm)	130.56	Steer Arm Length	125.98

Table 5: Steering System Specifications Table

Using the existing suspension geometry, the final steering geometry was obtained. The values shown above in table 5 display the final defined steering values. The steer ratio, c-factor (steering rack travel per revolution), steering arm length, and Ackermann values are all found using an iterative process as described in the following section. The majority of those values are set by the steering rack, with the steering arm length and Ackermann values being determined by upright geometry.

Steering rack and rack mount

	Kaz Technologies	Pro-Werks Stiletto
Specification	Value	Value
Weight	3 lbs	2.74 lbs
Materials	Gear: Steel, Case: Aluminum	Gear: Steel, Case: Aluminum
Rack Travel	3.25 in	4.5 in
Pinion Rotation	246 degrees	315 degrees
Rack Travel/Rotation	4.75 in/rotation	5.14 in/rotation
Mounting System	Outboard Collar Mounts	Inboard Bolt Holes
Sensor Integration	Yes	No
Cost	$670	$328

Table 6: Steering rack specs

		Kaz Technologies		Pro-Werks Stiletto	
Decision Factor	Weight	Score	Value	Score	Value
Steering Range (Angular)	7	10	70	8	56
Linear Motion Range	9	6	54	8	72
Cost	8	4	32	9	72
Durability	10	10	100	4	40
Weight	4	7	28	10	40
Totals			284		280

Table 7: Design Decision Matrix

Kaz design

Based upon the steering rack decision matrix in Table 7, the Kaz steering rack was the best option, primarily due to its high durability which can be attributed to the long length of the case surrounding the rack, to supports the rack in any side loading events with precision bushings at the ends of the case. The load is then transferred to the outboard mounts. On the Stiletto rack, the moment is transferred from the rack ends to the bolts, which are very close to the rack centerline. The rack is also not supported outside the narrow case, which will lead to premature wear during travel since in all cases except neutral steer, there is a force vector which results in an axial force and a moment about the pinion axis.

The Kaz rack was installed in the assembly model and the upright was optimized for this steering rack. This was done by creating a sketch using the existing geometry of the car, such as frame width and kingpin location at rack height. The rack travel was used in the sketch by creating three different steering arm positions, full lock(inside), neutral, and full lock(outside). The steering angles were set by the maximum steering angles from neutral as determined in Steering Design Parameters section above. This left the steering arm length to be fully defined. The arm length was initially determined for a parallel steer configuration for proof of concept. Ackermann geometry was added later.

Redesign for Stiletto

Unfortunately, the Kaz steering rack was discontinued for the 2016 year, with a model being available in 2017. All parts were sold out, meaning the steering system needed to be redesigned for the Stiletto rack becaues it was the only other steering rack within the allocated budget.

The uprights and rack mount were redesigned in the same fashion as the original Kaz rack design. The rack travel was updated and the upright moment arm lengths were therefore updated. The mounting system modified the rack mount significantly. The other major modification would be in the ends of the steering rack. The Stiletto came stock with tie rod ends, which would mean the tie rods would have to include clevis ends. This would cause a complicated and heavy tie rod design, so clevis ends were designed to mate with the steering rack and dust boots to maintain the original functionality.

Clevis End Design and Manufacture

Figure 83: Steering Rack Clevis End Manufacture and Installation

A mounting plate was designed with the purpose of mounting and supporting the Stiletto steering rack. Using a removable mounting plate allows for future adjustment of the steering rack location and position. It was determined early on that the steering rack would be mounted further back in the driver compartment to allow for an easier transmission angle onto the uprights. A steering wheel angle of 7 degrees of tilt upward was chosen after trial and error testing as the most comfortable steering wheel angle for the drivers to still work with packaging constraints. The steering rack would need to be mounted with a 7 degree angle forward to properly meet up with a 90 degree miter box to give a resultant 7 degree steering wheel tilt. This factor was considered into the design of the steering rack mounting plate. Figure 84 displays the 3D SolidWorks model of the mounting plate with a 7 degree channel to properly tilt the steering rack forward.

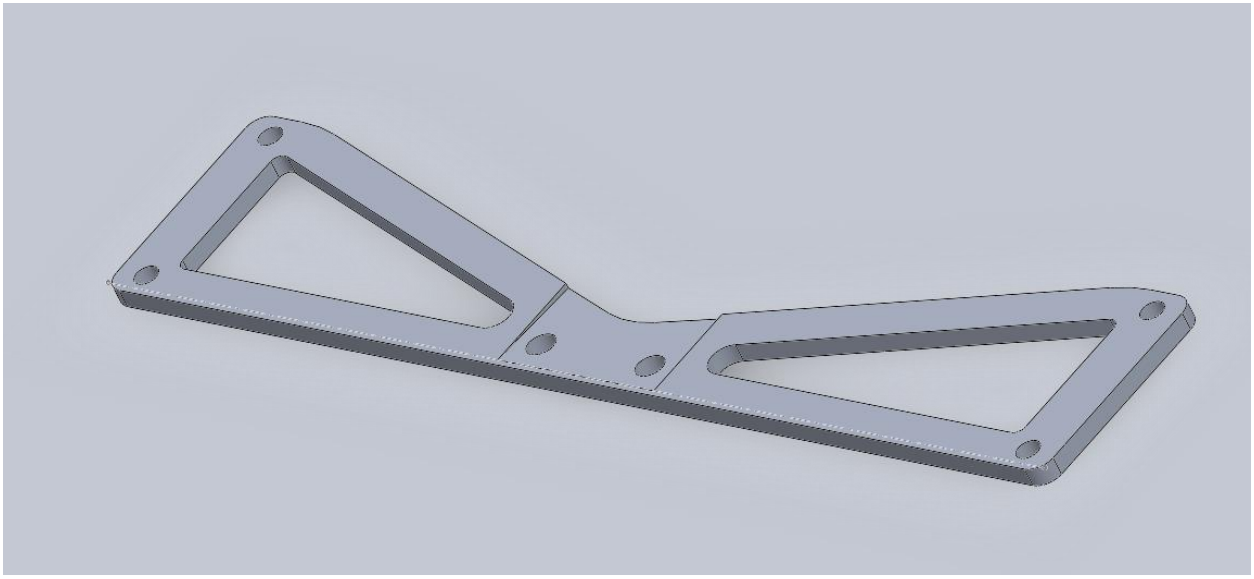

Figure 84: Steering Rack Mounting Plate

With a design chosen for the steering rack mount an FEA analysis was performed to ensure the part will not fail due to excess side loadings. To simulate the worst case rollover or side impact to the front tires a 500 pound force was applied across the two mounting holes of the steering rack. The mount was fixtured at the four frame mounting holes. The overall thickness of the part was ¼ inch and the material chosen was 6061-T6 aluminum for its lightweight and overall strength of 39890 psi. The maximum von Mises stress across the mounting plate was 2003 psi which gives an overall safety factor of 20. Considering the uncertainty of the forces that will be applied to the steering rack a factor of safety of 20 was conservative and acceptable. Figure 85 displays the von Mises stress evenly across the mounting plate.

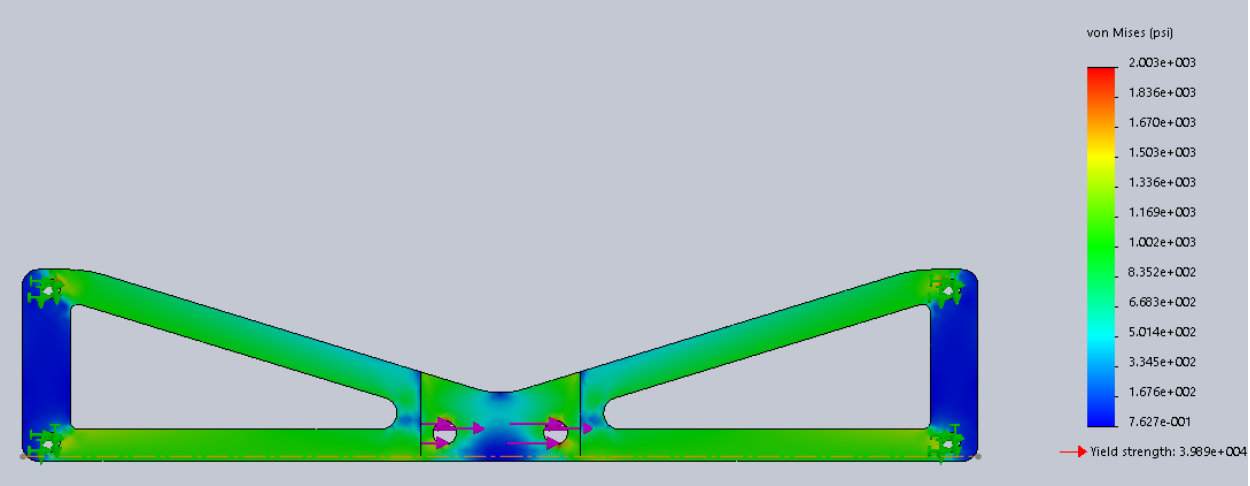

Figure 85: Steering Rack Mounting Plate Stress Analysis

The mounting plate was outsourced to a local machine shop to be cut on a water jet machine. Due to the complexity of the part shape and the complex fixturing which would be required to hold the part in a CNC milling machine it was practical to get it cut on a water jet to save time. The water jet machine was able to hold a tolerance of +/- .002 inches. The part was cut out of ¼ inch 6061 T6 aluminum plate. Once cut an additional operation was needed to mill the 7 degree channel in the center of the part. A Bridgeport manual milling machine with a ½ inch 4 flute endmill was used. Using a 7 degree angle gauge block and fixturing hardware the part angle was set on the milling table and the part was fixtured into place. From the SolidWorks model the overall depth of the channel was evaluated and the depth of the mill was set. The Width of the channel was milled by repeatedly milling from the center outward until the proper width was achieved. To offset the height of the steering rack from the mounting plate a parallel shim plate was made as an insert for the angled channel to lift the steering rack.

The tabs were manufactured using two separate operations on a CNC milling machine. ⅝" square stock steel was loaded into a CNC milling machine for the drilling operation for the mounting hole. For the second operation the part was rotated 90 degrees where a ¼ inch mill created the fish mouth feature which easily joined the tab to the frame. The steering rack mounting plate was fastened to the tabs using four ¼ -20 bolts.

Uprights (steering)

Steering Geometry

With the basic geometry defined for the uprights, the steering arm could be added to finalize the designs. As stated in the 'Steering Rack and Rack Mount' section, the moment arm of the steering rack was fully defined at a parallel steer position to create the initial geometry. With the moment arm defined, the height was chosen to be based upon the rack height to minimize steering effort and bump steer throughout suspension travel. The tie rod end should always be used in double shear, so two parallel moment arms were used to transmit the steering forces on the upright.

Ackermann Geometry

On road vehicles, the rate at which each wheel turns with respect to each other determines how the car will turn at both low and high lateral accelerations. This concept can be understood easiest in the low lateral acceleration case, for which weight transfer and tire slip is negligible. In this case, a pure Ackermann steering configuration would be ideal, since the inside wheel will turn with a smaller radius than the outside wheel as seen in the figure 86.

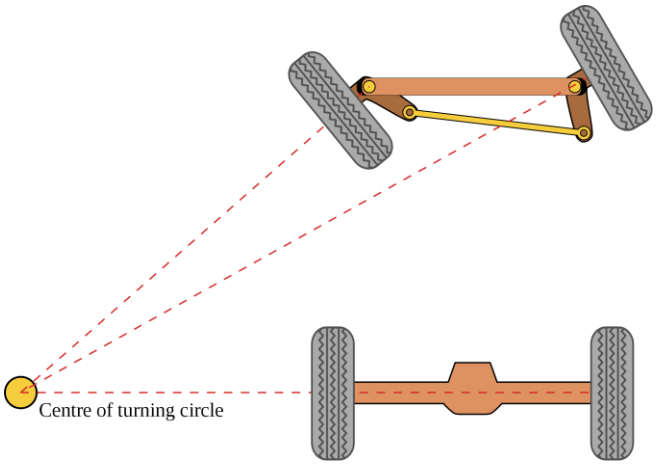

Figure 86: Ackermann Steering Instant Center Turning Diagram (Cite Wikipedia)

This geometry can be easily defined if the wheelbase, kingpin locations, and moment arm lengths are known. The geometry must be set up as seen in figure 87. A straight line must be made at neutral steer to the center of the rear wheelbase from each of the kingpins at the specified height. The steering pickup location will lie on that line at a point which is the distance of the moment arm length from the kingpin. This is what is considered a 100% Ackermann geometry.

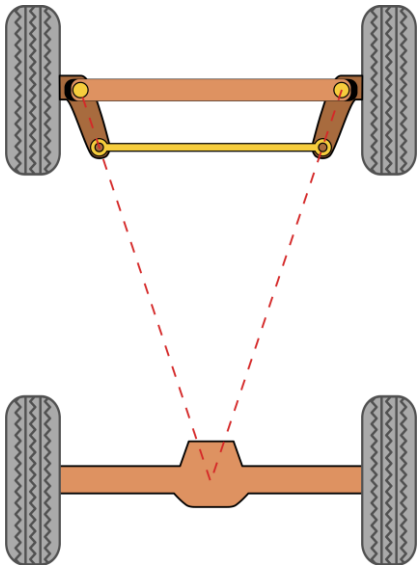

Figure 87: Ackerman Steering Instant Center Static Diagram (Cite Wikipedia)

Following research from the Milliken Book (CITATION), the important correlation between Ackermann steering geometry and handling at different lateral accelerations was made. At low lateral accelerations, an Ackermann geometry system would be ideal, yet at higher accelerations which a racecar would see, a parallel steer or even reverse Ackermann system would be preferable.

Other than this information, there was no quantifiable perfect geometry since each system had drawbacks. A parallel or reverse Ackermann system would be difficult to steer at low speeds, such as during a low speed run or moving the vehicle through the pits. Reverse Ackermann geometry is also difficult to achieve without longitudinal translation of the steering rack since the pickup points for the steering arms are on the outboard side of the kingpins. While this is possible to package at low steering angles, at higher steering angles collision becomes a major issue between the tie rod, upright, and wheel.

In order to properly validate this system, several Ackermann percentages were selected. This will allow the testing of each position to determine the optimal Ackermann position for each track, since the endurance might require a different Ackermann percentage than the autocross track or skid pad track. 5 tie rod pickup locations were designed, including 90%, 70%, 50%, 25%, and a parallel steering location. Reverse Ackermann positions were designed, but when collision detection was run, the tie rods would collide at the higher steering angles and were therefore eliminated from the system.

Optimization of Steering Force

Driver fatigue was found to be a significant issue in the WPI 2015 FSAE competition vehicle, most notably in the endurance event. The endurance track, as can be seen in the bottom of figure 88, is a circuit style course which consists of 22 laps of a 1km lap with three straight sections, and moderate corners. A higher speed can be carried through the corners unlike in the tight corners of the autocross course shown in the top of figure 88.

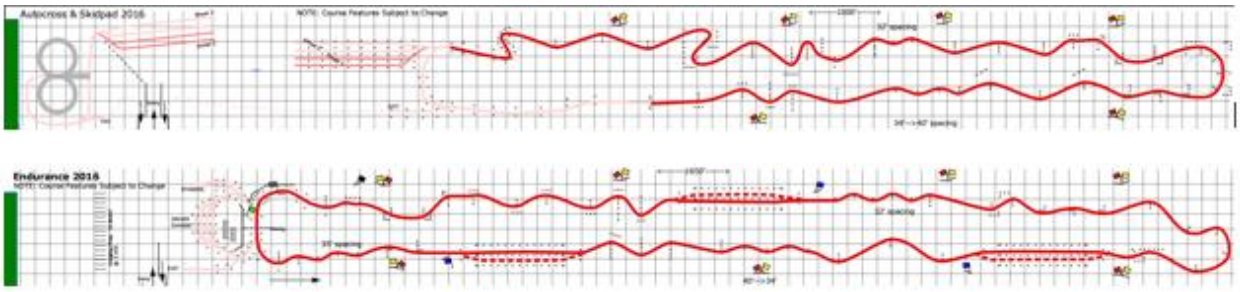

Figure 88: FSAE Michigan 2016 Proposed Autocross and Endurance Tracks

Due to the length of the endurance event, the system was optimized for this event since driver fatigue will be much more significant. The average steering angle will be relatively low, and there is an even number of right and left hand corners, so the steering should be symmetrical and optimized for low steering angles, but able to handle the hairpin corners of the autocross track.

The system was optimized to have the lowest steering force at neutral steer to allow the driver to make fast steering changes in slaloms and tight corners, along with making countersteering in a loss of traction situation easier. The tie rods were aligned with the steering rack in both the longitudinal and vertical axis

to create 90 degree transmission angles at neutral ride and neutral steer during a parallel steer scenario. For Ackermann geometry, the only section of the system that reaches a 90 degree transmission angle is the outside tie rod when the wheel is turned, while the inside tie rod reaches a higher, less efficient transmission angle. During a dynamic turning situation, the parallel steer will require more force per degree to turn from neutral, while with an Ackermann geometry the opposite will actually occur. This is due to weight transfer in the corner. The dynamic center of gravity will shift to the outside wheel, therefore creating more friction force on the contact patch. The outside tie rod-upright assembly will be at a 90 degree transmission angle during a moderate steering angle, while the inside, less loaded assemble will be at the more inefficient transmission angle. This results in a steering system which is easy to steer at higher lateral accelerations.

Tradeoffs and Design Considerations

There are several factors that contribute to the steering force which are left as variables not defined by geometry, yet bounded in most cases. For instance, on a normal road vehicle, the steering wheel may rotate approximately 1000 degrees from lock to lock. In this scenario, the driver must reposition their hands if the needed steering angle exceeds 180 degrees from neutral. In order to eliminate time lost during repositioning and increase safety, the maximum steering angle from neutral was set to 160 to safely and comfortably allow the driver to navigate the hairpin corners of the autocross track. If the system was truly optimized for only steering force, the steering angle would be increased along with the moment arm length to allow for a lower input force. If the input angle in this case is set to the maximum angle, the steering force will be minimized.

Geometry driven sketch of different Ackermann positions

In order to finalize the Ackermann positions that would be integrated into the upright design, the range of motion calculations were done at each selected Ackermann percentage. The upright stock was donated, and with the width of 3”, the maximum Ackermann percentage that was able to be achieved was 90%. These percentages were calculated by comparing the 100% Ackermann position to the parallel steer position, and then taking percentages of the resultant angle. All remaining locations other than 90% Ackermann and parallel steer were geometry driven by evenly spacing the locations at the nearest discrete Ackermann percentage. As with the parallel steer calculation, the rack travel was defined, the max angular travel was defined by the bounds of max wheel rotation. Tie rod lengths and moment arm length were defined by the neutral steer model for each, with the extreme positions being set to equal length.

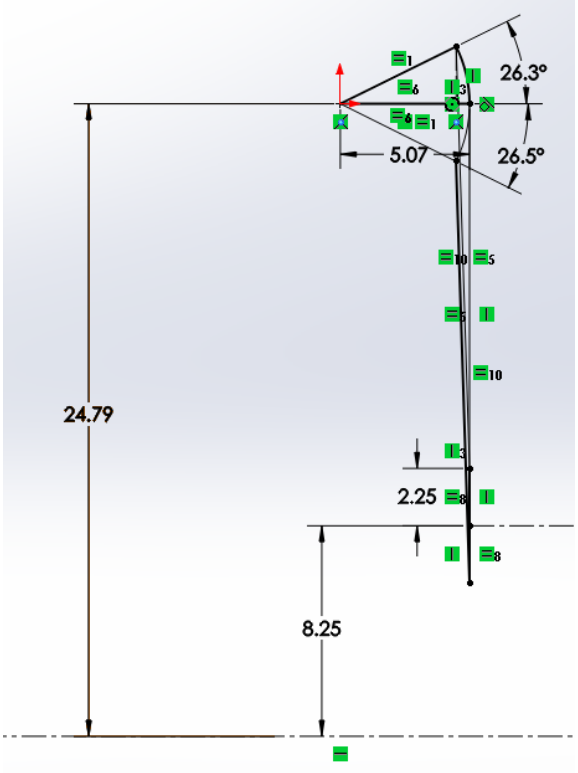

Figure 89: Parallel Steering Layout Sketch

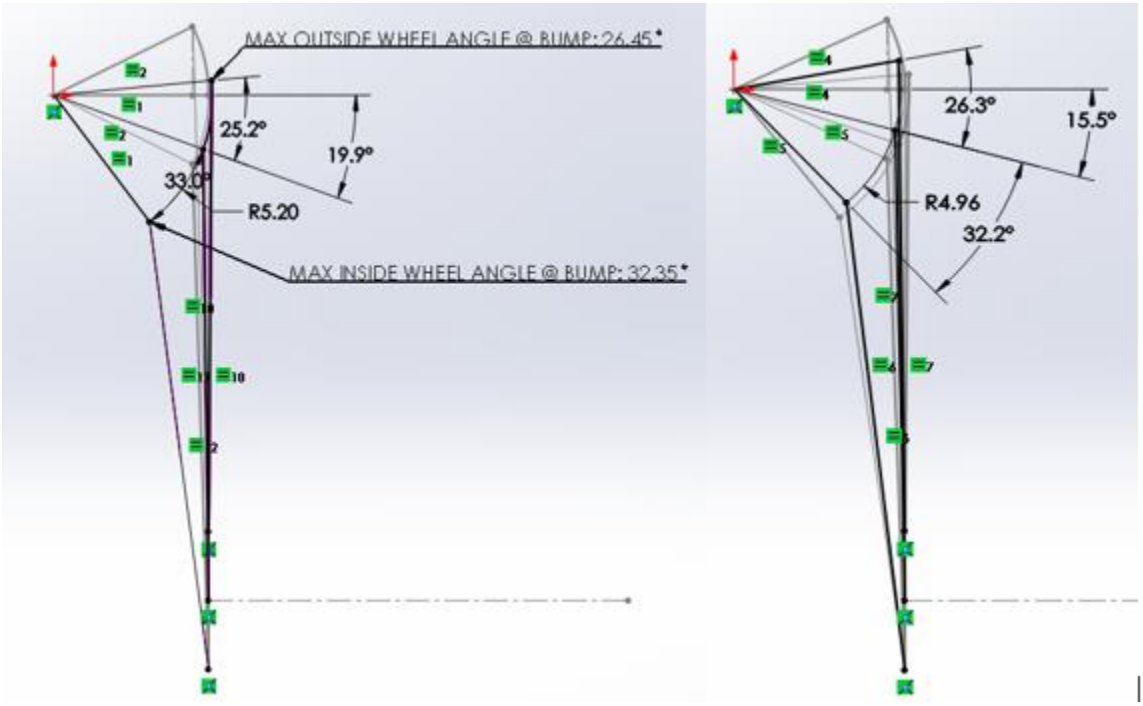

Figure 90: 90% and 70% Ackermann Position Layout Sketches

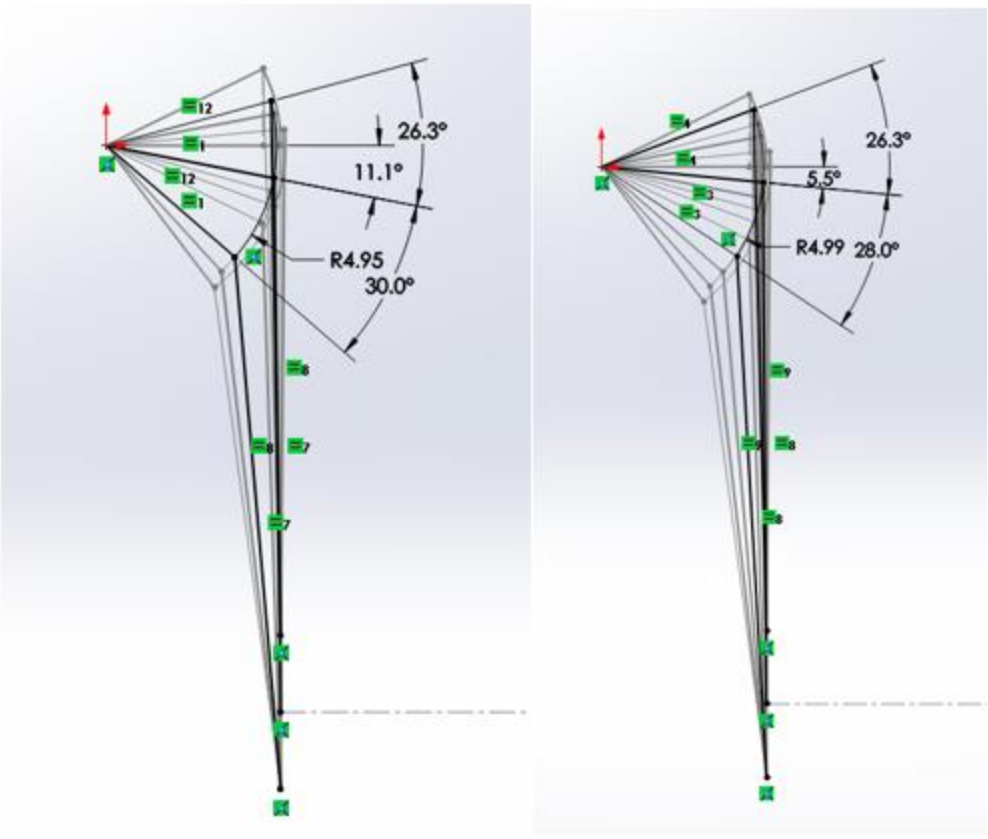

Figure 91: 50% and 25% Ackermann Position Layout Sketches

Initially, the angle was set to drive the sketch using the max inside angle of 33 degrees as seen in figure 90, but often this resulted in an outside angle over 26 degrees, which was the acceptable maximum. In these cases, as seen in figure 91, the system was driven using an outside angle of 26 degrees to avoid collision.

Tie Rod Design

Background and Design

To transmit the force from the steering rack to the upright, a link must be attached between the two components, which in this case is referred to as a tie rod. Since there is translation, and rotation in two axises, tie rod ends must be used to prevent binding of the system.

The design intent behind these components is to have a strong and stiff component which is lightweight and limits play in the system. The tie rod must be adjustable to accurately change the degree of toe in or out. A right and left hand threaded nut welded to each end with right and left hand thread tie rod ends were selected for the basis of the design. A thin walled tube was chosen for the member since it allows a lightweight design while maintaining a moderate section to improve stiffness.

Steering Gearbox Design

Reasoning behind steering box

Unlike previous sections of the steering system, the steering shaft is entirely packaging driven due to the fact that the steering rack is fully defined vertically, laterally, and longitudinally while the steering wheel must be positioned in a comfortable driving position while still staying within SAE specifications. The main area of concern is rule T6.5.7, which states that no section of the wheel at any steering position may be above the top of the front roll hoop. Following an on-campus study of several students ranging from average students to amateur racing drivers, the comfortable range of steering wheel inclination in the designed seating position was found to be 10-35 degrees of inclination forward. The longitudinal position was determined to be most comfortable approximately 5 inches rearward of the front roll hoop. The vertical height was found to be most comfortable as high as the rules will allow, therefore a buffer distance of 0.25" was designed into the model to account for tolerance stackup of machining and welding tolerances.

With the steering wheel in this position, the below geometry was created in the side view profile.

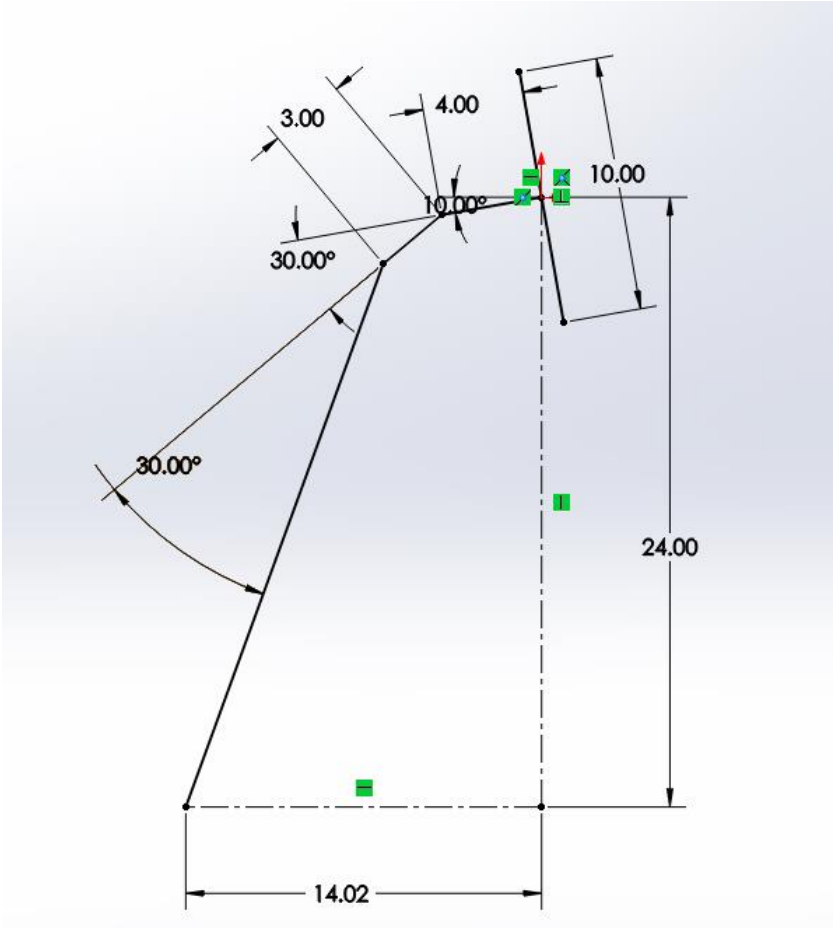

Figure 92: Steering Shaft Sideview Layout Sketch

As can be seen in figure 92, the distance from the centerline of the steering wheel to the centerline of the steering rack is over 14". This configuration is not necessarily a strong construction due to the very short upper and intermediate shafts. Each shaft will need to be supported to avoid idle degrees of freedom which could cause the system to lock up. The bearings for the shafts will need to be placed very close to each other, and only radial load ball bearings would be able to be used due to the lack of room for shaft collars to transmit axial load to a roller bearing or spherical roller bearing. The other major problem this initial configuration exhibits is the high angle between each shaft, which would have to be increased to meet the packaging requirements to 40 degrees for each u-joint. A normal u-joint becomes very inefficient at transmitting torque at high angles, and while high angle u-joints do exist, the gears have large amounts of backlash, which is unacceptable in a steering system requiring a very high reverse efficiency. U-joints also do not transmit rotation at a constant speed with respect to the input speed, causing a non-linear steering speed. This can be mitigated by properly phasing two u-joints, but due to the large angle, a geared system will have to be used. Below, figures 93 and 94 show the potential speed variations relative to the angle between the input and output shafts ("Ackermann Steering Geometry.").

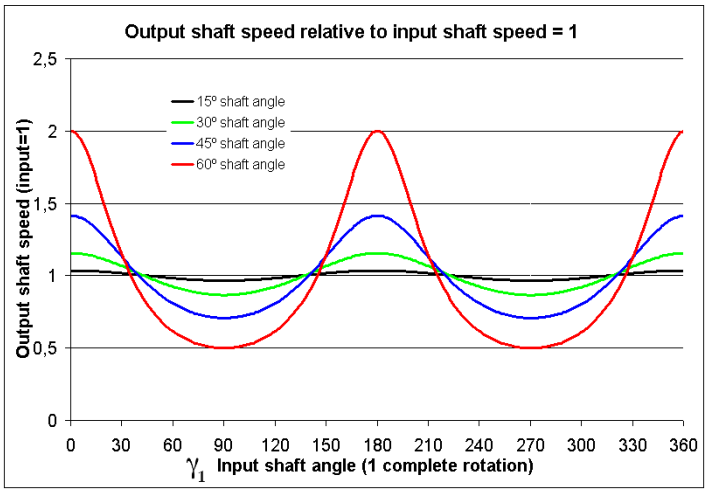

Figure 93: Universal Joint Non-Linear Output Velocity Normalized (speed/angle) ("Universal Joint")

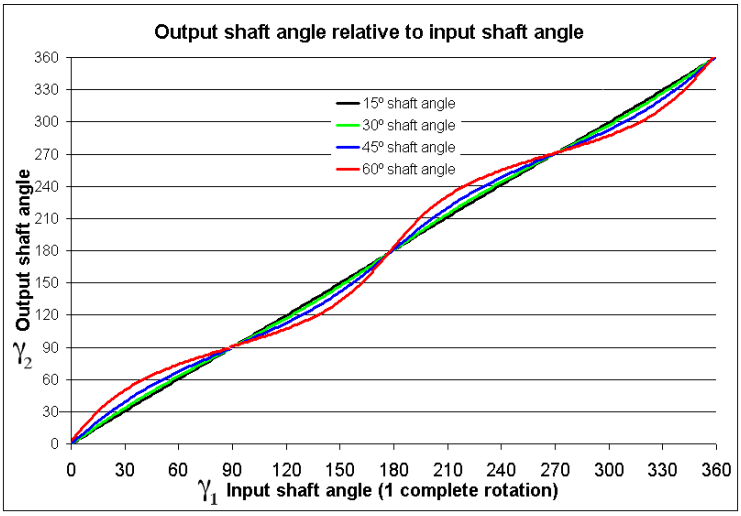

Figure 94: Universal Joint Non-Linear Output Velocity (angle/angle) ("Universal Joint")

Gearbox Design

Gear Selection and Design Constraints

After analysis of the steering side view geometry was done, it was determined that the longitudinal distance could be reduced through the use of a right angle gearbox, thus eliminating the intermediate shaft, all u-joints, and lengthen the upper shaft. This increases support area for the upper shaft and allows for better packaging of the lower section of the steering shaft.

In order to allow the system to transmit torque at an angle of 90 degrees, bevel gears were selected, and example of which can be seen in figure 95. Due to the total pinion angle of the steering rack being comfortably in the acceptable steering angle range, a bevel gear reduction was not needed. During testing of several bevel and miter gear sets, it was found that straight cut bevel and miter gears did not have a smooth mesh and had an unacceptable amount of backlash. To remedy this situation, spiral bevel gears were selected to provide a smooth, constant mesh with minimal backlash, which is done by always having a section of the teeth in mesh at one time, unlike straight cut gears where only small sections are in constant mesh at one time.

Figure 95: 90 Degree Miter and Spiral Miter Gear Sets (Gearvalves)

Bearing Selection

During the operation of miter gears, the gear set experiences both axial and radial loads. In a spiral miter gear set, the system becomes more complex as the components are not normalized to the standard coordinate system and force vectors need to be calculated. In order to handle large radial and axial loads during dynamic use of the system, tapered roller bearings were selected. Unsealed bearings were selected for ease of maintenance and assembly along with low cost, even though sealed bearings offered greatly improved dust and particulate protection.

Case Design and Geometry

Typically a gearbox design includes a sealed case with all components in an oil bath. With a system for which wires needed to be routed through the steering shaft and weight is a major concern, an oil filled gearcase was not feasible. An open construction design was created, utilizing welded frame members for mounting. The main structure of the gearbox consists of three bearing housings, two diagonal braces, one rear diagonal brace, and the mounts. Each component was designed to be easily manufacturable using a waterjet to decrease manufacturing time, with all additional milling and tapping operations to be done afterwards. Plate stock 6061-T6 was chosen for its moderate strength, low weight, low cost, and high availability. Lightweighting was done to all diagonal braces, as these were larger, load bearing components which had unnecessary large areas of material which could be easily removed to save weight while remaining structurally sound.

The upper tapered roller bearings were separated axially as far as packaging would allow to decrease the radial force that would be necessary to counteract the moment created from a sideloading of the steering wheel. The full model can be seen in figure 96 and the cross section can be seen in figure 97.

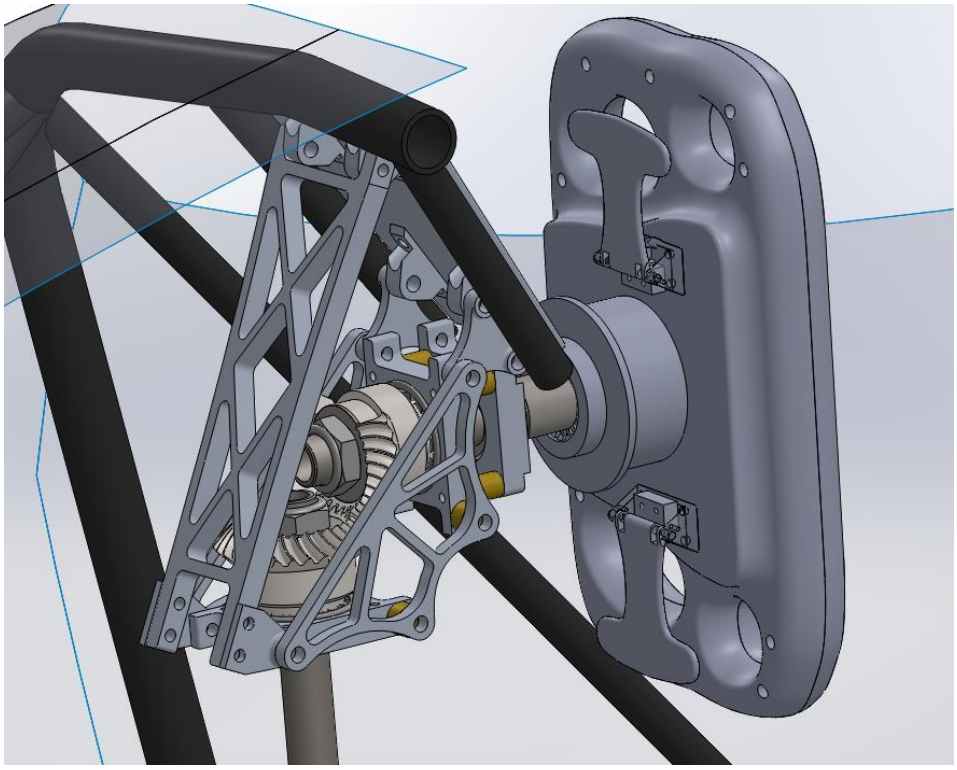

Figure 96: Revision 1 Steering Wheel with Steering Gearbox

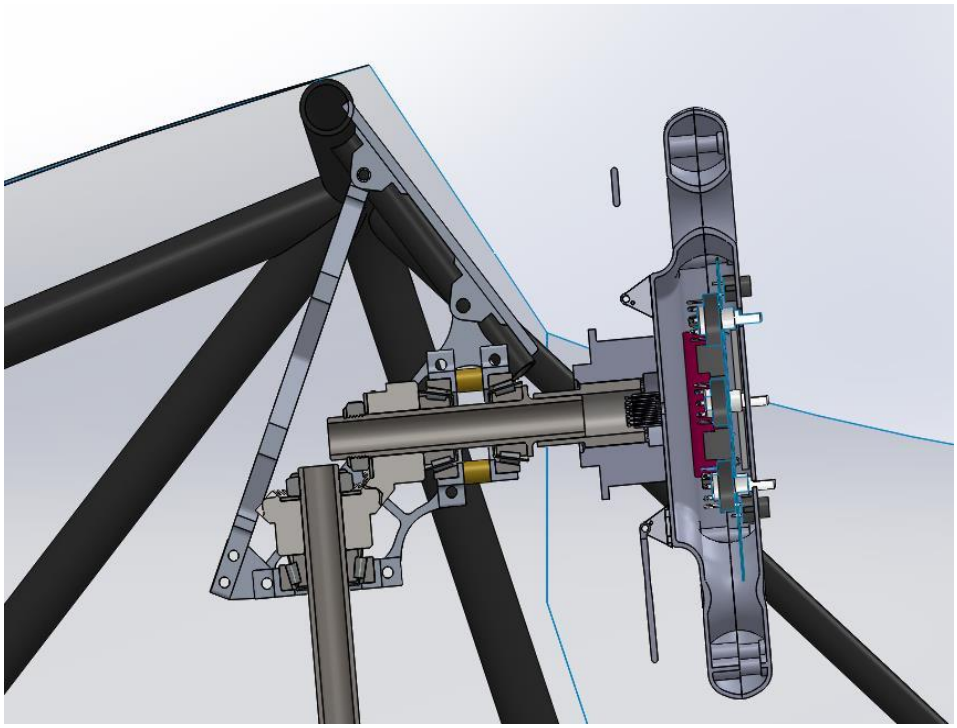

Figure 97: Steering System Cross Section

Steering Position Sensor Integration

To monitor steering position to analyze and validate suspension and steering performance both during and after a track event, a steering position sensor needed to be integrated into the steering system. Initially, the Kaz rack was to be used with the integrated position sensor, but due to unavailable parts, the system needed the steering position sensing with the new steering rack. The open gearbox design was optimal for this, since two rotating shafts were easily accessible, with very well defined geometry, and minimal tolerance stack to cause potential integration problems. The upper shaft was to route all electrical connections to the steering wheel, which left the lower shaft for position sensing. Figure 96 shows revision 1 of the steering gearbox, with gears which were not available for purchase during the manufacturing process. The system was redesigned for a gear set from Boston Gear and a new fixturing system was created. The upper and lower shafts were tapped, and a ½" bolt was used to provide the preload force to the bearings. This bolt on the upper shaft was drilled and chamfered to allow all wires to pass through, while the lower shaft was drilled and counterbored to allow for a small neodymium magnet to be pressed into the bolt head.

The position sensors designed by the 2016 Formula SAE Vehicle Electrical System Design team used magnetic field sensing to accurately locate position. The custom circuit board with sensor was mounted via a 3D printed mount, which was bolted to the diagonal braces as seen in figure 98.

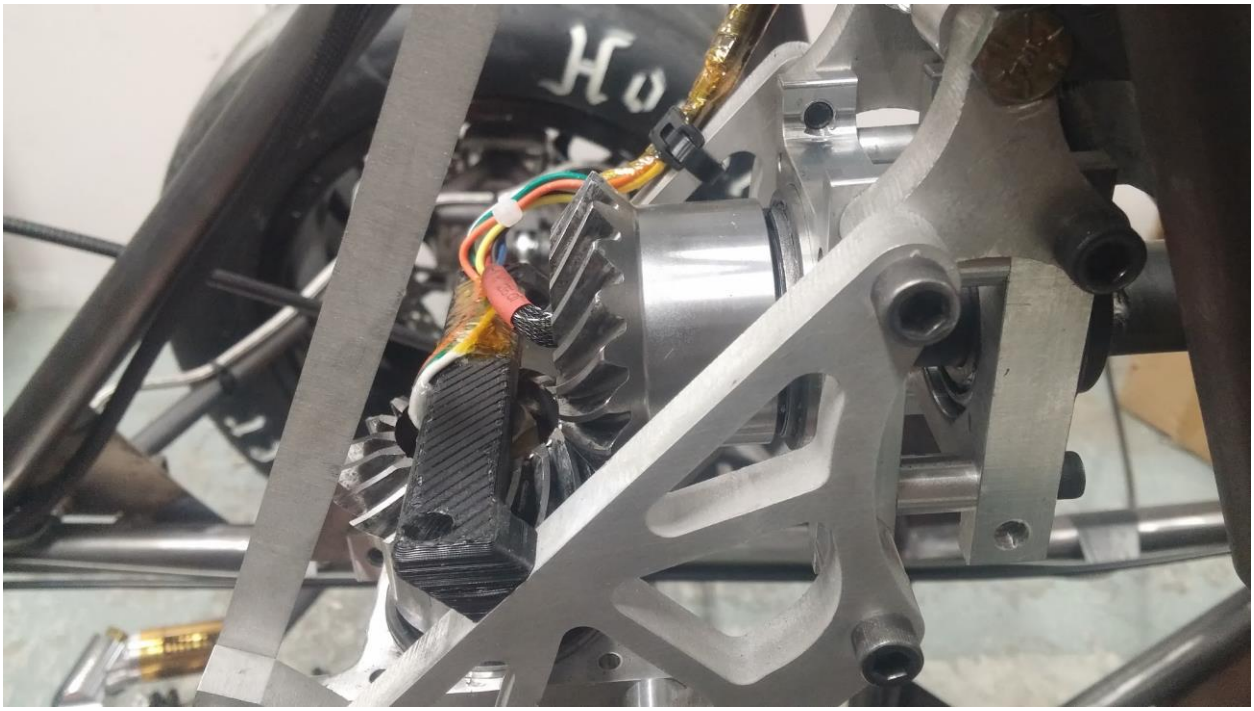

Figure 98: Steering Gearbox Sensor Integration Close-Up

Integration of Custom Pogo-Pin Connector

On the rearward end of the upper shaft, a splined section was welded on to interface with the quick disconnect hub mounted to the steering wheel. The steering wheel required a 4-pin connector which needed to be plugged in as the quick disconnect hub was connected. To solve both the problem of phasing and alignment, a pogo-pin connector was used to mate with a slip plate. The pins were aligned in concentric rings, with concentric rings of copper on the slip plate. The slip plate and pogo-pin connectors were designed by 2016 Formula SAE Vehicle Electrical System Design team, with the slip plate being manufactured at Osh Park while the pogo-pin connector was machined in-house.

Manufacturing

Several components were sent to Vangy Tool in Worcester, MA for waterjet cutting, which include the two diagonal braces, front diagonal brace, front diagonal brace mounts, and the two triangular rear mounts. All holes were undersized by 0.05" to prevent the oversizing of holes. Each hole was drilled and reamed to exact size. All secondary operations including drilling and tapping were completed prior to fitment.

The bearing housings were CNC milled in 5 operations following initial facing operations. The upper and lower steering shafts were manually turned, and a keyseat was milled following turning operations. The shafts were tapped to ½"X13 and the flanges were welded. The lower shaft was welded to the spline adapter for the steering rack, whereas the upper shaft was welded to the spline that mates with the steering wheel hub.

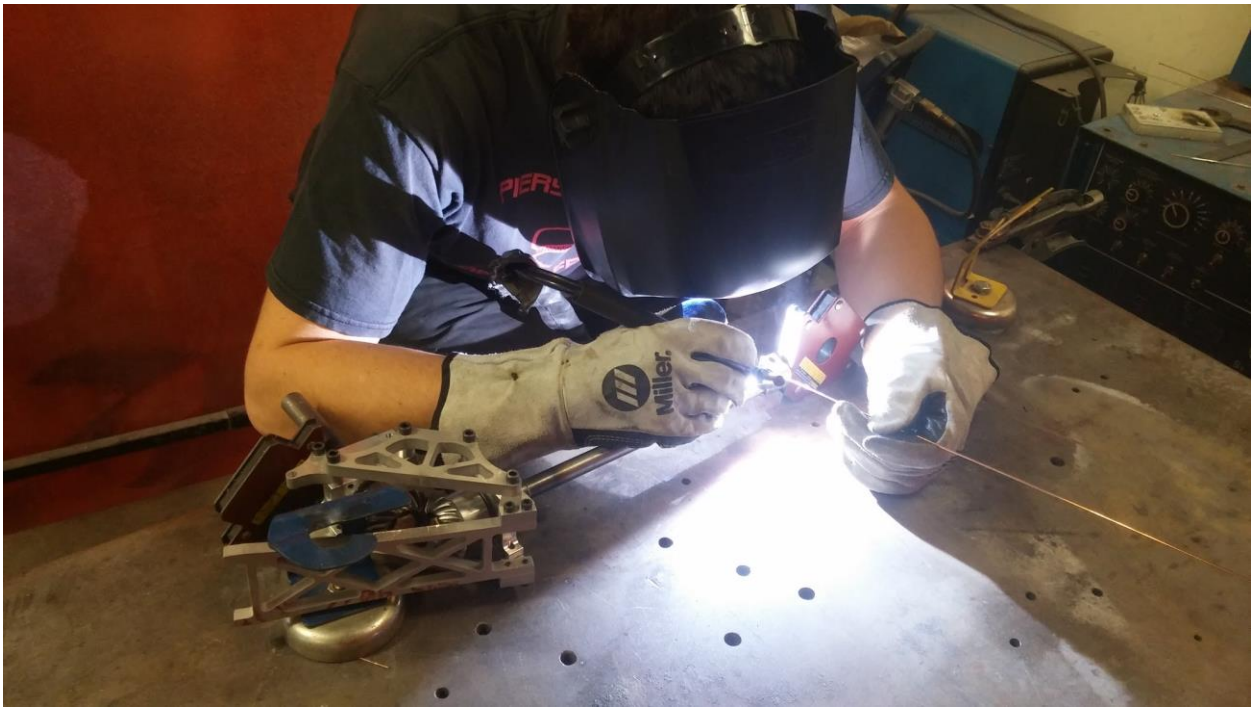

Figure 99: Steering Gearbox Welding

Figure 100: Steering Gearbox Parts Prior to Final Assembly

Assembly

Correct torque settings

During the initial assembly, the system was found to freely turn as expected. The steering gearbox was installed in the car with the remainder of the steering system and wheel assemblies. The preload bolts were tightened to roughly 30ft-lbs. The steering was tested and was found to be very difficult. After careful analysis, the only system with significant resistance was the gearbox. The preload was set to zero and the system was tested again, revealing the problem as there was minimal system resistance. Through a series of tests, the torque was set to 28 in-lbs using a torque wrench. The bolts were secured with red Loctite.

Selected lubricant

During the assembly process, several lubricants were tested to find the ideal lubricant for the steering gearbox. Since the system could not be submerged in oil, a thin coating needed to be applied prior to assembly. This coating needed to properly reduce friction while not attracting particles. The first test was done with a graphite lubricant since this dry coating would not attract particles. This coating had little effect, and a white lithium grease was applied following cleaning. This lubricated well, but was messy and attracted particles. Finally, Kluberplex BE 31-102 was tested courtesy of the Higgins machine shop, and this performed well and met all constraints. A thin coating was applied to all roller and thrust bearings.

Testing of wheel

The steering system on the 2015 FSAE competition vehicle was found to take 11.3 ft-lbs of torque to operate in a static condition. This system was noted by all drivers and the ergonomics judge at the 2015 FSAE competition as being very hard to operate. The 2016 steering system was designed to only require 6.5ft-lbs of torque. During testing following final installation, the system was found to only require 4.1 ft-lbs of torque in a static condition, which is about 3 times easier to operate than the 2015 system. The variation from the calculations can be attributed to conservative tire grip calculations.

Steering wheel

Revision 1

The initial design of the steering wheel was modeled after the 2015 WPI FSAE competition steering wheel. Instead of using two parallel aluminum plates with 3D printed internals, the wheel was to be constructed of initially fiberglass, and then for the final revision, with carbon fiber. The basic shape and styling was similar, with a hollow shell type with integrated handles. The wheel needed to adhere to SAE rule T6.5.6, which state that the wheel may contain no concave sections, so the wheel could be only a small variety of shapes from a circular style to a more rectangular configuration.

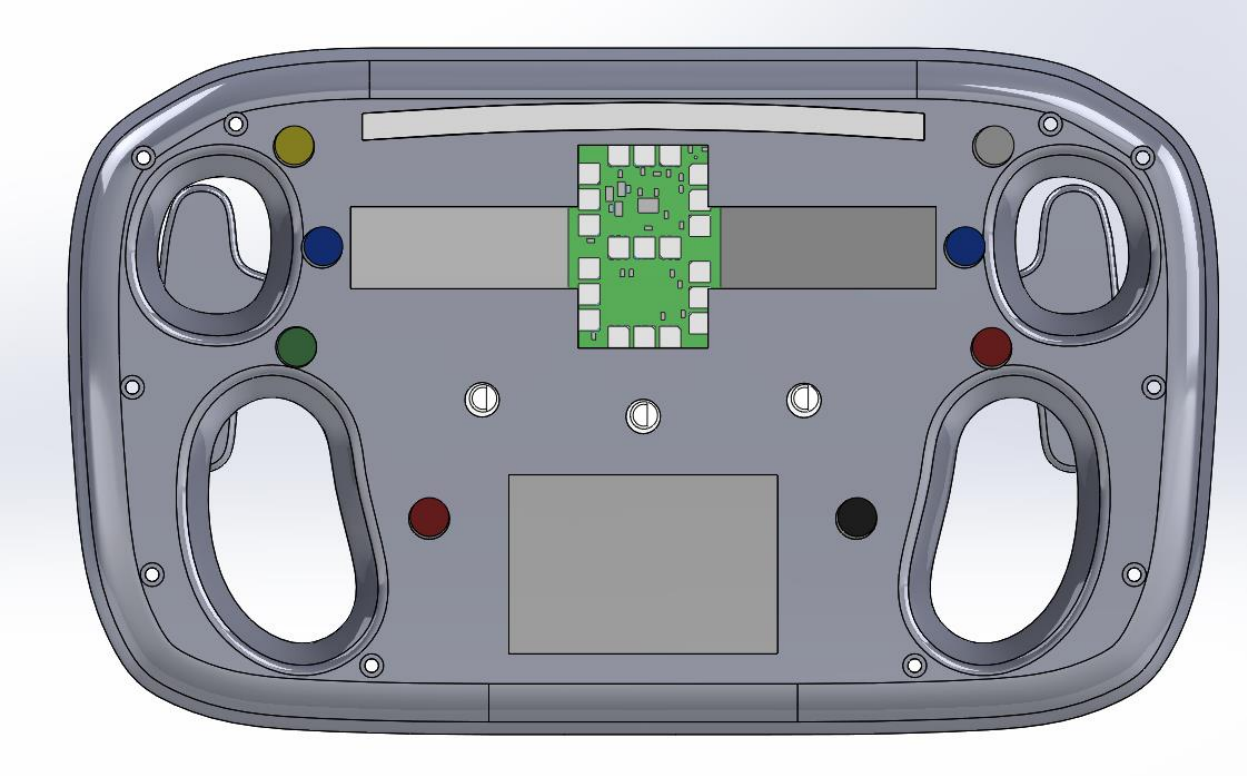

Figure 101: Steering Wheel Rev 1

To create the geometries pictured in figure 101 using fiberglass or carbon fiber, precise molds needed to be created. Using these molds, the parts would be laid up using a wet layout technique and the parts would be vacuum bagged. Since there was not an autoclave available, prepreg fiberglass or carbon fiber were not able to be used.

The main problem that was found with the mold making process was material selection. Metal molds would be ideal due to their strength and the ability to make very precise shapes. Aluminum would be the only metal that would be selected due to the machinability, yet billet aluminum of the needed dimensions was too costly for this project. Lower cost materials involved sheet insulation foam, laminated veneer lumber, MDF, and closed cell machining foam. Sheet insulation foam, such as Owens Corning Foamular

boards were experimented with during the 2015 bodywork build, and while offering a very soft stock for easy machining and shaping, the material melted when exposed to the epoxy used with the fiberglass and carbon fiber. Sealing methods on the molds included using aluminum tape in order to isolate the foam from the epoxy. This material was not selected due to the poor surface finish the tape would give, along with the very low strength of the molds.

MDF was chosen as it has a higher strength and considerably better consistency than LVL, while it is much cheaper than machining foam and available at any local hardware store. It can be laminated to any shape or size.

The part was divided at the center plane to form the mold parting line. Each part file was converted into a mold shape, and draft angles were considered to allow for the part to pull from the mold after curing. Each mold half was machined from laminated MDF using sharp carbide insert router bits. The 3D mold roughing operation was done with a ½" straight flute router bit, with the parallel planes finishing operation being completed with the ¾" ball end router bit. A final finishing operation was completed with an extended ¼" ball endmill. The top half of the mold can be seen in figure 102 with the lower half of the mold in figure 103.

Figure 102: Top Half of Steering Wheel Mold

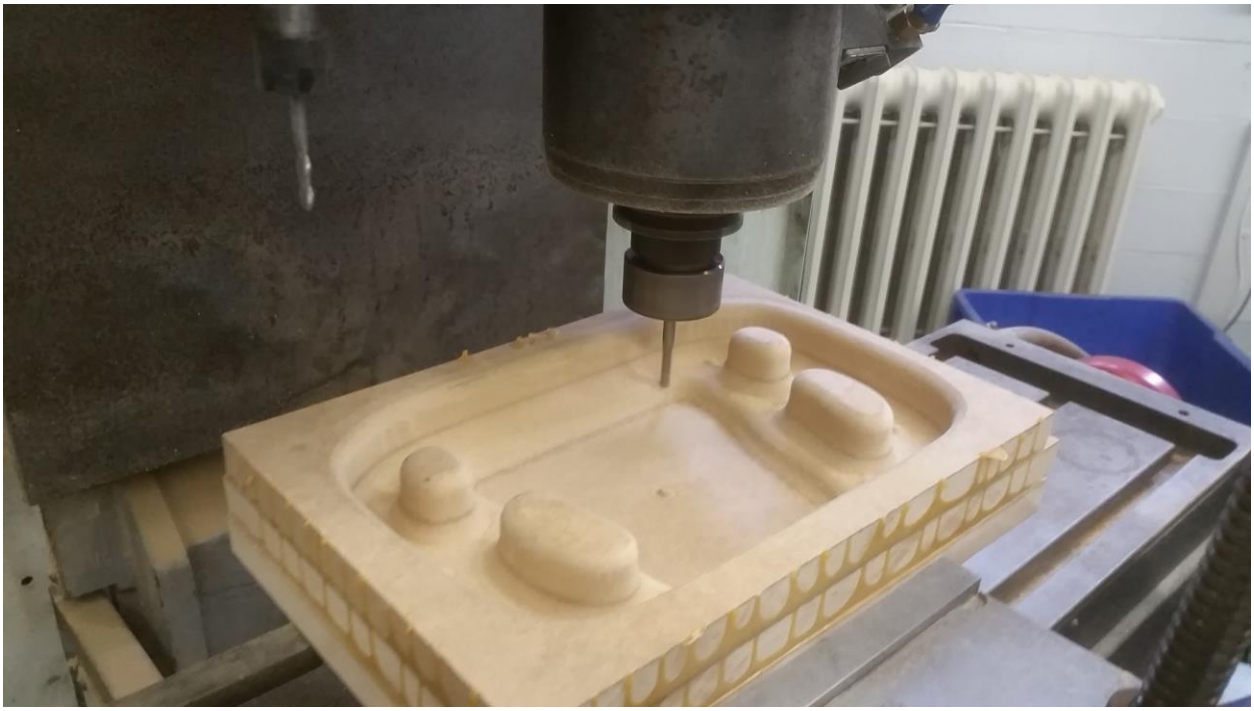

Figure 103: Bottom Half of Steering Wheel Mold

Following machining, the molds were sanded and epoxy was applied in two coats to seal the molds. After each coat, the molds were sanded using high grit sand paper. The epoxied molds can be seen in figure 104. The fiberglass was applied after mold wax and PVA release material was applied and the system was vacuum bagged. Unfortunately, the part did not release well from the mold due to the high curvature areas and large flat areas of the mold. In order to complete a working steering wheel model, the approach needed to be modified along with the steering wheel geometry.

Figure 104: Steering Wheel Molds Sealed

Revision 2

The design of the steering wheel was modified to improve manufacturability. The new design featured a carbon fiber plate which would be waterjet to the correct shape, with an aluminum case that would be mounted on the back to house the electronics. A ¼" carbon fiber plate was selected to allow a light part with a very high strength. 7075-T6 billet aluminum was selected for the case since the high strength was required even at a high cost, since the steering wheel is the primary method of interface between the driver and vehicle, and the driver needs to be able to safely control the vehicle at all times. The second revision of the steering wheel can be seen in figure 105.

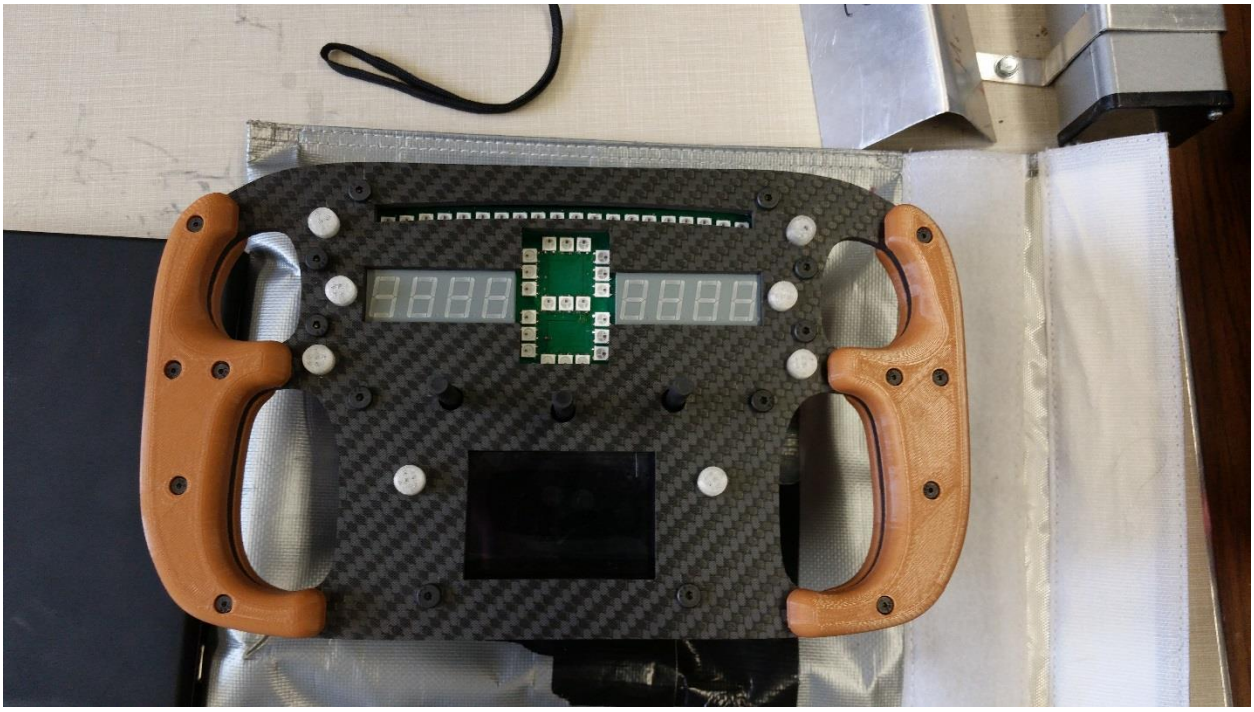

Figure 105: Steering Wheel Rev 2

The case was machined in three different operations following the initial facing operations. The first included drilling and tapping of mounting holes, with the second included a 3D mold roughing and z-surface finishing operations to pocket the internals of the steering wheel. The finished internal section of the wheel can be seen in figure 106.

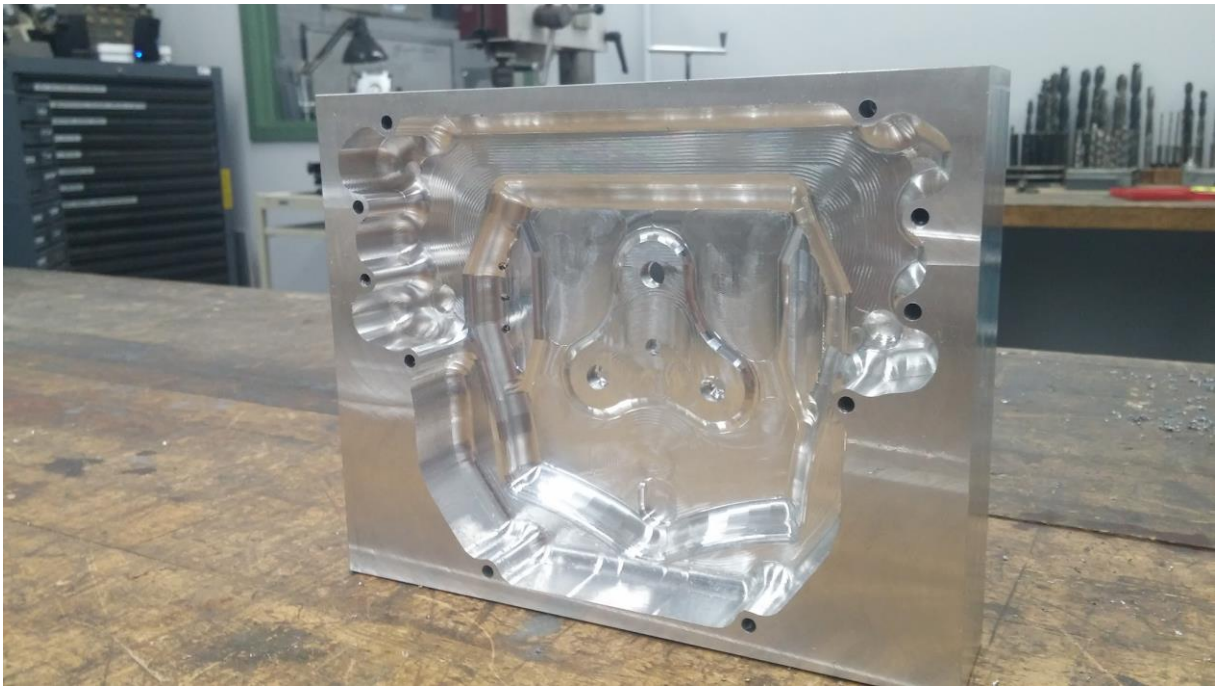

Figure 106: Finished Internal Section of the Back of the Steering Wheel

The part was bolted to a sacrificial plate from the underneath, and the remaining material was removed using similar operations to those used in the previous operation. The machined part can be seen in figure 107. The finished part was cleaned and then brought to a local company to be anodized red to improve surface toughness.

Figure 107: Finished Steering Wheel Back Plate

Connectors and switch parts

Manufacturing the Pogo-Pin Connector

The pogo-pin connector needed to mate with the slip plate connector inside the slip plate connector housing, which was mounted inside the steering spline. The diametric tolerancing needed to be within 0.001” of spec to allow for a close slip fit of components. The connector was turned to exact diameter, and then milled in two operations as seen in figure 108.

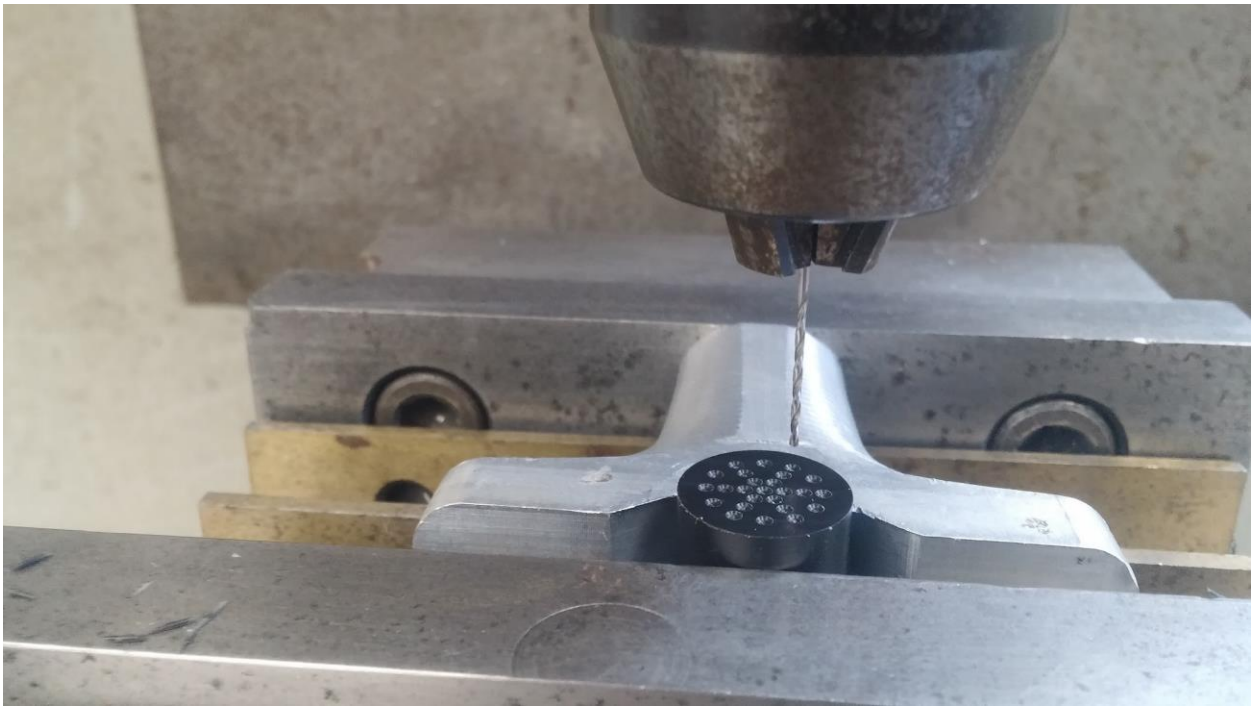

Figure 108: Pogo Pin Connector Drilling Operation

Integration with Slip Plate

The slip plate connector housing was machined and then pressed into the splined section and held with red loctite. The fitment between the housing and the connecter were check and confirmed to be a close slip fit. The system was then checked with the tapped connector being mounted to the wheel, and the quick release hub was used to drive the alignment of the system. The components meshed properly and the electrical connections were tested with positive results. The connector housing can be seen installed in the spline with the pogo-pin connector in figure 109.

Figure 109: Finished Pogo Pin Connector

Button molds and Button Manufacturing

Due to the entirely custom steering wheel, special buttons needed to be made to allow the driver to actuate all button controls including the paddle shift controls. The buttons on the front plate were chosen to be molded using an aluminum mold with epoxy being used as the part material. The main knobs were chosen to be 3D printed due to the complex geometry to reduce machining time. The bushings and buttons for the paddle shifters were turned manually from delrin to allow a self lubricating button that will not bind.

Brakes

Design Parameters

The brakes are a vital safety system for formula race cars. At the formula SAE competition out in Michigan one of the dynamic events evaluates the ability of the racecar to stop and lock up all four of its wheels at once. Knowing this our team design the brake system around these FSAE requirements to pass the brake event at the 2016 FSAE competition in Michigan.

Design

The brake system works off of hydraulic pressure produced by the compression of a master cylinder. This hydraulic pressure compresses a set of brake calipers which causes friction and stops the car. Using an iterative design process on Microsoft Excel a design sheet was set up with the necessary calculations to determine the forces on the braking system for a particular instance and easily compare and modify system parameters. The car was designed to have a 50/50 weight distribution in a static position. With a total weight of 550 pounds that puts a total of 275 pounds on the front and rear tires of the car. In a dynamic braking situation a portion of the weight is going to be transferred to the front tires of the car based on the center of gravity location. Knowing the relative mass, center of gravity height, wheelbase length, and expected braking deceleration in G's the team calculated the weight transfer onto the front wheels of the car during a lockup situation utilizing equation 3 below.

Equation 3: Weight Transfer

$$W_{transfer} = \frac{W_{total} * H_{CG} * F_{braking}}{L_{wheel\ base}}$$

$$W_{total} = Total\ Weight\ of\ car$$

$$H_{CG} = CG\ Height$$

$$F_{braking} = Intended\ Brake\ Deceleration$$

$$L_{wheel\ base} = wheel\ base\ distance$$

The effective weight acting on the front tires in a lock up situation is the sum of the static weight on the front tires and the weight transferred which was previously calculated. For the initial weight calculations the team determined an effective front wheel weight of 445 pounds. The effective weight acting on the rear tires of the car in a lock up situation is the difference between static weight acting on the rear tires of the car and the weight transferred onto the front tires. The team determined the rear wheels would experience a weight of 104 pounds

To ensure the brake components chosen were properly sized for the requirements of the car the required braking torques to completely lock up the wheels were calculated for the front and rear of the car. The car

is designed to use tires with a radius of 10 inches in the front and rear. With the effective weights on the front and rear wheels calculated above and a designed stopping force of 1.5 G's the team calculated the front wheel torque of 570 foot pounds and rear wheel torque of 134 foot pounds using equation 4 below.

Equation 4: Required Braking Torque

$$T_{wheel} = W_{effective} * R_{tire} * F_{braking}$$

$$W_{effective} = effective\ weight\ on\ the\ tires$$

$$R_{tire} = Tire\ Radius$$

$$F_{braking} = \ Intended\ Braking\ Deceleration$$

The proportion of the torque required to lock up the front and rear tires is 81 percent in the front and 19 percent in the rear. To properly lock up all four tires the actual brake bias of the system needs to closely match this initial proportion. The brake system consists of a brake pedal which applies a mechanical advantage to a set of master cylinders which build hydraulic pressure to compress the brake calipers. Since the brake system consists of components assembled into a series system and each component affects the next it was necessary to calculate the output rotor torque based on the force onto the brake pedal. Figure 110 below displays the system of equations used to determine the brake torque starting from the force applied to the brake pedal.

$$F_{out} = R_{pedal} * F_{in}$$

• Brake Pedal Output Force

- F_{out}= Force applied onto master cylinder
- R_{pedal}= The brake pedal lever ratio
- F_{in}= The force applied by the driver's foot onto the pedal

$$P_{line} = \frac{F_{out}}{A_{master_{cylinder}}}$$

• Master Cylinder Output Pressure

- P_{line}= The pressure in the brake lines
- F_{out}= Force applied onto master cylinder
- $A_{master_{cylinder}}$= Area of master cylinder piston

$$F_{clamp} = P_{line} * A_{caliper}$$

• Brake Caliper Clamping Force

- F_{clamp}= brake caliper clamping force
- P_{line}= The pressure in the brake lines
- $A_{caliper}$= Area of brake caliper piston (x2 for brake calipers with two pistons)

$$F_{friction} = F_{clamp} * \mu_{pad}$$

• Friction force of brake pads

- $F_{friction}$= The friction force from the brake pads
- F_{clamp}= brake caliper clamping force
- μ_{pad}= friction coefficient of brake pads (average brake pads= 0.4)

$$T_{brake} = F_{friction} * r_{rotor}$$

• Brake Torque

- T_{brake}= Torque applied by brakes
- $F_{friction}$= The friction force from the brake pads
- r_{rotor}= Radius of brake rotor

Figure 110: System of Equations for Brake System

A Microsoft Excel file was used to compute the system of equations listed above and results were compared for many brake component setups. Iterative design was used to examine and compare the performance of each setup with the required brake torque the team calculated earlier on in this section. Both the brake torque ratio and the torque values of the front and rear wheels of each setup were then compared to the required brake torques and proportions calculated earlier. The full excel sheet with the brake calculations can be found in appendix A.

Part Specification

The team chose to use two Wilwood compact remote flange master cylinders to package the brake system in the front of the car. A ¾ inch master cylinder was used for the front brakes and a ⅞ inch master cylinder was chosen for the rear brakes. For the brake calipers the team went with Wilwood Dynalite Single IIIA calipers for the front wheels and Wilwood PS-1 calipers for the rear wheels. This setup through the calculations gave a resultant brake torque of 558 foot pounds of force in the front and 134 foot pounds of braking torque in the rear. The brake distribution of the total braking torque was 80.5 to 19.5 which matched the required brake torque ratio of 81 to 19. On the brake pedal is a simple bias bar adjustment which allowed us to slightly adjust the brake performance.

System Integration and Assembly

To assemble the brake system the team carefully planned how to rout the hard and soft brake lines along the frame. The main objective was to minimize the required brake line length and number of line fittings needed since each additional connection could be a plausible failure point. Figure 111 below is top down diagram displaying the layout of the brake lines.

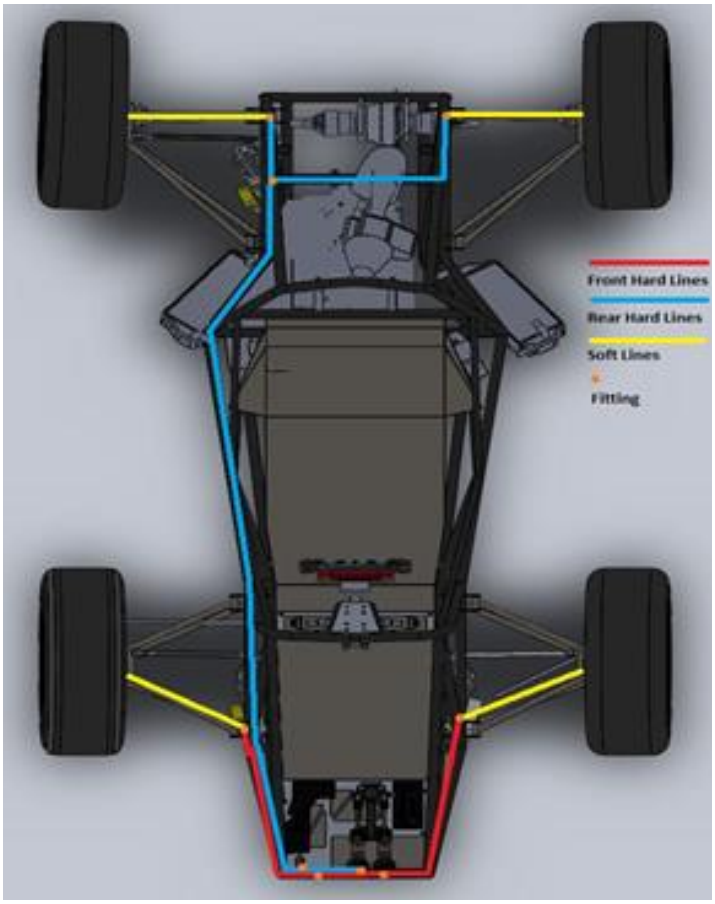

Figure 111: Brake Line Layout

To integrate the brake system into the driver telemetry system which monitors and records data on all of the driver's inputs as well as the behavior of the system two pressure sensors were installed in series in both the front and rear brake lines allow the team to monitor the pressure being applied onto the brake as well as determine if there is a fault in the brake system during testing if a pressure loss is observed. In locations where a hard brake line is connected to a soft brake line a tab was created on the frame as a hard mount for connecting the two lines.

Drivetrain

The drivetrain of the car is centered around the Yamaha YFZ450R engine package. The team decided this would provide the best results under the requirements of the car. With a 5 valve head and large aftermarket part market this engine is light, efficient and easily modified for power gains. The integrated 5 speed sequential shift transmission allows for easier packaging and reliability of the whole system without compromising the time needed to shift gears. In order to adapt the engine package to the vehicle, a final drive assembly was manufactured to transmit torque to the rear wheels. This utilizes a limited slip differential that can be adjusted to the handling requirements set by the suspension and steering systems. Fuel metering is handled by a custom EFI system based around the Haltech Elite 1500 ECU.

It was decided to not modify the internal components of the engine to improve reliability. The team had no prior experience with this motor, so modifications to performance could not be compared with a stock baseline. The timeline also did not allow for multiple dynamometer tunes. In the spirit of data collection throughout the vehicle systems, multiple sensors were used in addition to the standard EFI system provide future teams to better understand the YFZ450R.

Engine Packaging

The 2016 WPI FSAE chassis was specially designed to package the chosen engine. By minimizing unnecessary space around the engine the frame can be smaller, and therefore lighter. The factory engine mount locations are interfaced to three frame crossmembers using custom brackets. On the front of the motor, there are two nearly identical brackets on the left and right side that support front and bottom mount points on the motor to the two front engine mount tubes on the frame. These are slightly different shapes to account for packaging differences on either side. The two rear brackets are identical and connect the rear frame mount tube to the rear engine mount point. All four of the brackets utilize the same clamping methods to allow for engine alignment and ease of removal. On the frame side, the brackets mount to 1” frame tubes in the same way a two piece shaft collar would. The engine mount points utilize a simple rod through the engine block to clamp the brackets to the side of the engine.

Figure 112: Engine mounts (right) with differential carriers (2 parts on left)

Engine Systems

Fuel System

The fuel system is composed of three main components that deliver a constant fuel pressure to the engine intake. The fuel pump is packaged within the fuel tank to minimize the number of fittings that need to be connected to the tank. The third component is the single fuel injector, mounted in the intake runner. In a standard return style fuel system, the pressure regulator is mounted on the fuel rail and is connected to the intake manifold through a vacuum hose. The pressure differential across the injector is kept constant even as the pressure in the intake varies, which simplifies the calculations done within the ECU when it controls the injector. A return less fuel system has the pressure regulator mounted on the fuel pump output within the fuel tank. The single fitting on the tank output supplies a constant 47 psi which reduces the plumbing in the fuel system. While this does add another function the Haltech ECU must compensate for, it is well within its ability to do so. Mounting the fuel pump inside the tank does take up valuable space for fuel storage, however the advantages of this system are much greater. Since there is only one line connecting the fuel tank to the injector, less hose is needed. This reduces cost and pressure losses in the hose and less fuel is lost in the lines after the tank has run dry. The OEM fuel pump supplied by Yamaha for the YFZ450R was used since it is within the size, power consumption, and fuel supply requirements set by the design team.

The design of the fuel tank was driven mainly by operating requirements and packaging constraints. After researching the fuel economy of engines of similar size and type, efficiency scores from past FSAE competitions, and calculating theoretical fuel use rates for the engine, a minimum capacity requirement was set to 4.5 liters. A rough CAD model estimated the pump's volume to be .25 liters, which set the volume requirement of the tank model to 4.75 liters. From there, the fuel pump was packaged in the designated frame cavity and the tank designed around it to maximize internal volume. The first revision had a total volume of 5.2 liters without the fuel pump. Since this was well over the required value, the tank was shortened on one side to allow for better access to electrical connectors and the right engine mount adjustment screws. The second revision of the tank had a volume of 4.8 liters without the pump. This satisfied the requirements and manufacturing was completed by hydro-cutting and TIG welding 0.125" aluminum plates. The top panel of the tank had two holes CNC cut before welding, one for the fuel pump mount and one for the filler neck. Once the fuel tank assembly packaging had been validated in the frame, two rings were CNC milled to clamp the fuel pump to the tank. The lower ring was welded to the tank and featured 10 tapped holes for the pump retaining ring to mount to. This provided a rigid clamping force between the tank and the fuel pump without the need to drill and tap through the top of the fuel tank.

Two solutions were considered to prevent the fuel pump from losing its fuel source under high accelerations. First, a baffling system composed of fuel safe foam or internally welded baffles would prevent the fuel from moving around the tank at high velocities, while still allowing all of the fuel to sink to the pump pickup and tank drain as the tank is emptied. This would increase the cost and manufacturing time of the tank, as well as take up some of the limited volume inside the tank. The second method that was considered was a sump that would allow the pump to sit at the lowest point in the tank. This would

trap all remaining fuel in an almost empty tank. After studying the sump style pickup on the fuel pump and the packaging within the frame, the team decided on the sump type tank. The low hanging sump packaged the fuel pump nicely in the frame, and increased the volume of the tank, rather than decreasing it , and the same additional cost and time to manufacture as the welded baffle solution.

For initial engine testing, the OEM Yamaha YFZ450R fuel injector was used. During testing and intake runner design, it was clear this injector had little to no known operating values available to the team. With the possibility of making more than the manufacturer's intended horsepower or lower fuel economy, it was decided to purchase a new injector. A standard GM fuel injector was purchased through a discount from Five-O motorsports, who supplied the properly sized injector for our flow requirements and a datasheet of information needed by the Haltech to calculate the injector duty cycle. The injector was used in the design of the intake runner and fuel supply adaptor. A simple hose barb feeds the injector once installed, which is connected to the fuel pump output by ⅜" ethanol safe fuel hose.

Additional features of the fuel system include a fuel flow sensor, Schrader valve to measure fuel pressure, and a clear filler tube to see when the tank is filled to maximum capacity. The fuel flow sensor and pressure measurement port are located in line with the fuel feed hose between the fuel pump and the injector, and the filler neck is connected to the top of the fuel tank.

Fuel Tank Requirements

- Minimum fuel capacity of 4.5 liters
- Method to prevent fuel starvation under high accelerations
- Integration of YFZ450R fuel pump
- Method to drain all fuel from tank
- Mount to frame using nonrigid fasteners
- Must not contact seat pan
- Design for manufacture by welding of flat panels
- Must not leak under normal operation

Figure 113: Checking fuel tank for leaks

Intake Manifold

The intake manifold is a key feature in a powertrain, as it controls the amount of air that is allowed into the engine. The more air that can make it into the cylinder, the more power the engine can make. There are four main components to the intake manifold, the throttle body, restrictor, plenum, and runner. Each of these effects different properties of the manifold and must all be packaged and balanced in a way to provide maximum airflow under the designed RPM range. In order to limit the power of competition vehicles, Formula SAE requires a 20 millimeter circular restrictor be placed between the throttle plate and the intake port. In order to make the maximum power output under this restriction, the intake plenum and runners must be tuned to the RPM range used most during the autocross and endurance events. Since this is the first year WPI's formula team has worked with the YFZ450R, some assumptions must be made with regards to engine performance and fuel economy. Stock performance curves were found for the engine chosen, and compared with the expected speeds during competition. With the final drive and transmission gear ratios set by the engine manufacturer and packaging constraints, it was decided to increase the engine power in the 5500-6000 RPM range in order to provide a more linear torque curve and better fuel economy. Tuning in the 9000 RPM range would also increase the powerband of the motor and likely provide a greater maximum HP rating, however the fuel economy and reliability of the engine would be reduced.

The part that most significantly affects engine torque is the intake runner. During each intake stroke, a rarefaction wave is created at the intake port. This wave propagates down the intake runner until a large enough air mass reflects the wave back down the runner. In the case of the intake manifold, the intake plenum is the air mass and the length of the runner determines the time it takes for the wave to travel from the intake port to the plenum and back to the intake port. If the runner length is tuned such that this wave arrives at the intake valve the moment that it opens on the next cycle, the pressure at the valve can be raised above ambient pressure. By increasing the amount of air the engine can intake on each stroke, the engine torque can also be increased. The diameter of the intake runner can be determined based on the displacement of the engine and the maximum RPM of the engine. It was decided to use the same internal diameter throughout the runner length as the Yamaha throttle body, in order to reduce variations in flow. The length of the intake runner was determined based on the tuned RPM, speed of sound, and duration of intake valve opening. Equation shows that tuning to 5500 RPM requires an intake runner length of 5.25 inches. Since this number can be influenced by many factors such as intake port area, size of restrictor, shape of camshaft lobes, and intended RPM range of the engine, it was decided to manufacture the intake runner in a way that would allow changes in the length after tuning of the engine. Once these basic intake runner dimensions are determined, the runner can be designed to allow airflow to efficiently enter the intake valves. A simple bellmouth was added to allow efficient air flow from the plenum to the runner.

Equation 5: Tuned intake resonance RPM

$$\frac{speed\ of\ sound\ (720 - Intake\ duration)}{12 * (2n - 1)l} = Tuned\ RPM$$

The intake restrictor limits the maximum power of the engine by limiting the maximum rate that air can enter the engine. Maximum air flow, or choked flow, occurs when the velocity of the air through the restrictor equals the speed of sound. This can be easily calculated using the cross-sectional area of the restrictor and the speed of sound at operating air temperatures. It was calculated that a 450cc engine operating at 120% VE at 10,000 RPM would intake 0.0495 m^3/s of air. In a 20mm restrictor, this correlates to a mach number of 0.517, well below the limit of 1. Since this is an extremely high VE towards the top of the RPM range of the motor, choked flow should not occur during normal operation. In order to reduce the effect of the restrictor on intake performance, various restrictor cross-sections were considered to decrease the pressure loss across the minimum diameter. The most simple of these cross-sections is the converging-diverging restrictor. In this case, both sides of the restrictor converge towards the minimum diameter cross section point. A converging and diverging angle is determined that will best reduce the pressure differential across the restrictor. The paper "Space Advantage Provided by De-Laval Nozzle and Bell Nozzle over Venturi" shows that while a highly-efficient venture restrictor is possible, it is not feasible within most packaging constraints. This study shows that a highly-efficient restrictor can instead be manufactured using a de Laval nozzle on both the converging and diverging side of the restrictor that will reduce the packaging size without significantly reducing performance. After performing multiple iterations of flow simulation of various sizes and restrictions, a restrictor length and cross section could be determined that best fit the performance and packaging constraints.

Under current FSAE rules, there are two types of throttle control that are allowed. The first is a purely mechanical cable or linkage throttle control that connects the throttle pedal directly to the throttle plate. The second connects the throttle pedal electronically to an actuator in the throttle body which controls the position of the throttle plate. Electronic throttle-control (ETC) is, in principle, much more reliable and safer than a traditional mechanical throttle linkage. In a mechanical linkage, the ECU detects throttle position using only one sensor mounted to the throttle plate. It then determines fuel and ignition timing based upon this value along with the manifold air pressure and engine speed. When using ETC, the ECU requires two pedal position sensors along with two throttle position sensors. Each sensor must agree with its paired sensor, within a certain margin of error, in order for the driver to have control of the engine throttle. Should a failure occur within any of the four sensors, the throttle position defaults to 0%. This system has the added benefit of applying safety measures during certain implausible conditions, such as an object becoming lodged in the accelerator pedal causing a full or partial throttle condition while the brakes are being applied. In addition to the added safety measures, the ECU is aware of throttle movements in the before they happen and can correct for small changes in power demand such as necessary during idle. After considering the added benefits over a mechanical throttle, it is clear that ETC would increase the reliability and tuning range of the car.

The size of the throttle body was chosen based on the diameter of the throttle bore, availability of an electronic throttle body and the amount of modification needed to satisfy FSAE rules. In order to compete with an electronic throttle body, FSAE requires two forms of mechanical power that can independently return the throttle plate to shut, should a failure occur. Under ETC rules, this is typically satisfied by one return spring and one actuator. The bore of the throttle body was determined by measurement of the OEM Yamaha throttle body and a fluid calculation based on the displacement of the cylinder and maximum operating RPM of the engine. This was determined to be 1.875" inches in diameter. A Nissan/Denso

model throttle body was chosen because it was readily available and satisfied all size and functional requirements without any modifications.

The intake plenum was designed around the runner size, restrictor position, and the packaging with in the engine bay. Due to the position and orientation of the intake port on the engine, it was not possible to create an intake manifold that was completely linear. While this would be the most efficient way to reduce turbulence and pressure loss through the intake manifold, it would not fit within the packaging of the car. Since an efficient restrictor requires the lowest diverging angle possible, it was decided to mount the restrictor and throttle body above the intake port, and use the plenum volume to efficiently provide air to the runner entrance. Since the plenum has the highest cross-section throughout the intake manifold the sharpest turns can be made along the cross section centerline with the least energy loss. With the intake runner and restrictor set to definite size and shape and locations, the intake plenum went through multiple iterations of flow simulation to provide the most efficient manufacturable plenum possible. The final iteration of the intake plenum provided little to no additional pressure loss, and allowed for an increase in runner length without exceeding the roll envelope, defined as a straight line in the side view from the top of the main roll hoop and tangent to the rear tires.

Due to the widely organic shape of all intake manifold components, manufacturability was a concern throughout the design process. Initial revisions were designed to reduce pressure loss throughout the system and improve engine performance in the intended RPM ranges. Once the ideal shapes had been determined, they were modified to provide an easily manufacturable shape with minimal changes in pressure loss. The runner was split into two pieces, the injector holder/intake port entrance, and the bell mouth. Both pieces were machined from aluminum to resist degradation from fuel deposits. This two-piece design allows for modification of runner length through change in bellmouth parts without the remanufactured of the injector holder. The restrictor was also manufactured from aluminum, both through turning and milling. The throttle body is mounted to the restrictor entrance through a welded flange with a gasket between the throttle body and flange. A 3D printed restrictor was considered, however it was decided to use aluminum for added strength and tolerance since the throttle body is the supporting member for the entire intake manifold. The intake plenum was originally manufactured using 3D printed ABS, however readily available printers were not available to print the size plenum out of one piece. In order to reduce the number of joints and improve structural rigidity in the plenum, the final version was manufactured using fiberglass vacuum molded onto two CNC milled MDF mold halves. The two plenum halves were then glued together encasing the runner bellmouth and restrictor diverging end.

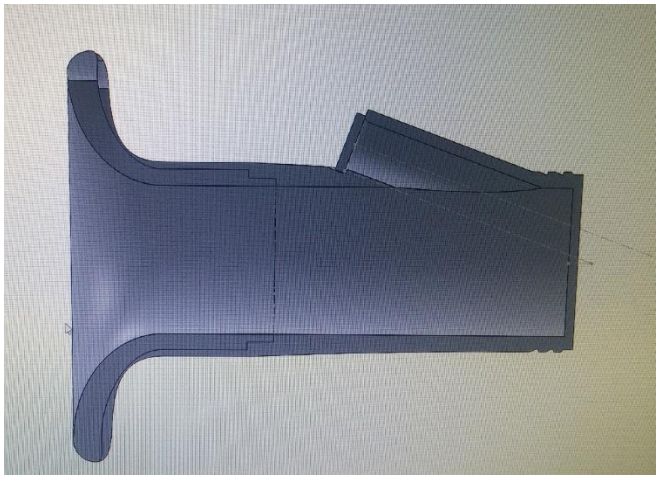

Figure 114: Intake bell mouth and runner design

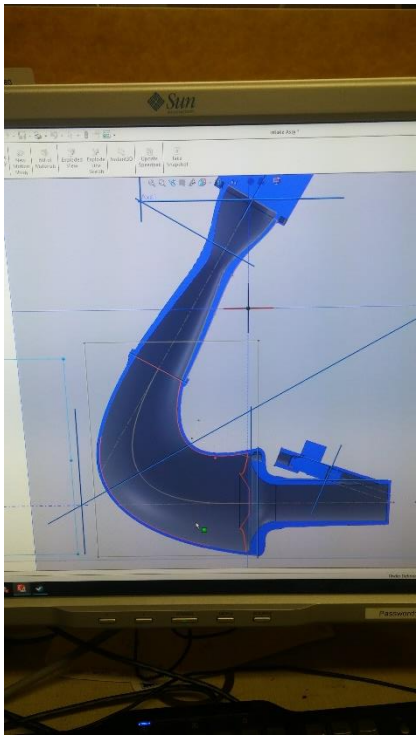

Figure 115: Intake designed for manufacturability

Intake Manufacturing

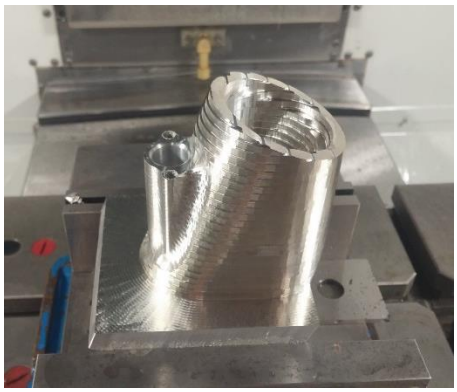

Figure 116: Intake runner operation 1

Figure 117: Intake runner operation 2

Figure 118: Intake runner operation 3

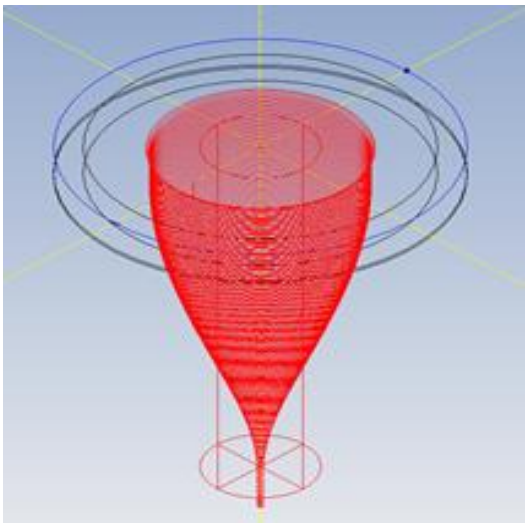

Figure 119: Tool Path for Mill Op

Figure 120: Positive molds for intake plenum

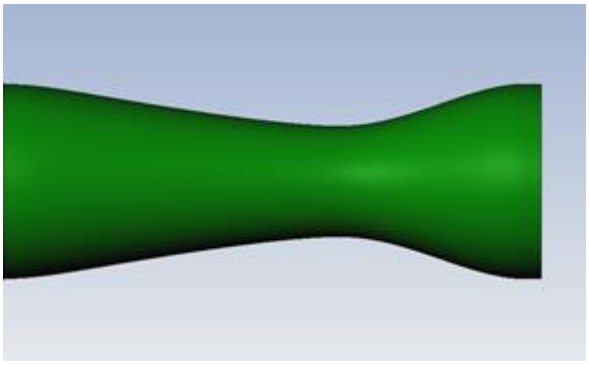

Figure 121: Simulation for Lathe Op

The restrictor was done using the ST30 as well as the VM2. Originally the plan was to use the lathe for the entire part however the length of the part as well as the minimum diameter required the use of a small

boring bar sticking far out from the holder. This caused unacceptable amounts of deflection and chatter as the inside of the restrictor had to be as smooth as possible for optimal air flow. Some of this chatter was due to the part and tool hitting resonant frequencies. To solve this problem, spindle speed variation was used to keep the part from resonating however this was not effective enough, although it did reduce the chatter. The final solution was a mill op to do the internal shape. Because the part was so tall it required us to put a vice on its side for fixturing and using a long ¾ Endmill to minimize deflection.

Figure 122: Fixturing for Mill op of Restrictor

The one problem however was tramming the part vertically so the hole would be in the proper location. After running both sides it was noticed that they appeared slightly off, but by an acceptable margin.

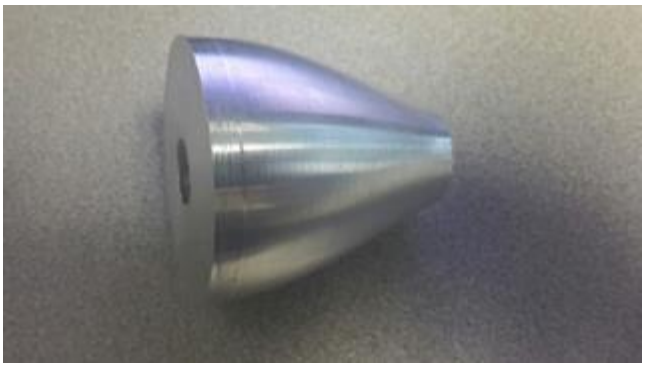

Figure 123: Restrictor Plug for Tailstock

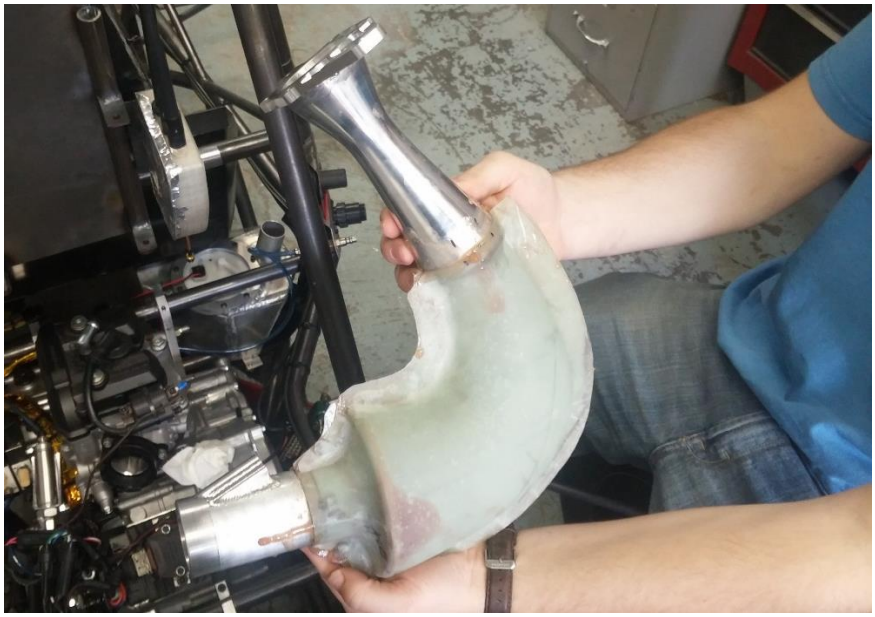

Figure 124: Intake assembly before painting

To run this long, now hollow part, on the lathe without having extreme deflection of the part the machines tail stock had to be used. However, since the part was hollow in a unique shape, a plug had to be machined to insert in one end for the tailstock to go into. There was some elastic deformation of the side being clamped however with the use of the tailstock the clamping force of the two was enough to hold the part straight and in place. With the use of the tailstock it is possible to make the walls much thinner and the restrictor much lighter.

Exhaust System

The exhaust system of an engine is just as important as the intake when it comes to power and efficiency, especially at the header and exhaust port. However, there were only so many modifications available to the team this year to improve the flow of the system. Packaging and material requirements drove the exhaust system, with some tuning available in the length of the runner.

In the same way the intake runner oscillates a rarefaction wave upon each intake event, the exhaust runner oscillates a positive going wave on each exhaust stroke. By tuning the size and length of the runner, a low pressure pulse can be timed to arrive at the exhaust port when it opens. This will remove more exhaust gasses than the engine is capable of punching out, leaving more room for fresh air and fuel in the next cycle. Since the exhaust port on the YFZ450R is located on the front side of the engine, the OEM solution is to use a u shaped tube to guide the hot gases toward the rear of the vehicle. During heavy operation, the exhaust header can reach temperatures exceeding 1000F. The OEM solution utilizes titanium for the first 18 inches of the header tube. This u shaped header could not be easily modified with the resources available to the team and since the inner diameter is within the ideal range for operation, it was decided that no modifications were needed. Tuning of the header length could be made by shortening the section of tube between the titanium header and the muffler. This length was limited to the legal location of the muffler, 17.5 inches behind the centerline of the rear axle, and a maximum of 23.7 inches off the ground. The steel section of the exhaust was also modified to accept a wideband O2 sensor for ECU fuel control.

The team had originally planned on testing multiple muffler types and sizes on the exhaust of the YFZ450R, however time and budget constraints did not allow this year. The OEM muffler was used since it was already in stock and satisfied the requirements of the FSAE rules.

Cooling System

FSAE rules require engines to use only distilled water in the cooling system, to prevent toxic spills, should a leak occur. Since the YFZ450R has a coolant pump built in, the only item that required design were the radiators, cooling fans, plumbing, reservoir and pressure relief valve.

Once the size and water flow of the radiator had been decided, radiators within the price and packaging constraints were researched. It was also decided to use a radiator with a standard pressure relief cap, to simplify the reservoir design. Multiple radiators were found, including an aftermarket generic radiator, OEM YFZ450R and the OEM WR450 radiators. Due to unavailability of engine data for cooling, only the stock radiators were considered. The WR450 radiators were chosen over the YFZ450R radiator since the YFZ450R uses one large radiator, with two smaller radiators being preferable for packaging with dual sidepods.

The specifications for the radiator fans needed to take the basic engine efficiency calculations into effect by allowing all heat energy to be dissipated by the radiators to simulate a worst case scenario. The below calculation in figure 125 displays the equations used.

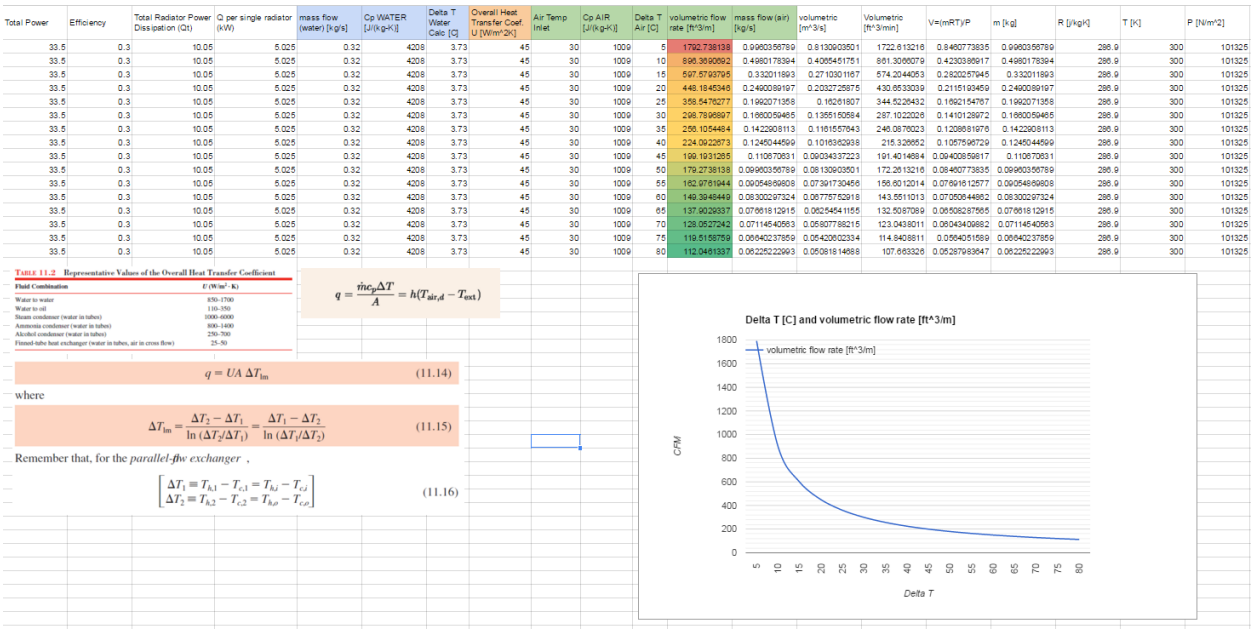

Figure 125: Radiator Fan Calculations

The total predicted engine power was set to 33.5kW, with 30% of engine power going to heat production. Basic heat transfer equations were used to determine the rate of airflow across the radiator that would be necessary to dissipate 10kW of power. This is the case of running the engine at peak power with no additional airflow (vehicle stationary) in a steady state condition. A factor of safety of 2 was used to select radiator fans to ensure proper vehicle cooling even under component failure. Two 150CFM fans were selected. With one fan running and only heat transfer being considered through that radiator, the air temperature would increase 60°C, which is acceptable since in nearly all cases the exit temperature will be much lower due to airflow due to vehicle movement and both radiators transferring engine heat with both fans running.

Tuning and Sensors

ECM choice

In an EFI setup, an ECM takes in data from engine sensors and calculates the amount of fuel and ignition timing the engine requires under every possible scenario. The most basic system requires an engine load source, throttle position sensor, engine RPM, and air and coolant temperature sensors. The engine load is derived from a manifold air pressure (MAP) or mass airflow (MAF) sensor. This information is coupled with engine RPM and air temperature to calculate the estimated mass of air entering each cylinder. The ECM then calculates how long to hold open the fuel injector for the requested air fuel ratio, and times it's opening according to the crankshaft position. The same is done with the ignition coil timing, which relies on the same inputs as the fuel timing source. Depending on the complexity of the ECM, engine type and performance requirements, many control strategies can be employed to provide increased fuel economy, torque, throttle response, etc.

The first step in tuning was to choose the ECM that would best suit the engine and vehicle combination. While the YFZ450R is a 4 stroke piston engine, it does not have a camshaft position sensor, only a crankshaft position sensor. This means the ECM can determine the crankshaft speed and exact piston location but not the stroke the engine is currently on (intake vs power stroke.) This is commonly used in smaller engines, or engine that do not need to meet strict fuel economy standards. The solution is to employ a method called wasted spark where fuel and ignition outputs that normally operate once every 4 strokes now operate every other stroke. The chosen ECM had to be able to operate under these settings, up to 10,000 RPM and provide many standard control strategies to allow the vehicle to be tuned to the fuel economy and power performance targets. Many ECMs, usually low cost ones, only provide the minimum required tables for engine tuning. These tables have a maximum size and resolution that suits most hobby engine tuners. Another important requirement for the ECM is the ability to communicate with the custom electronics designed for the 2016 FSAE vehicle, preferably through CAN bus. After researching aftermarket ECMs that fit the requirements of the vehicle, a few models had been narrowed down. Since the team had prior experience with Haltech's tuning software and positive experiences with their technical support, the Elite 1500 was chosen. This ECM meets every requirement and allows for many common tuning tables, including anti-lag, traction control, and electronic throttle.

Tuning

By the end of A-term, the engine had been mounted in a test stand, plumbed for coolant and fuel and wired to the ECM. Without having a MAF sensor calibrated to the anticipated airflow range, it was necessary to use speed density, or MAP sensor based tuning. In this method, the ECM predicts the density of the air in the intake manifold using the MAP sensor and air temperature sensor. Theoretically, every other engine revolution draws in exactly the displacement of the engine. In reality, flow resistance, gas inertia, resonance and mechanical limitations limit the amount of air that can enter the cylinder. Volumetric efficiency (VE) is a measure of how much air is actually entering the engine relative to the air in the intake manifold. If the air density in the cylinder at the end of the intake stroke is the same as the air density of the intake manifold, then the engine is at 100% VE. Speed density tuning utilizes aVE table to calculate how much air is actually entering the cylinder. This table uses the engine speed and MAP sensor readings, since those are the two conditions that most affect the VE of the engine. The VE values in this table are set by the tuner, and can reach over 100% under certain conditions. Using fuel and ignition tables from other YFZ450R tuners, a rough VE and timing table was setup. Basic settings were input to the Haltech, including base timing, engine size, type and, number of cylinders. The engine was cranked until a firing event occurred, and cranking fuel and timing were adjusted to allow the engine to start most reliably. Under initial testing, the engine started only once every few attempts at cranking. Many times it would simply backfire and continue cranking. It was later determined that the fuel and ignition settings were multi-point and distributor type which did not permit a wasted spark setup. After discussing with Haltech's technical support, they were changed to sequential for fuel and direct fire for ignition. This allowed the engine to startup almost every time, and more reliably once the cranking fuel and timing were adjusted further.

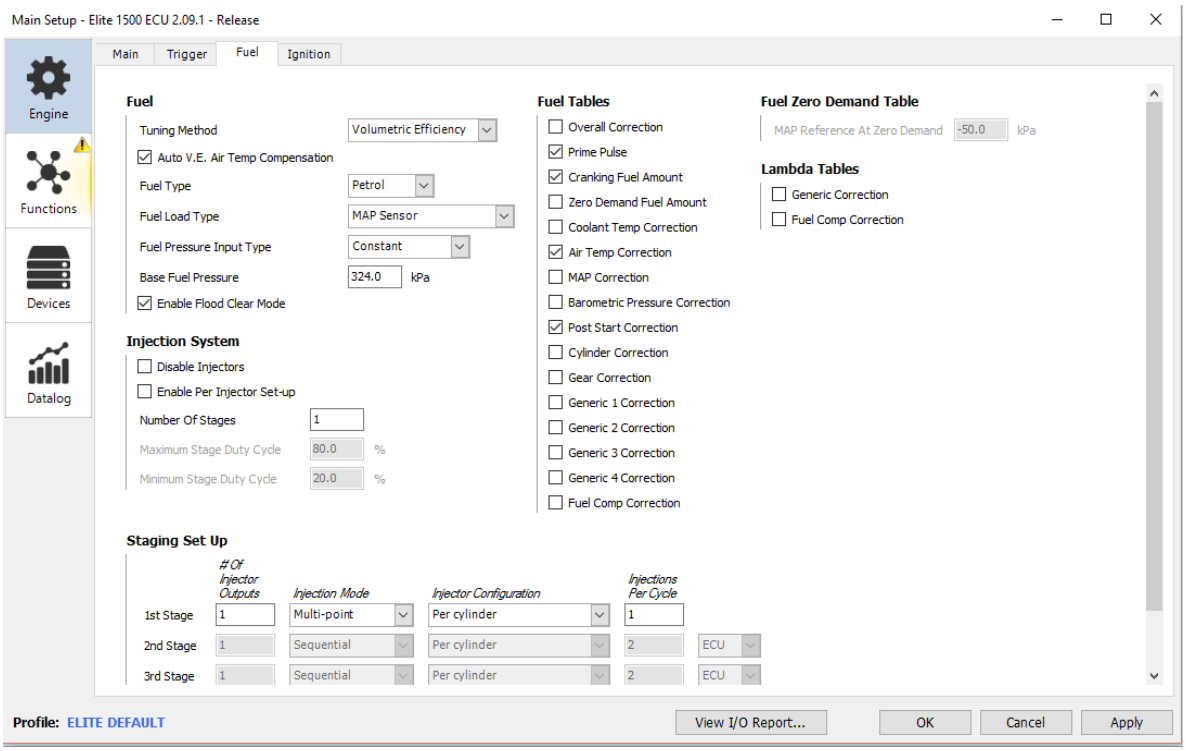

Figure 126: Initial (incorrect) fuel settings

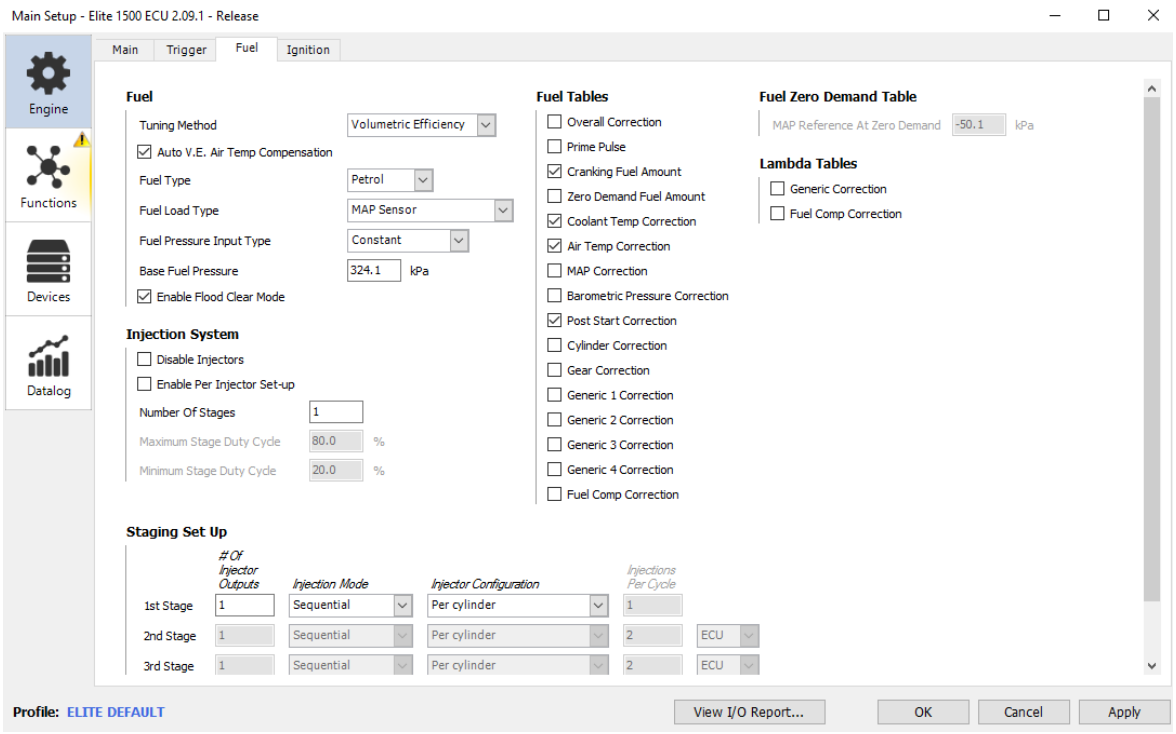

Figure 127: Correct fuel settings

Once the engine could be reliably started under hot and cold conditions, AFR measurements and mid load dynamometer tests were done. The o2 sensor, which measures the amount of oxygen molecules in a

mixture of gasses, was enabled in the ECM along with the long and short term fuel trim functions. This o2 control function allow a fuel table to be corrected to a better approximation of the volumetric efficiency of the motor. While the stoichiometric ratio of air to gasoline is 14.7:1 (air to fuel ratio, or AFR) it is almost always necessary to run the engine at a lower value under load, such as 12.5:1. This allows for some extra fuel to cool the internal engine components without significantly sacrificing fuel economy. Under light loads, the target AFR is significantly closer to stoichiometric, around 14.3:1. The o2 control function reads the amount of oxygen in the exhaust gasses to determine if the engine is running rich or lean. The ECM then compares this value to the target AFR from a table, and corrects the VE table accordingly. After just a few minutes of light to mid load running, the VE table was adjusted from figure 128 to figure 129.

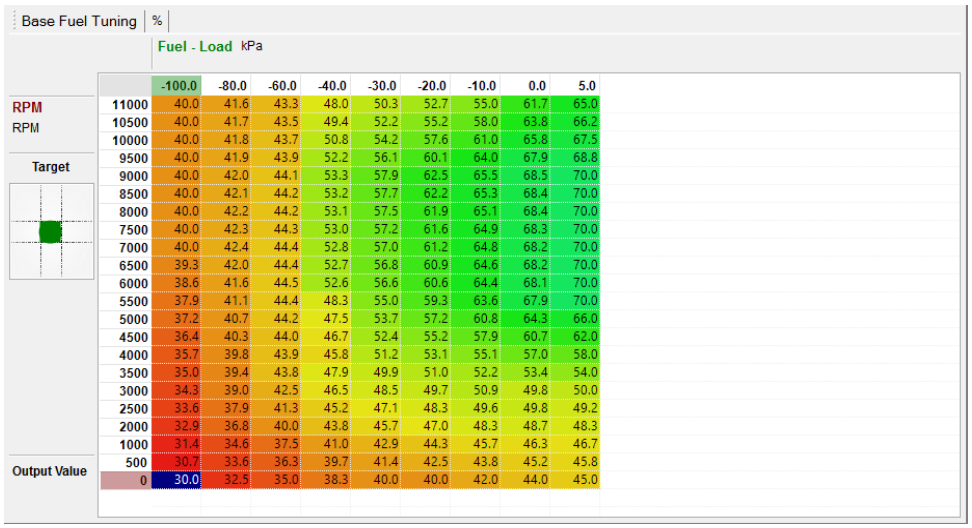

RPM \ Fuel - Load kPa	-100.0	-80.0	-60.0	-40.0	-30.0	-20.0	-10.0	0.0	5.0
11000	40.0	41.6	43.3	48.0	50.3	52.7	55.0	61.7	65.0
10500	40.0	41.7	43.5	49.4	52.2	55.2	58.0	63.8	66.2
10000	40.0	41.8	43.7	50.8	54.2	57.6	61.0	65.8	67.5
9500	40.0	41.9	43.9	52.2	56.1	60.1	64.0	67.9	68.8
9000	40.0	42.0	44.1	53.3	57.9	62.5	65.5	68.5	70.0
8500	40.0	42.1	44.2	53.2	57.7	62.2	65.3	68.4	70.0
8000	40.0	42.2	44.2	53.1	57.5	61.9	65.1	68.4	70.0
7500	40.0	42.3	44.3	53.0	57.2	61.6	64.9	68.3	70.0
7000	40.0	42.4	44.4	52.8	57.0	61.2	64.8	68.2	70.0
6500	39.3	42.0	44.4	52.7	56.8	60.9	64.6	68.2	70.0
6000	38.6	41.6	44.5	52.6	56.6	60.6	64.4	68.1	70.0
5500	37.9	41.1	44.4	48.3	55.0	59.3	63.6	67.9	70.0
5000	37.2	40.7	44.2	47.5	53.7	57.2	60.8	64.3	66.0
4500	36.4	40.3	44.0	46.7	52.4	55.2	57.9	60.7	62.0
4000	35.7	39.8	43.9	45.8	51.2	53.1	55.1	57.0	58.0
3500	35.0	39.4	43.8	47.9	49.9	51.0	52.2	53.4	54.0
3000	34.3	39.0	42.5	46.5	48.5	49.7	50.9	49.8	50.0
2500	33.6	37.9	41.3	45.2	47.1	48.3	49.6	49.8	49.2
2000	32.9	36.8	40.0	43.8	45.7	47.0	48.3	48.7	48.3
1000	31.4	34.6	37.5	41.0	42.9	44.3	45.7	46.3	46.7
500	30.7	33.6	36.3	39.7	41.4	42.5	43.8	45.2	45.8
0	30.0	32.5	35.0	38.3	40.0	40.0	42.0	44.0	45.0

Figure 128: Initial VE map

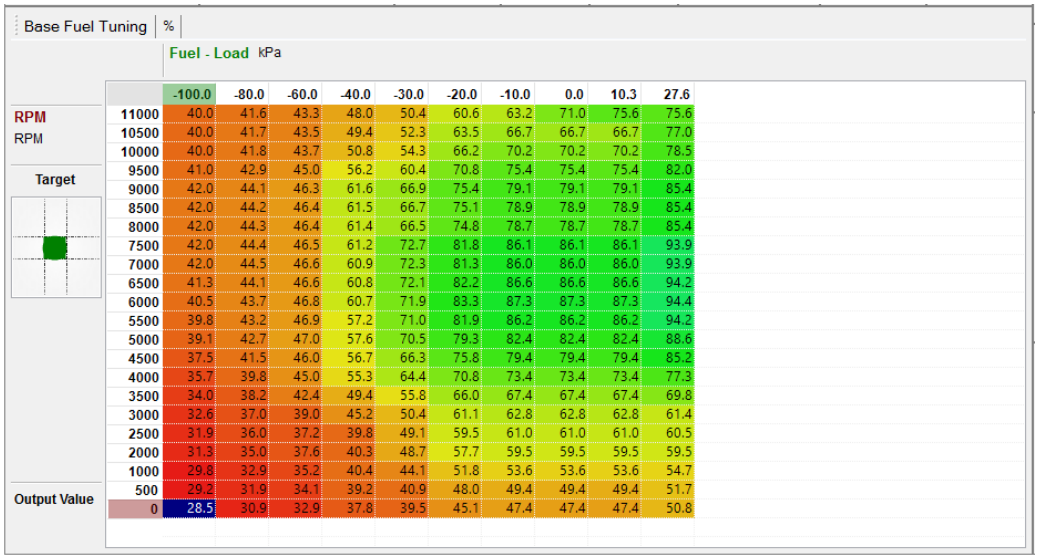

RPM \ Fuel - Load kPa	-100.0	-80.0	-60.0	-40.0	-30.0	-20.0	-10.0	0.0	10.3	27.6
11000	40.0	41.6	43.3	48.0	50.4	60.6	63.2	71.0	75.6	75.6
10500	40.0	41.7	43.5	49.4	52.3	63.5	66.7	66.7	66.7	77.0
10000	40.0	41.8	43.7	50.8	54.3	66.2	70.2	70.2	70.2	78.5
9500	41.0	42.9	45.0	56.2	60.4	70.8	75.4	75.4	75.4	82.0
9000	42.0	44.1	46.3	61.6	66.9	75.4	79.1	79.1	79.1	85.4
8500	42.0	44.2	46.4	61.5	66.7	75.1	78.9	78.9	78.9	85.4
8000	42.0	44.3	46.4	61.4	66.5	74.8	78.7	78.7	78.7	85.4
7500	42.0	44.4	46.5	61.2	72.7	81.8	86.1	86.1	86.1	93.9
7000	42.0	44.5	46.6	60.9	72.3	81.3	86.0	86.0	86.0	93.9
6500	41.3	44.1	46.6	60.8	72.1	82.2	86.6	86.6	86.6	94.2
6000	40.5	43.7	46.8	60.7	71.9	83.3	87.3	87.3	87.3	94.4
5500	39.8	43.2	46.9	57.2	71.0	81.9	86.2	86.2	86.2	94.2
5000	39.1	42.7	47.0	57.6	70.5	79.3	82.4	82.4	82.4	88.6
4500	37.5	41.5	46.0	56.7	66.3	75.8	79.4	79.4	79.4	85.2
4000	35.7	39.8	45.0	55.3	64.4	70.8	73.4	73.4	73.4	77.3
3500	34.0	38.2	42.4	49.4	55.8	66.0	67.4	67.4	67.4	69.8
3000	32.6	37.0	39.0	45.2	50.4	61.1	62.8	62.8	62.8	61.4
2500	31.9	36.0	37.2	39.8	49.1	59.5	61.0	61.0	61.0	60.5
2000	31.3	35.0	37.6	40.3	48.7	57.7	59.5	59.5	59.5	59.5
1000	29.8	32.9	35.2	40.4	44.1	51.8	53.6	53.6	53.6	54.7
500	29.2	31.9	34.1	39.2	40.9	48.0	49.4	49.4	49.4	51.7
0	28.5	30.9	32.9	37.8	39.5	45.1	47.4	47.4	47.4	50.8

Figure 129: Updated VE map

Definitions

AFR: Air fuel ratio

ATS: Air temperature sensor

CTS: Coolant temperature sensor

ECM/ECU: Engine control module/Engine control unit

MAP: Manifold air pressure

MAF: Mass air flow

VE: Volumetric efficiency

Final Drive

Yamaha yfz450r couples a racing performance engine with a high performance sequential 5-speed transmission. In the OEM application, this engine transmits its power to the ground through a chain drive to a differential, a solid rear axle or a single rear tire in the motorcycle application. With a simple sprocket output, it was decided to transmit this power to the wheels in the same fashion it would be in an ATV. In order to maximize the handling characteristics of the vehicle, it was obvious that a differential was necessary. Once the rear suspension type had been decided, the rear axles could be designed. These axles will transmit torque from the differential to the rear hubs, and further to the wheels.

Differential

A differential is a mechanical device that allows the driven wheels of a car to rotate at different speeds while allowing drive torque to still be applied. Many high performance cars utilize some type of limited slip differential, which only allows a certain amount of speed or torque difference between the two output shafts. On high lateral acceleration turns, the inside wheel may not be able to transmit all of the torque required to accelerate the car forward. In this case, the limited slip differential forces some of the drive torque to be transmitted to the wheel with more grip. In some cars, it is beneficial to omit a differential all together. This is called a solid rear axle, and is usually done for cost reduction and design simplicity.

Drive type	Cost	Value	Weight	Value	Durability	Value	Handling ability	Value	Tunability	Value	Total
Weighting	4		8		7		9		9		
Solid Rear Axle	9	36	9	72	7	49	2	18	1	9	184
Differential	5	20	5	40	6	42	6	54	3	27	183
LSD	2	8	4	32	4	28	9	81	7	63	212

Table 8: Comparison of differential types

Table 8 shows that in order to satisfy the tunability and handling requirements of the vehicle, a limited slip differential is necessary. There are many different methods of resisting differential rotation in a drive axle. The most common are clutch pack, viscous, and torsen which each have their own characteristics under various driving conditions. The torsen differential uses an intricate set of gears that allow different output shaft speeds, but only a limited amount of differential drive torque. Once one wheel begins to spin faster than the other, the differential begins to lock up. The greater the driving torque and differential speeds, the greater the lockup of the differential. The clutch pack type utilizes clutch plates locked to the output shaft that are forced against clutch plates locked to the differential housing. This type of differential remains locked until a large enough torque differential is applied between the output shafts. A clutch pack LSD benefits from the relatively easy replacement of worn out clutch packs, and the ability to adjust the torque at which the differential breaks free. A viscous differential uses a fluid, usually oil, to resist the differential shaft speeds. This design is similar to the clutch pack type, except it uses the resistive flow of oil between separated clutch plates, instead of contact friction. The lockup increases with differential output shaft speed, so the faster it slips the more it locks. Viscous differentials are usually more expensive and require a specific type of oil that needs to be changed often under heavy driving conditions. The design requirements for the differential state that the lockup amount, whether based on differential speed or torque, must be adjustable for the tuning of handling characteristics. The differential must also be robust under the designed drive torque for the entire length of the endurance event, and within the budget of the vehicle. The clutch pack differential from the front axle of the Honda TRX350 was chosen because it fell within the designed drive torque of the vehicle, had easily adjustable clutch pack preload, and did not cost anything since it was already in stock.

In the OEM application, this differential is installed within a sealed case and is driven by a mitre gear pinion. In order to preserve the lifetime of the clutch packs, and ensure the differential operates as intended, a sealed case had to be designed that would accept the chain drive used in the car. In order to best interface with the differential output, the OEM axles and seals were purchased and CAD models were created of all components. It was decided to manufacture the case from 6061-T6 5" round aluminum since it was readily available, and the necessary features could be easily machined within WPI's facilities. The case needed to assemble onto the differential and interface with the deigned faces on the differential housing. It also needed to be mounted between bearings on the car, and spin to the RPM of the wheels at maximum vehicle speed. This required two balanced case halves, with some type of seal between them. The output shaft seals were also required to be fixed in the correct position, concentric to the differential centerline and spaced axially from each end of the differential. It is also crucial that the drive torque does not stress the housing in a way that would allow a sealing surface to leak. After careful packaging of the differential gear assembly within the housing, it became possible to clamp the housing on the surfaces that would normally interface with the bevel gear. This would allow for sufficient torque transfer to the differential gears, while also increasing the rigidity of the housing. One housing half was designed to fit inside the other, so an o-ring could be used to seal the joint.

After considering the transmission gear ratios, competition speeds and the torque curve of the motor, an ideal range of final drive ratios was determined. Packaging constraints in the vehicle showed that the largest possible sprocket would be a 38 tooth, which fell at the lower end of the ideal range. Since a sprocket with the correct number of teeth was in stock, a simple sprocket adapter was manufactured to adapt this part to the bolt pattern on the differential case.

Differential Manufacture

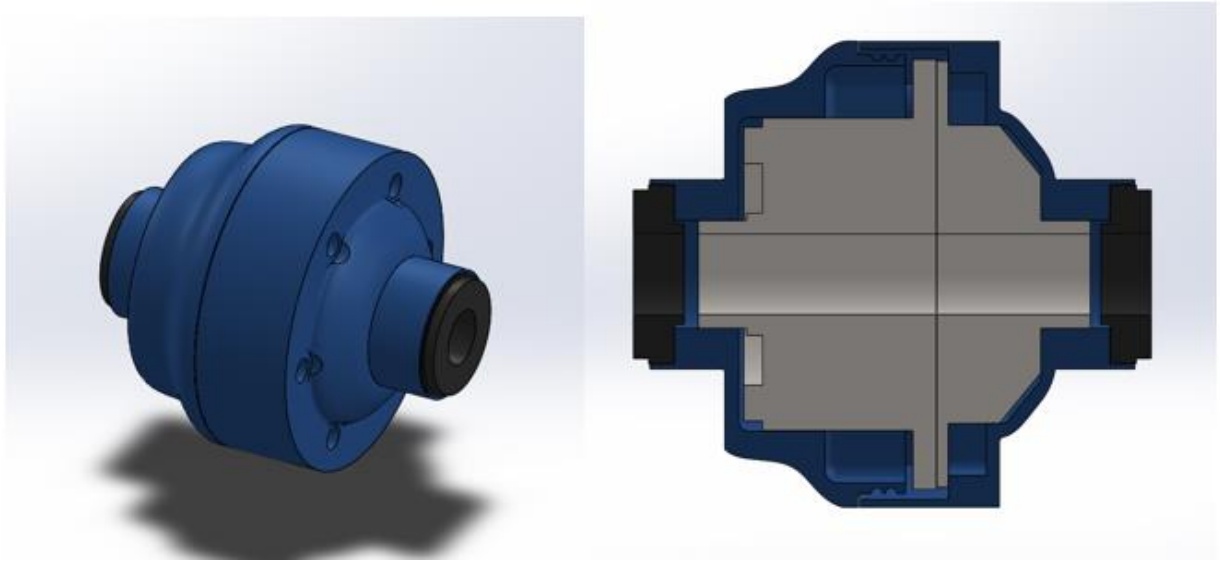

Figure 130: Differential Case and Section View

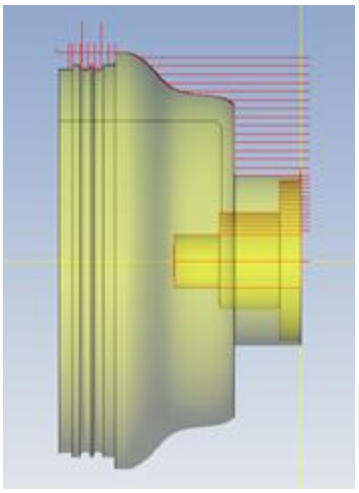

Figure 131: Lathe Tool Path for Large Diff Case

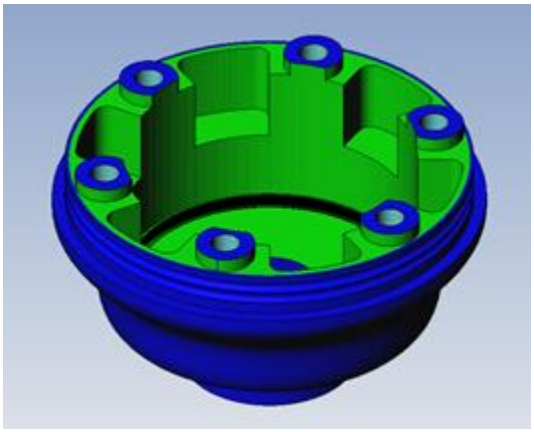

Figure 132: Mill Simulation for large diff case

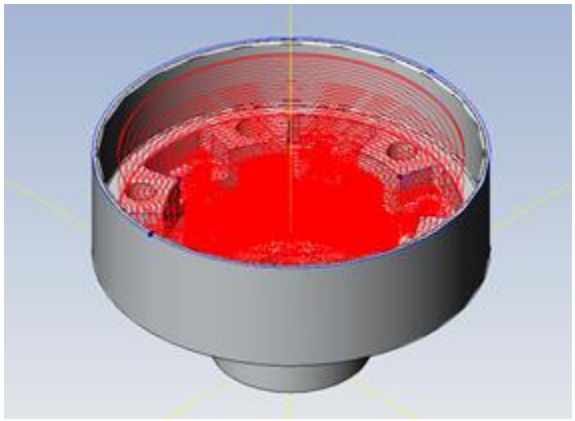

Figure 133: Mill tool path for Small Diff Case

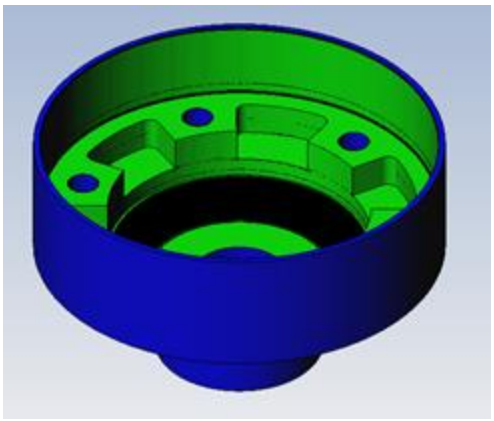

Figure 134: Mill Simulation for small diff case

Both sides of the differential were made using one lathe operation on the ST30 as well as 2 mill operations using the VM2. The softjaws already made for the ST30 were reused. A left handed 35 degree turning tool was used to make the groves on the larger half of the diff. More of the softjaws had to be machined down to ensure there was enough clearance while still being able to hold on to the part. During the mill operation a three jaw chuck insert in the mill with pre-existing soft jaws however the clamping force was insufficient causing the part to pull out and crash.

Figure 135: Crashed Diff

Figure 136: 11. Broken Jaws

Softjaws were made in order to hold the piece with enough clamping force in order for the peace not to pull out of the vice as well as the operations themselves were made much more conservative as the part was very top heavy with a large moment around the outside (dropping depths of cut, step overs and feeds all by at least 25%). After this was done the parts came out fine, the only areas with some concern were the internal pocket corners being the same size as the ¼ EM that was used causing for large spikes in load on the tool which is potential for breaking the tool.

Half Shafts

In the TRX350 application, the differential is set slightly off center to allow for the drive shaft to pass from the rear to the front of the engine. This means the two output shafts are different lengths. After researching the possibility of cutting custom splines, it was decided to purchase two of the longer Honda half shafts. These shafts could be easily extended, and require much less manufacturing time with increased reliability over custom shafts. The longer of the two half shafts was slightly shorter than the shortest requirement on the car, which allowed for maximum support once the axles had been cut and extended. Multiple methods were considered to extend the axles, with varying levels of reliability and manufacturability. It is widely accepted that a round tube is the lightest and strongest method of transmitting torque. The size of this tube was chosen based on the diameter of the half shafts, the range of torque that needs to be transmitted and the method of manufacturing for reliability and weight savings. The extensions pieces were to be turned using tools readily available in the Higgins machine shop. The sections to be pressed onto the half shafts, which have a diameter of 0.73”. The ID of the tube must be a nominal size smaller than this, so it can be accurately bored to an interference fit tolerances using a boring bar. The OD of the tube must be sufficiently greater than the half shaft diameter, so a method of rigidly connecting the two in the overlapping section is possible. The OD of the shaft would be turned down in just the center section to reduce weight. This center section OD was specified to transmit the maximum output torque of the engine (35 ft-lb), since this could value be possible in just one shaft under extreme cornering conditions. The maximum stress in a tube under torsion can be found using the following equation:

Equation 5: Maximum Stress

$$\sigma = \frac{Mc}{I} \text{ where } I = \frac{\pi}{2} \times (r_o^4 - r_i^4) = \frac{\pi}{2} \times (r_o^4 - r_i^4)$$

Since the tube will be manufactured from chromoly steel, a yield strength of 63.1 ksi can be used. With the exception of the section that will be press fit onto the existing half shafts, the ID is chosen to be 0.625". The value c is chosen at the maximum stress location, r_o in the case. In order to simplify calculations, an OD of 0.75" was chosen first. Entering this information into the formula:

Equation 6: Moment of Inertia

$$I = \frac{\pi}{2} \times (0.375in^4 \quad - 0.3125in^4) = 0.01608in^4$$

Equation 7: Stress

$$\sigma = \frac{Mc}{I} = \frac{420in - lb \times 0.375in}{0.01608in^4} = 9793psi$$

Equation 8: Factor of Safety

$$FOS = \frac{Yield\ Strength}{Maximum\ stress} = \frac{63.1ksi}{9.793ksi} = 6.44$$

While a small amount of additional weight savings could be found by further reducing the OD, a thinner wall section would reduce the rigidity of the tube and subject it to greater vibrational stress at high wheel speeds. The transition from the hollow tube extension section was manufactured to reduce stress on the part. Fillets on changes in diameter and overlapping sections so no part of the wall thickness is less than the hollow section ensured no stress concentrations would take place. The final overall length of the two completed axles were manufactured to allow the tripod joint to sit in the center of its range at ride height. Multiple methods of torque transmission were explored to connect the half shafts with the extension tube. One such method discussed was using welds to connect the two parts, either radially at the end of the tube or in plug welds through holes in the tube wall. Another method used, a pin, or set of pins, pressed into holes cross drilled in the two parts. Ultimately, it was decided to use plug welds through the tube wall. While this method permanently connected the parts and risked damaging the rubber boots, proper precautions were taken to ensure the shafts were not overheated and remained straight and balanced. The set of six evenly spaced plug welds into each half shaft end was completed without issue. Calculations in equations 9 through 11 were done to determine the size and number of welds necessary to safely transmit torque through the interfacing section. The size of the plug hole is recommended to be greater than or equal to two times the thickness of the material. Since the wall thickness at the interfacing section is 0.125 inches, a minimum hole diameter of 0.25 inches was necessary. Since the thickness of the half shaft stub

is significantly greater than the thickness of the tube wall, a hole diameter of 0.3125 inches was used. The minimum number of welds could then be determined using the following formulas:

Equation 9: Area of Weld

$$A_{weld} = \frac{i \times \pi \times d^2}{4} = \frac{i \times \pi \times 0.75in^2}{4}$$

Equation 10: Force on Weld

$$F = \frac{420in - lb}{0.375in} = 1120lb$$

Equation 11: Strain

$$\tau = \frac{F}{A_{weld}} \qquad \tau = \frac{\tau_{yield}}{FOS} = \frac{80ksi}{10} = 8\ ksi$$

$$8000\ psi = \frac{1120lb}{0.25 \times i \times \pi \times 0.5625in^2}\ i = 0.32$$

While this estimation shows only about one third of one weld is needed on each end to provide a factor of safety of 10, it was decided to use more welds in the final product. At least one weld on both sides of the tube were recommended to balance out each other. Two more pairs of welds were added to each end to compensate for the potential for poor weld qualities, and the unknown half shaft alloy. The final product used six welds on either half shaft stub.

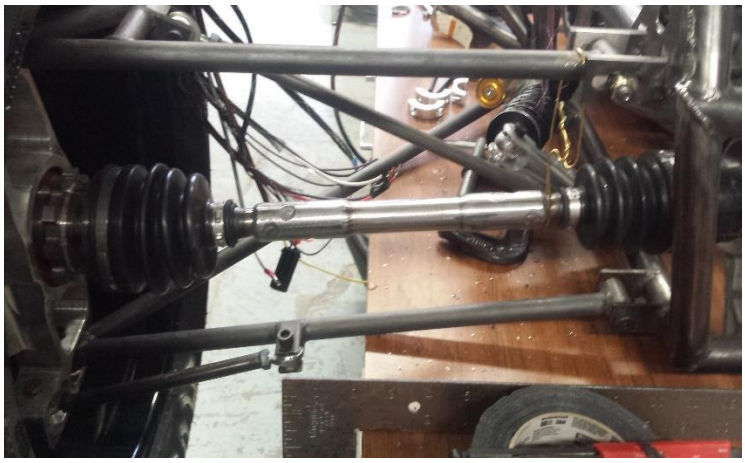

Figure 137: Left axle with welded extension

Rear Hubs

The rear hubs were designed in parallel with the front hubs, since they are the main interface between the suspension and the tire. In order to simplify manufacturing, the rear hubs were created identical to the front hubs, with the exception of the wheel bearing preload hardware and the addition of a torque transmission method. Besides supporting the rear of the vehicle, the rear hubs must also transmit the drive torque to the wheel. Since the half shafts had been specified to be sourced from a Honda TRX350, the

outer CV joint spline had to be interfaced with the hub. After calculating the stress on each spline tooth in the 6061-T6 hub, it was determined that a splined hub would be more than strong enough for the highest drive torque. However, there was no readily available method of creating a female spline in the hub. Since most alternative CV joints would have a similar output spline and would complicate the manufacture of the axle extensions, the team decided to stick with the TRX350 CV joints. Therefore, a practical method of creating a spline in the hub was necessary. After studying the tooling available to the team, it was decided to use the TRX350 wheel hub to interface with the axle spline. The central part of the two hubs were then machined to a spline shape that could also be machined in the hubs. This shape is essentially 0.28in diameter circles equally spaced around two slightly different diameter patterns. This way, a 0.25in endmill, a commonly available tool, could be used to manufacture each piece. The steel spline insert is held into the hub by friction from an interference fit, and spiral snap ring. This spline provided more than enough surface area on each part to prevent shearing of the splines. The method of failure for this spline would likely be through stretching of the hub as torque is applied to the rounded spline teeth. However, the hub is completely encased in this region by the wheel bearing, so no yielding should occur.

Figure 138: Rear hub spline design with steel spline insert installed

Chain Drive and Tensioner

After the differential, axles and engine had been aligned in the CAD model, the chain drive could be designed. The chain must be aligned between the engine and differential sprockets. Since the team are using ATV type o-ring chain, no half links are available. Therefore a method of tensioning the chain is needed. Another issue that arose was the alignment of the engine with the rear frame tube. The height of the engine sprocket and the size of the final drive sprocket placed the chain just tangent to the rear frame tube. In order to keep the chain from running along the tube, a guide had to be manufactured. Black delrin was machined into the curve that most gently guided the chain below the frame tube. The guide was fixed to the tube using the same shaft collar method as the engine mounts.

Figure 139: Chain guide

With the guide taking up most of the length of the top section of chain, the tensioner was packaged on the bottom of the chain. Due to the lateral location of the chain relative to the bottom suspension pickup frame tube, a simple steel arm could be machined and welded to the frame tube. This would allow a spring tensioned arm to be mounted to it. The arm length and neutral position was determined based on the idler sprocket diameter and length of chain that needed to be tensioned. Initially the tensioner was designed using a maximum deceleration engine torque, since this is the only time the bottom chain is in tension. However, initial testing while driving and on the dyno showed that a stronger tensioner was required. It was decided to manufacture a bracket mounted to the idler support bolt on the opposite side of the tensioner arm. This bracket was then connected to an arm mounted on the frame tube above the chain using a 5/16-18 bolt. This bolt provided a fixed adjustment of the tensioner arm position.

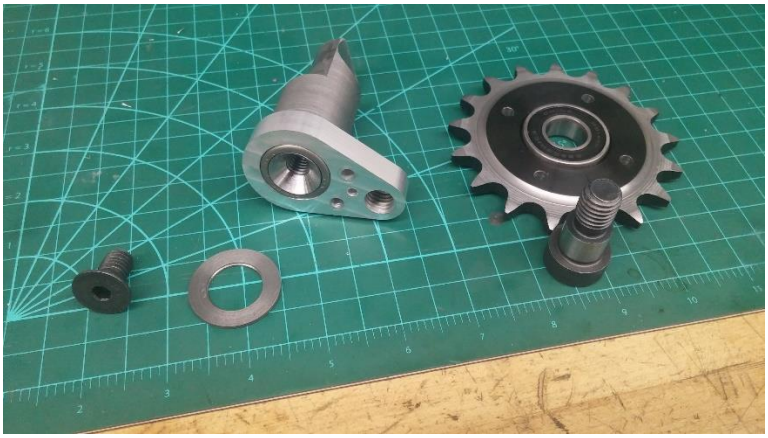

Figure 140: Chain tensioner parts

Transmission and Pneumatics

One of the most competitive features of the YFZ450R is the 5 speed sequential shift transmission. In order to get the lowest potential shift times, it was decided to use a pneumatic shift system powered by a compressed air tank. This system would add less than 10lb to the car, and would allow for semi-auto or full automatic shifting when paired with the electronic modules that were developed in parallel. Force and travel measurements were taken of the clutch and shift shafts to determine the smallest pneumatic actuators that could be used reliably. The smaller the actuators, and the less often they are used, the longer each air tank will last.

The pneumatic cylinders were selected by using the measured torque and rotation needed for actuation, and optimizing the output arm length based upon nominal bore and stroke dimensions. The system was defined to operate under normal conditions at 100 psi, yet a lower pressure of 80 psi may be used during the endurance event to save power. Figure 141 shows the clutch cylinder calculations with the yellow row containing the selected cylinder. The initially selected cylinder (in stock) was shown in the dark orange row, which was not selected due to its excessively large size and volume.

	Clutch Cylinder								
	80 PSI Regulated								
	Bore	Area	Pressure	Force (Linear)	Arm Length Needed	Rotation	Stroke	Torque(inlbs)	FOS
	0.5	0.19625	80	15.7	2.229299363	0.645771823	1.341625848	35	1.0
	0.625	0.306640625	80	24.53125	1.426751592	0.645771823	0.8586405426	35	1.0
	0.75	0.4415625	80	35.325	0.9907997169	0.645771823	0.5962781546	35	1.0
	0.875	0.601015625	80	48.08125	0.7279344859	0.645771823	0.4380819095	35	1.0
Selected Cylinder	0.875	0.601015625	80	48.08125	1.59	0.645771823	0.9568858868	76.4491875	2.2
	1	0.785	80	62.8	0.5573248408	0.645771823	0.3354064619	35	1.0
	1.125	0.993515625	80	79.48125	0.4403554297	0.645771823	0.2650125131	35	1.0
	1.25	1.2265625	80	98.125	0.3566878981	0.645771823	0.2146601356	35	1.0
Stock Cylinder	1.25	1.2265625	80	98.125	3.18	0.645771823	1.913771774	312.0375	8.9
	100 PSI Regulated								
	Bore	Area	Pressure	Force (Linear)	Arm Length Needed	Rotation	Stroke	Torque(inlbs)	FOS
	0.5	0.19625	100	19.625	1.78343949	0.645771823	1.073300678	35	1.0
	0.625	0.306640625	100	30.6640625	1.141401274	0.645771823	0.6869124341	35	1.0
	0.75	0.4415625	100	44.15625	0.7926397735	0.645771823	0.4770225237	35	1.0
	0.875	0.601015625	100	60.1015625	0.5823475887	0.645771823	0.3504855276	35	1.0
Selected Cylinder	0.875	0.601015625	100	60.1015625	1.59	0.645771823	0.9568858868	95.56148438	2.7
	1	0.785	100	78.5	0.4458598726	0.645771823	0.2683251696	35	1.0
	1.125	0.993515625	100	99.3515625	0.3522843438	0.645771823	0.2120100105	35	1.0
	1.25	1.2265625	100	122.65625	0.2853503185	0.645771823	0.1717281085	35	1.0
Stock Cylinder	1.25	1.2265625	100	122.65625	3.18	0.645771823	1.913771774	390.046875	11.1

Figure 141: Clutch Cylinder Calculation Table

The shift cylinder was calculated in the same manner as the clutch cylinder. A 7/8" bore with a 1" stroke single acting cylinder was chosen for the clutch cylinder, as it retained a factor of safety of 2.2 at 80 psi, and could therefore safely operate at 40 psi to allow several operations under compressor failure to allow the vehicle to safely exit the track. The shift cylinder that was selected as seen in figure 142 was a ¾" bore with a 1" stroke double acting, with ½" stroke being used to shift up or down from the neutral position.

	Shift Cylinder									
	80 PSI Regulated									
	Bore	Area	Pressure	Force (Linear)	Arm Length Needed	Rotation	Stroke (Up/Down)	Stroke (Actual)	Torque(inlbs)	FOS
	0.5	0.19625	80	15.7	3.694267516	0.1308996939	0.4821986719	0.9643973438	58	1.66
	0.625	0.306640625	80	24.53125	2.36433121	0.1308996939	0.30860715	0.6172143	58	1.66
	0.75	0.4415625	80	35.325	1.641896674	0.1308996939	0.2143105208	0.4286210417	58	1.66
Selected Cylinder	0.75	0.4415625	80	35.325	1.932	0.1308996939	0.2521766034	0.5043532067	68.2479	1.95
	100 PSI Regulated									
	Bore	Area	Pressure	Force (Linear)	Arm Length Needed	Rotation	Stroke	Stroke (Actual)	Torque(inlbs)	FOS
	0.5	0.19625	100	19.625	2.955414013	0.1308996939	0.3857589375	0.771517875	58	1.66
	0.625	0.306640625	100	30.6640625	1.891464968	0.1308996939	0.24688572	0.49377144	58	1.66
	0.75	0.4415625	100	44.15625	1.313517339	0.1308996939	0.1714484167	0.3428968333	58	1.66
Selected Cylinder	0.75	0.4415625	100	44.15625	1.932	0.1308996939	0.2521766034	0.5043532067	85.309875	2.44

Figure 142: Shift Cylinder Calculcation Table

The system was originally designed to operate from a 3000 psi paintball tank which was regulated to 100 psi. As seen in figure 143, the system could theoretically operate for 1064 shift cycles, which included an upshift (no clutch) and a downshift (clutch and shift). Due to the potential for rapid operation of the shift and clutch cylinders, the main air tank would both not be able to properly supply regulated air and would experience a temperature drop. A ballast tank was added to the system to store regulated air for immediate use, and testing proved the tank to hold enough air to operate the clutch and shift cylinder ten times. The temperature drop during rapid usage remained an issue due to the decreased system efficiency at lower temperature. A worst case scenario of 60% efficiency was used to predict a total of 638 shift cycles, or 29 cycles per endurance lap. The calculations can be seen in figure 143.

Storage Pressure	3000	psi	
Storage Volume	37	in^3	
Operating Pressure	100	psi	
Up/down shift volume (1/2 shift piston)	0.220893	in^3	
Clutch Volume	0.60132	in^3	
Volume per shift	1.043106	in^3	1 up +1 down + 1 clutch
Max number of shifts	1,064.13	shifts	Theoretical, no pressure/temp loss, etc
60% system efficiency	638.48	shifts	
22 laps in endurance	29.02	shifts per lap	

Figure 143: Pnuematic System Overall Calculations

Lap simulator software calculated 30 shift cycles per lap, with a minimum of 20. A slim margin drove a system redesign. A compressor was selected to provide at least twice the necessary airflow at the desired pressure (0.0077CFM at 100psi). The smallest readily available compressor was able to provide this flowrate at 20% duty cycle.

Bodywork

Design Parameters

The design parameters of the bodywork are focused around safety and accessibility of the system components and driver.

Safety:

- Have no sharp forward facing edge
- Close out the drivers cockpit
- Reduce foreign object damage in the engine compartment
- Protect the radiators from FOD

Accessibility:

- Be removable without modification of other parts of the car
- Not restrict airflow to the radiators
- Easily interface and mount to the car
- Easily interface and mount to the undertray

With these design parameters satisfied, the remaining design choices were made with aesthetics in mind. Aerodynamic considerations beyond basic visual streamlining were ignored given a lack of time and resources to make well informed changes in the bodywork to reduce drag.

Design

The bodywork was designed in SolidWorks with three lofted surfaces on one half of the car, each mirrored about the centerline plane. The primary surface from the nose cone to the rear engine cover is referenced as the main bodywork, while the sidepods and nose cone cap form the additional two surfaces.

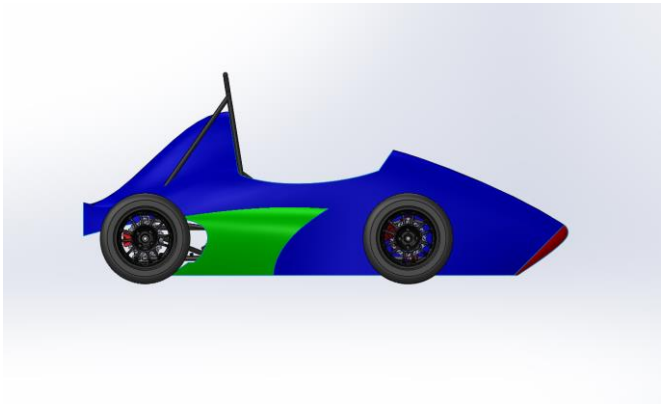

Figure 144: Bodywork Design

Main Bodywork

The main bodywork is a single lofted surface with surface trims around the cockpit opening and rear suspension. This surface was formed from a series of cross sectional curves contoured to the frame. The upper guide curve forms the upper contour of the bodywork at the center plane. The lower guide curve was sketched offset to the ground plane in order to interface with the unknown ride height of the undertray. The ground-facing surface of the bodywork was left open, as this area would be closed out by the undertray.

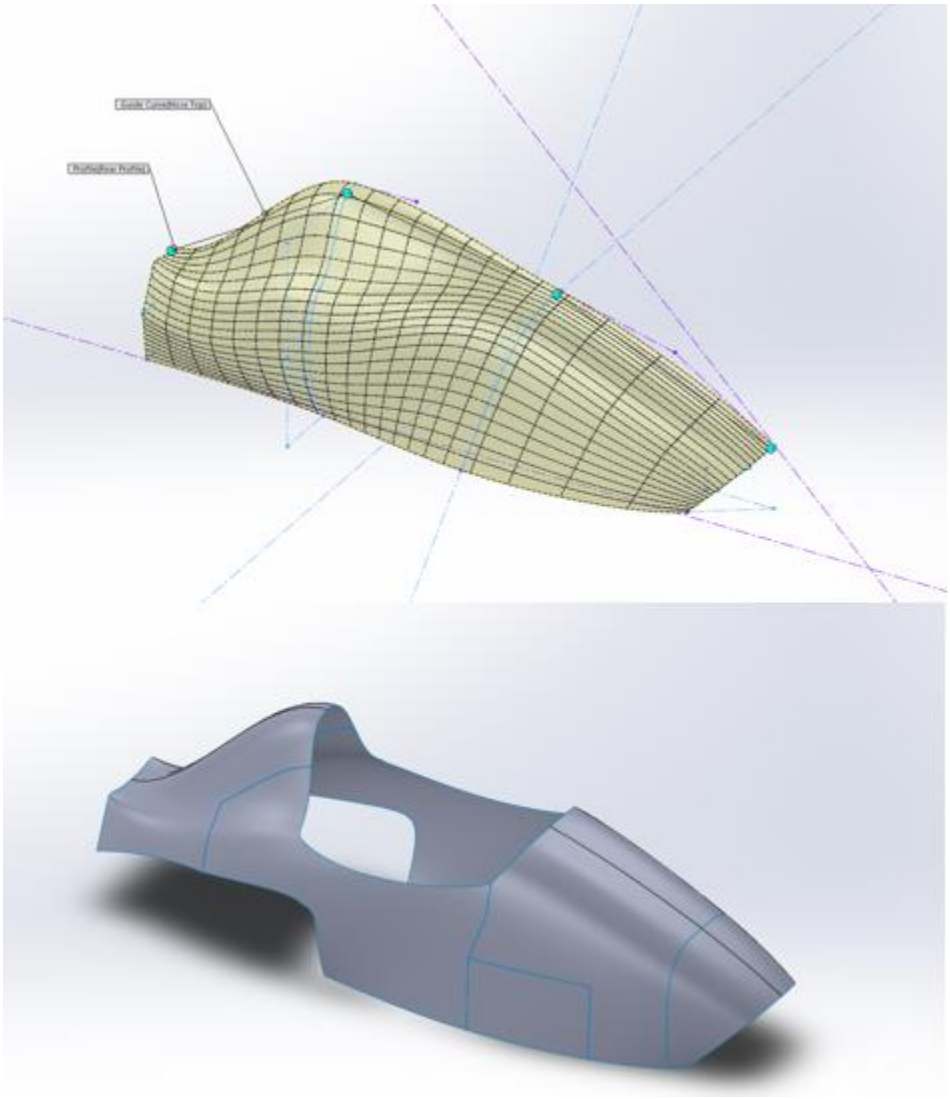

Figure 145: SolidWorks Modeling of Bodywork

The main bodywork was split into three smaller panels to allow for easy installation and removal. The first section consists of the nose cone area in front of the front roll hoop. The second panel extends from the front roll hoop along the sides of the side impact structure to the rear roll hoop support. The third panel closes off the rear of the car and covers the engine compartment. This division of panels was chosen

in order to make the car accessible. The rear engine cover meets the side panels at the rear roll hoop supports to allow for easy removal of the rear cover to access the engine. The contour around the radiators allows for installation of the bodywork without having to modify or remove the radiators.

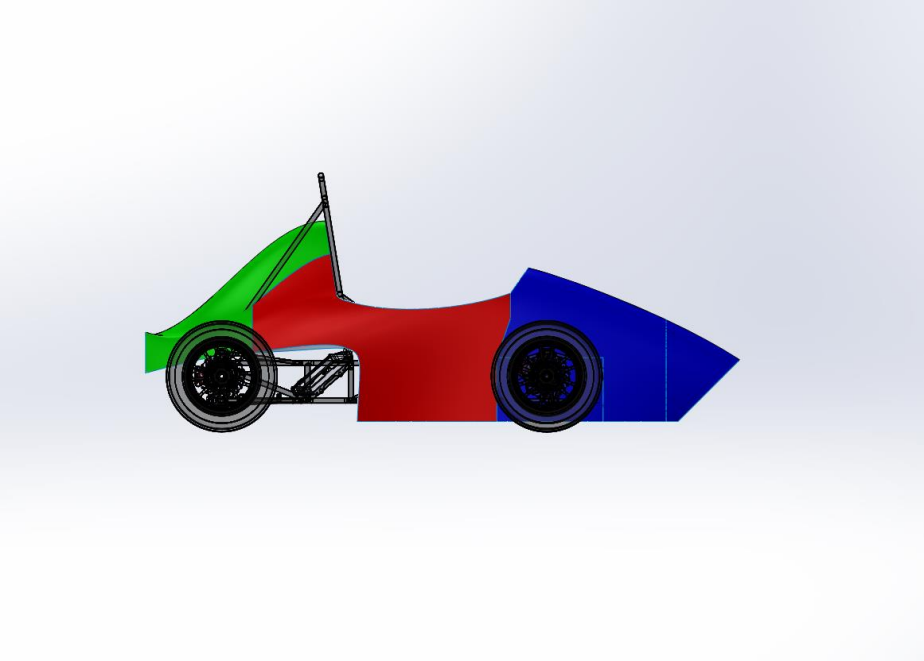

Figure 146: The Sections of the Body Panels

Sidepods

While traditionally a tool for improved cooling, the sidepods only serve as a protective cover for the radiators to protect from damage. All cooling needs are met by the radiator fans and thus the sidepods are simply streamlined within reason so as to not detract from the flow to the radiators.

Nose Cap

To meet the requirement for a legal nose, the radius of the nose tip was set to 2 in extending for 47.5 degrees above and below the forwards direction. This is above the requirements of 1.5 inches extended for 45 degrees above and below the horizontal.

Manufacturing

The manufacturing of the bodywork was done using a wet layup fiberglass vacuum bagging process. This process was chosen because it produces stronger parts than allowing parts to cure at atmospheric pressure, but is simpler than vacuum infusion.

MDF Molds

Composites require a molding surface to form the shape of the part. The mold surface must also be nonporous due to the fiberglassing process. Mold material and sealing strategies were explored in conjunction with Deufol SE, a team sponsor and partner. Materials such as laminated veneer lumber (LVL), modeling board (Renshape 450), and medium density fiberboard (MDF) were considered. MDF was chosen based on cost and machinability. The main bodywork and nose cap were manufactured from mdf molds using the process outlined below.

The molds for the three main bodywork panels were designed and manufactured by Deufol SE in Sunman, Indiana. While the resources were available on campus to complete these molds, the much larger CNC machines at the Deufol facilities were able to complete the large bodywork molds. Deufol was able to machine the three molds, one per panel, in five sections per side, ten in total. Due to the large size of the side panel and nose cone molds, these molds were manufactured in halves and joined at the conclusion of the machining process. This resulted in five mold sections per half the car, two sections forming the nose, two forming the side panels, and one forming the rear cover.

The nose cap mold was machined on campus. The nose cone molds were made in two parts out of four 3/4in thick mdf sheets glued together. It was fixture by screwing it into an mdf board with dowel pins to ensure the block was straight and then the board was bolted onto the table. A mold roughing operation was used to make the rough shape of the mold using a ¾ in router bit with a .1 in scallop height.

Then a mold finish operation was done using a ¾ in ball router bit in order to get the final shape of the mold. The CAM software, esprit, calculated the machining time for the mold to be rather long so to cut back on it drastically a much larger stepover, 15% to diameter, was used on the floor finish pass. This meant the mold had to be lightly sanded however it saved more time machining than it took to sand it. Another major issue that was run into with the mold was that the machine was data starved. Instead of running at the 200 IPM federate, it was actually much slower as the machine was constantly stopping and going. It took quite a bit of testing in order to get an acceptable cut for the roughing, the issue of the machine not having enough power to go the DoC's and step overs set kept causing problems so they were toned back quite substantially causing the machine time to go up dramatically.

Figure 147: Nose Cone Mold

Figure 148: Nose Cone Mold Roughing

While MDF proved to be easily machinable, the machined surface finish proved to be rough and very porous. Some small scallops were left on the mold surface from the machining process that were sanded off with rough grit paper. Various sealing materials were explored including gel coat, polyurethane, and two part epoxy resin. A few small machined surfaces were used as test pieces. Two layers of the epoxy resin with a fast hardener was the method that required the least amount of material and sanding and was chosen as the sealing method for all molds. The final mold surface was sanded with progressively finer grit paper, culminating in 800 grit sandpaper

Mold release was applied to the mold once sealed. 3-4 coats of sealing wax were applied to each mold and allowed to dry roughly 15 minutes between coats. Finally, two coats of Polyvinyl Alcohol were applied and allowed to dry to a film between coats.

Figure 149: Body Molds from Deufol

Figure 150: Mold Sealing Test

Vacuum Bagging Process

The vacuum bagging process used was the process as described by Fiber Glast Developments Corp. in "Vacuum Bagging Equipment and Techniques for Room-Temp Applications". Vacuum was provided by a vacuum pump hooked up to a large pressure tank with connection to a three port manifold. All vacuum bagging supplies were sourced from Fibre Glast and the West Systems 105 Epoxy system was used. For some molds the vacuum bag was sealed to a flange designed around the top of the mold surface in order to conserve bagging material. This method was prone to leaks and as such some parts were cured in a self contained bag that was much simpler to seal and prevent leaks. Three layers of fiberglass were used for all of the bodywork.

Sidepods

Three manufacturing strategies were explored with regards to the sidepods. Initially, MDF molds were designed in order to follow the same manufacturing process that was developed for the main bodywork.

Due to the small available machinable area on the Haas TM1, this method proved to be very resource intensive and impractical. Thus, an alternate strategy was developed in which thin flat fiberglass panels would be contoured to shape by laser cut cross sectional ribs in order to form the mold surface. The completed mold would then be treated with mold release and a part manufactured as normal in a vacuum bag. Due to significant scheduling constraints and small difficulties in implementing this strategy, even this method was deemed to be too time intensive. For the sake of time, the flattened contour of the sidepods were cut out of a flat composite plate, bent to shape around the radiators, and bolted to the car with angle brackets. This proved to be a very simple and lightweight implementation that was only possible for this application due to the single curve contour in the sidepod geometry.

Recommendations

While MDF molds provide a good work surface for multi-use applications, the cost and weight of these molds make for an impractical solution for one use applications such as this. In order to save time and materials, it is recommended for future project to continue the development of contoured plate molds such as was developed for the sidepods due to the numerous potential benefits offered with this strategy. Benefits include lower cost of material, less intensive manufacturing requirements, lower manufacturing time, and no need for mold sealant since the mold surface would already be made of non porous fiberglass.

Some issues were experienced when attempting to flatten the three dimensional shape of the sidepods into two dimensions. These issues could easily be resolved given more time, a closer attention to detail and a less rushed schedule.

System integration/assembly

The body panels were oversized during the manufacturing process to allow for trimming and fitting onto the car. The body panels were trimmed to fit around the suspension pickups in the front of the car as well as the radiators in the rear of the car by taking simple measurements with reference to each component. Body panels that were manufactured in halves were joined post-cure with strips of fiberglass tape interior to the part.

Steel sheet metal body tabs were welded to the frame as a base for creating body mounting tabs to secure the body panels to the car. The locations of these tabs were spread out to ensure the body panels were well supported. Figure 151 below displays the locations where these tabs were welded. The distance from the tab to the bodywork was used to create offset tabs that were coincident to the bodywork surface. D7 quarter turn fasteners from Southco were used to fasten the bodywork to the car. These fasteners were epoxied to the bodywork and allowed for simple installation and removal.

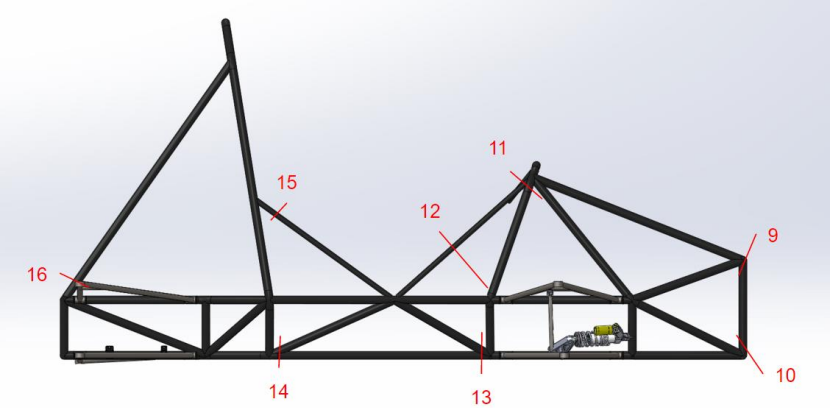

Figure 151: Body Mount Tab Locations

The riser tabs were designed for the ease of manufacturing. Every riser tab was fabricated from a 1 inch piece of 20 gauge aluminum sheet metal. The tab consists of two base sections with a width of ½ inch which bolt to the frame and an offset surface with a single hole for the D7 quarter turn fastener to mount to. The SolidWorks model of the basic tab design is displayed in figure 152 where the height of the tab is varied based on the required distance the body panels needed to be mounted. 10-32 bolts were used to fasten the body tabs to the frame.

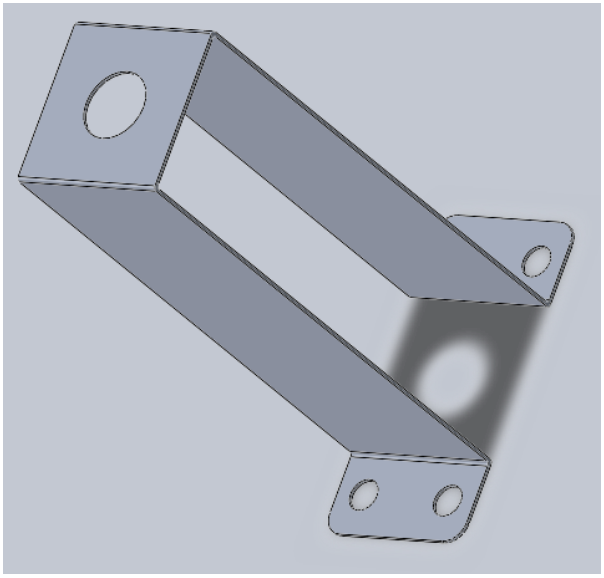

Figure 152: Body Mount Riser Tab Design

Aerodynamics

Background

The ultimate purpose of the aerodynamic package is to reduce the time it takes for the car to go around a track. In order to reduce lap times, downforce, weight, and drag must be properly balanced. A full length diffuser equipped undertray was selected for development in order to keep weight, drag, and development time low. Research into aero configurations of past FSAE cars as well as common findings from professional motorsport showed that an undertray/diffuser would produce significantly less drag than a winged configuration. While this reduced drag must be accompanied by a corresponding reduction in downforce, simulations showed that lap times could still be reduced to specification with this setup. Additionally, unlike wing systems which require the development of both the front and rear wings in order to maintain the balance of the car, the longitudinal balance of the car can be easily controlled with an undertray by adjusting the location of the center of pressure.

Lap time simulations using Optimum Lap were conducted in order to produce the design specifications for the aerodynamic components. Given an estimated weight of the entire aero system, a change in lap time could be found for any given change in the vehicle lift and drag coefficients induced by the undertray. Designs were produced iteratively using ANSYS Fluent, using two dimensional simulations in order to take advantage of faster computation times. The finalized design was manufactured using a honeycomb core composite structure in order to increase strength and reduce weight. Verification of the undertray performance was conducted with wind tunnel and on track testing.

Design Parameters

The aerodynamics package must:

-Decrease the average lap time of the car by at least 0.5% across a wide range of typical FSAE endurance and autocross tracks.

-Maintain the center of pressure within 100 mm of the center of gravity

- Obey all FSAE rules

Lap Time Simulations

Lap time software was used in order to develop the design specifications to meet these parameters. The free software Optimum Lap was chosen for this application. Before starting the simulation process, various car models were developed to represent potential changes in design. This involved entering engine performance, weight, and aerodynamic performance data. One model was developed to simulate the car without an aerodynamic package. Since the aerodynamic performance of the car could not be feasibly tested in the wind tunnel beforehand, these parameters were estimated from data collected by

other teams. Drag coefficients of 0.85 (Dahlberg, 2014) and 0.64 (Merkel, 2013) were averaged for an estimated drag coefficient of 0.7. Lift coefficients varied widely, from effectively zero (Merkel, 2013) to values as high as 0.3 from informal sources. These values were averaged for an estimated lift coefficient of 0.1.

Four additional car models were created in order to simulate the car with an aerodynamic package. Estimated values for the lift coefficient were found to be around -0.9 (Hammond and Flay, 2014) to -0.8. These models had drag coefficients ranging between 0.7 and 1.0 in increments of 0.1. These drag coefficients were chosen to represent an increase of drag from the base simulation. For each of the four models with an aerodynamic package, the weight of the car was increased by the estimated weight of the undertray (17.5 kg). This weight estimation was found using the known density of the honeycomb core material and the measured density of typical fiberglass parts previously manufactured for the car.

Given the wide range of potential initial lift coefficients, a study was conducted in order to examine the effect of this estimation on the simulation results. Two base lap times were set, all identical except for the lift coefficient which was set to the extremes of the expected possible initial lift coefficients of 0 and 0.3. A batch simulation was then run, varying the lift coefficient between 0.3 and -1 in order to be inclusive of the expected lift coefficient with an undertray installed. For each base lap time, the change in percent lap time per change in lift coefficient was plotted as shown in Figure 151. A linear trendline was used to find the maximum difference in percent lap time between these two cases, which was found to be 0.07%. This meant that the initial lift coefficient estimation had relatively little effect on the simulation results, with a maximum error of 0.07% change in lap time within the given range of initial lift coefficients.

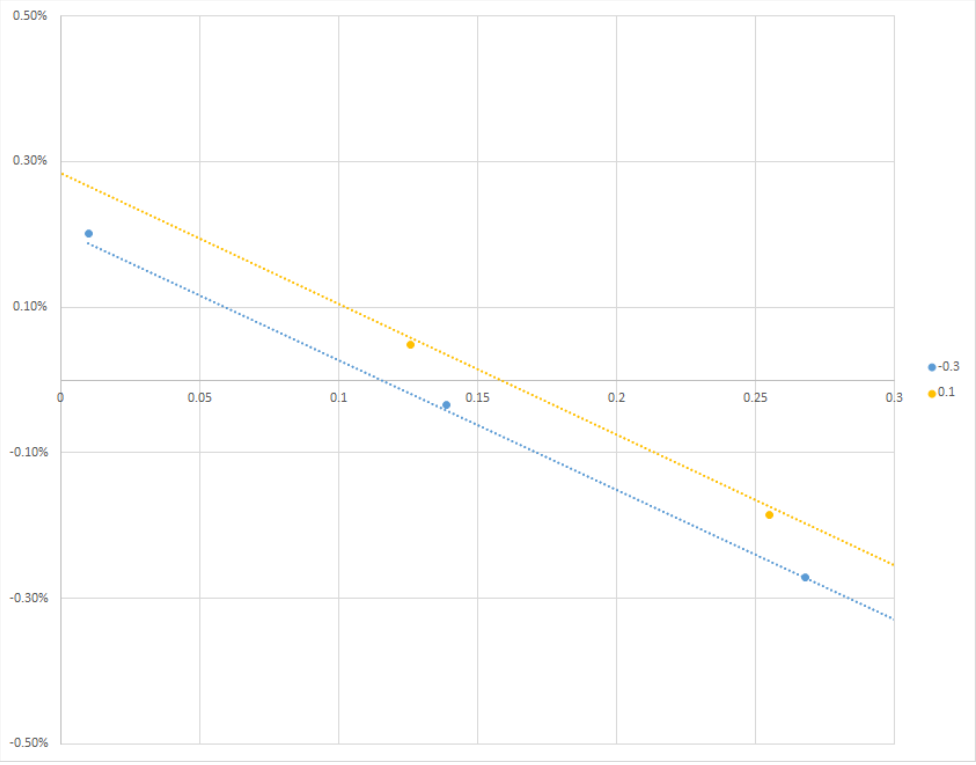

Figure 153: Change in percent lap time per change in lift coefficient

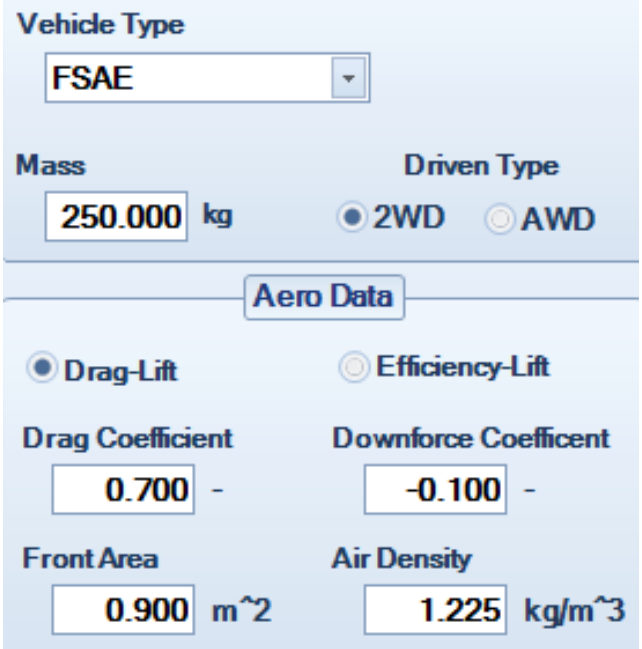

Figure 154: Model of the car in lap time software

The completed models were then used to perform simulations across six different FSAE tracks. The track list is shown below in Table 7.

Location	Event Type	Year
Austria	Endurance	2012
Germany	Autocross	2012
Germany	Endurance	2012
Michigan	Endurance	2014
Nebraska	Autocross	2013
Nebraska	Endurance	2012

Table 9: Tracks used in lap time simulation software

Five simulations were run for each track, one for each car model. The lap time of the non-aero car was recorded and used as the comparison for all other simulations. Batch simulations were run for each of the four cars with an aerodynamic package, sweeping across lift coefficient values between -0.2 and 1 with increments of 0.08. The lift coefficient and the corresponding lap time data were exported from Optimum Lap for analysis in Excel. The lift coefficient data was then translated into a change in lift coefficient with reference to the car model without and aerodynamic package. The lap time was also translated into percent change in lap time with reference to the baseline lap time. From this data, the necessary change in lift coefficient to achieve a 0.0%, -0.5%, -1.0%, and -1.5% change in lap time was found for each of the four car models. An example of these calculations are shown below in figure 155 for a car with an aerodynamic package with a drag coefficient of 0.7 at the Michigan Endurance track from 2014.

	A	B	C	D	E
1	**Cl0**	**-0.1**	**<--Cl with no aero**		
2	**Cd0**	**0.7**	**<--Drag coefficient with no aero**		
3	**T0**	**64.44**	**<--Lap time with no aero**		
4	**Cd**	**0.7**	**<--Drag coefficient with aero**		
5	**Lap time [s]**	**Downforce Coefficient [-]**	**% Lap time**	**Delta Cl**	
6	64.74941368	-0.2	0.48%	-0.1	
7	64.65594121	-0.12	0.34%	-0.02	
8	64.56438171	-0.04	0.19%	0.06	
9	64.47100747	0.04	0.05%	0.14	
10	64.37865269	0.12	-0.10%	0.22	
11	64.28709729	0.2	-0.24%	0.3	
12	64.19684191	0.28	-0.38%	0.38	
13	64.1056011	0.36	-0.52%	0.46	
14	64.01486704	0.44	-0.66%	0.54	
15	63.92501359	0.52	-0.80%	0.62	
16	63.83539448	0.6	-0.94%	0.7	
17	63.74824495	0.68	-1.07%	0.78	
18	63.66107316	0.76	-1.21%	0.86	
19	63.57531348	0.84	-1.34%	0.94	
20	63.49116664	0.92	-1.47%	1.02	
21	63.40739544	1	-1.60%	1.1	
22				0	
23	**slope**	**-0.0174**	0.00%	0.1666667	
24	**intercept**	**0.0029**	-0.50%	0.454023	
25			-1.00%	0.7413793	
26			-1.50%	1.0287356	

Figure 155: Example Calculations

The bulk data in columns A and B is the data imported from Optimum Lap. The bulk data in columns C and D is the imported data translated with reference to the values in cells B1 through B4. The average change in lift coefficient per change in percent lap time is represented in cell B23, and the percent change in lap time with no change in lift coefficient is represented in cell B24. The "slope" and "intercept" were then used to calculate the values in cells D23 through D26.

This calculation module represents data for one of the four car models with an aerodynamic package. The plot shown in figure 156 was then produced with four of these modules, one for each value of drag coefficient. This process was completed six times, once for each track. The resulting data was averaged across all tracks in order to minimize specific anomalies in track performance. The resulting plot was used to evaluate the final design against the design parameters. Given a change in lift and drag coefficients induced by the undertray, a percent change in lap time could be easily found.

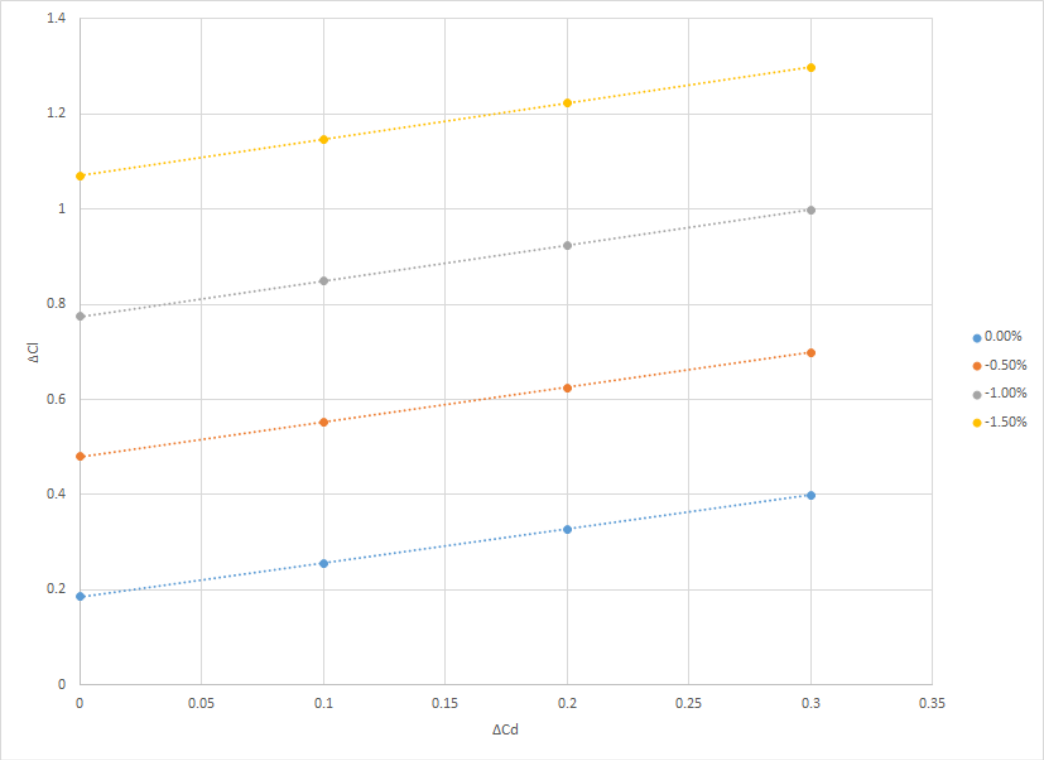

Figure 156: percent lap time as a function of change in lift and drag coefficients

Design

The design process was completed utilizing 2D Computational Fluid Dynamics Simulations in Ansys Fluent. Due to significant time constraints, only one final design could be tested and verified. Two dimensional CFD simulations were used in order to minimize the complexity and time needed to iterate the design. For each design iteration, the lift coefficient, drag coefficient, and center of pressure were found and compared to previous iterations. These parameters were used to guide the design and fix variables in the undertray geometry. Once all of the parameters were satisfied, the geometry was finalized.

CFD Methodology

The mesh was generated in a solution domain 5.5 meters in length and 1.7 meters high. A 20 layer inflation with a growth rate of 1.2 was used to capture the boundary layer on the undertray surface. The final mesh consisted of 8,943 nodes and 8,450 elements.

Six distinct boundary conditions were used. An 18 m/s velocity inlet and zero pascal gauge pressure outlet were used. Freestream was set to symmetry and the ground was a moving wall with an X component velocity of 18 m/s. The lower surface of the undertray was set as a stationary wall while the upper surface was set to a wall with a specified shear of 0 in x and y. A viscous standard k-epsilon turbulence model was chosen due to its popularity in automotive aerodynamics, and all parameters were left as default Fluent values.

Reference values were set as shown in Table XX. Lift coefficient and drag coefficient values were printed to console and recorded for each design iteration. The center of pressure was reported at the height of the center of gravity, 355.6 mm from the ground.

Area	0.9 (m2)
Density	1.225 (kg/m3)
Depth	0.914 (m)
Velocity	18 (m/s)

Table 10: Reference values for CFD simulations

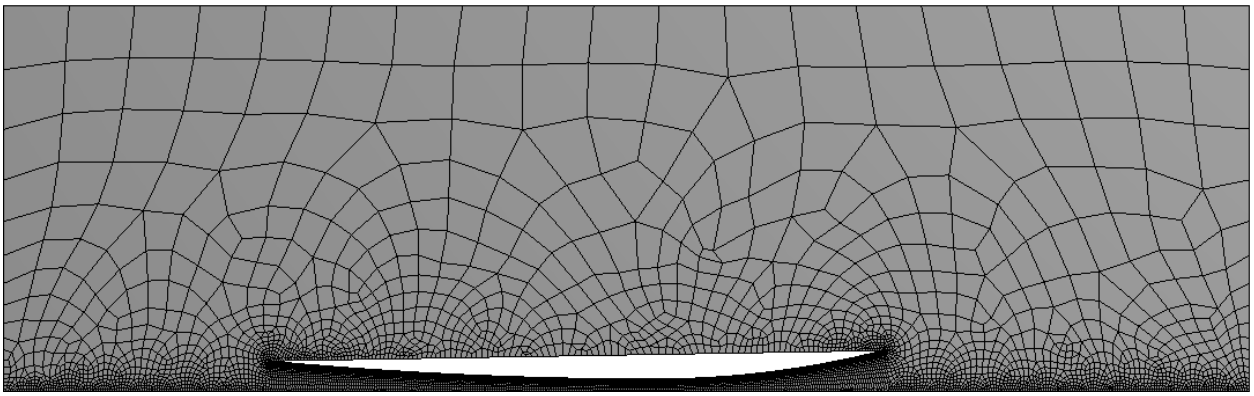

Figure 157: Example Mesh

Design Methodology

A two dimensional SolidWorks sketch was used to define the geometric bounds of the undertray. Ground clearance was defined using the known limits of suspension travel. Conditions under full jounce, braking, and acceleration were considered. The forward and rearward extents of the undertray were limited by the keepout zones defined in the FSAE rules. With this domain under the frame fully defined, the undertray was then sketched as a two tangent arcs, coincident to the front and rear keepout zones, shown in figure 158. The only remaining four variable geometry parameters were the height of the entrance and exit of the diffuser and the location of the diffuser entrance in both height and length. The diffuser entrance is defined at the point tangent to both the front and rear arcs of the undertray. A fifth dependent variable was created, the diffuser angle, defined as the angle of the line tangent to the rearmost point on the diffuser to the horizontal ground plane. The remaining geometry variables were fixed using a combination of simulation results and findings from researchers at the University of Southampton's RJ Mitchell Wind Tunnel.

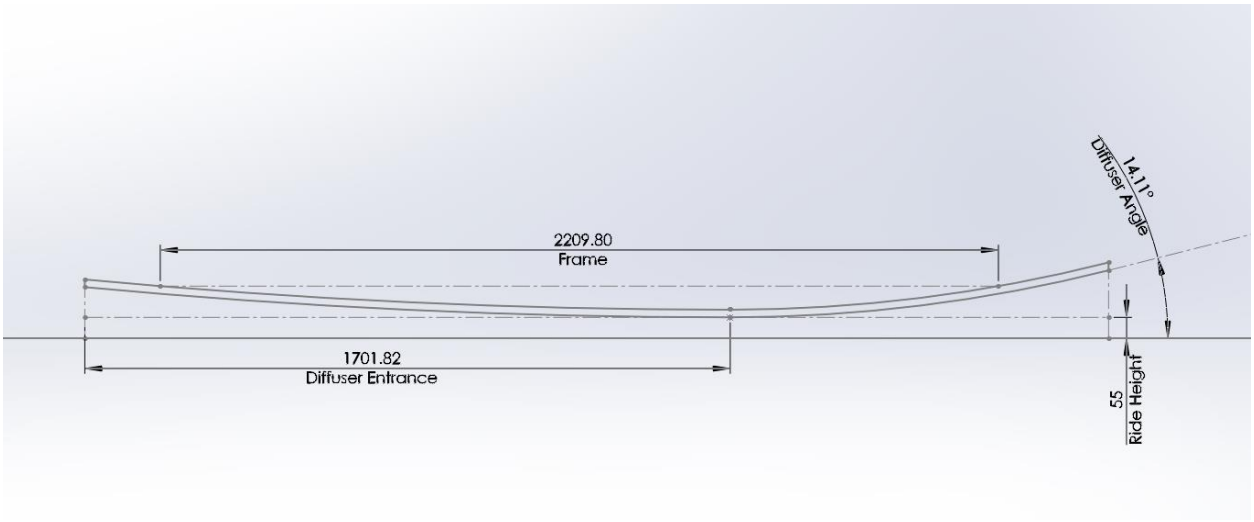

Figure 158: Undertray Geometry

Without the ability to collect data on stall behavior of the specific diffuser setup, data found from Ruhrmann and Zhang (2003) was used to define this behavior. Figure 159 shows the relation between lift coefficient, ride height, and diffuser angle. The geometry used to generate this plot was a diffuser equipped bluff body, with length x/d=9 and diffuser entrance at x/d=5. In order to apply this data to this geometry, "d" was calculated to be 300.74mm using a total undertray length of 2706mm. This diffuser location would correlate to roughly 1500mm from the front of the undertray. The target value of hr/d*theta was between 0.7 and 0.75 for maximum downforce. The ride height then became the variable geometry, dependent on the distance of the diffuser entrance behind the front of the car. This left only three remaining variable geometry parameters: the ride height, and the height of the front and rear of the undertray.

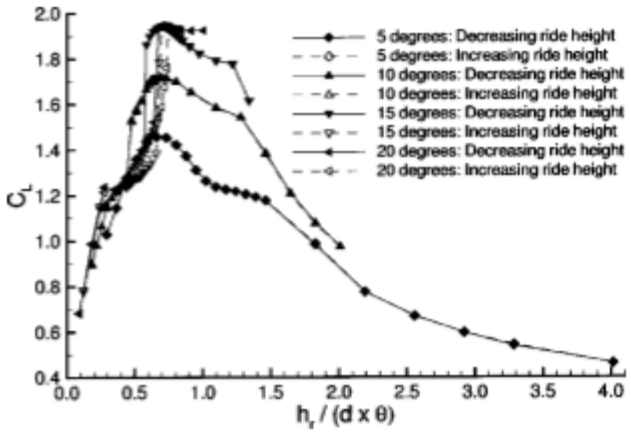

Figure 159: Lift coefficient as a function of undertray geometry

To fix the height of the rearmost point on the undertray, the fundamental workings of automotive diffusers was considered. In order to create the lowest possible pressure underneath the car, the change in flow area must be maximized. Given a fixed flow area underneath the car, this means the diffuser should expand to the largest area possible to achieve maximum downforce while staying within the physical bounds of the car. Therefore, the rearward diffuser arc was made coincident to the rearmost point on the frame, as this was the limiting geometric constraint.

Next, the forward most point on the undertray was fixed using simulation results. A few cases were examined in order to understand the general trends experienced when varying the height of the front of the undertray. Higher lift coefficients were experienced as the front of the undertray was lowered since the low pressure generated by the diffuser extended further forwards, as shown by figure 160. This figure shows the pressure distribution across the bottom the undertray for two different undertray configurations. The venturi shaped undertray (in red) shows a pressure peak roughly at the mid lenght of the car. This is in contrast to forward raked undertray (blue) where the pressure peak occurred at the very front of the car. While the forward raked configuration generated more downforce (cl=2.7 vs. 2.4 for this specific configuration), this change was also accompanied by a large shift in the center of pressure forwards (663 mm in front of the center of gravity vs. 128mm). Without a rear wing to counter balance, this configuration would promote heavy oversteer, especially at higher speeds. The venturi shaped undertray with the flared front does not experience this issue since the center of pressure is moved back closer to the center of gravity. Therefore, in order to shift the center of pressure the furthest rearward, the front of the undertray was made coincident with the front most point on the frame.

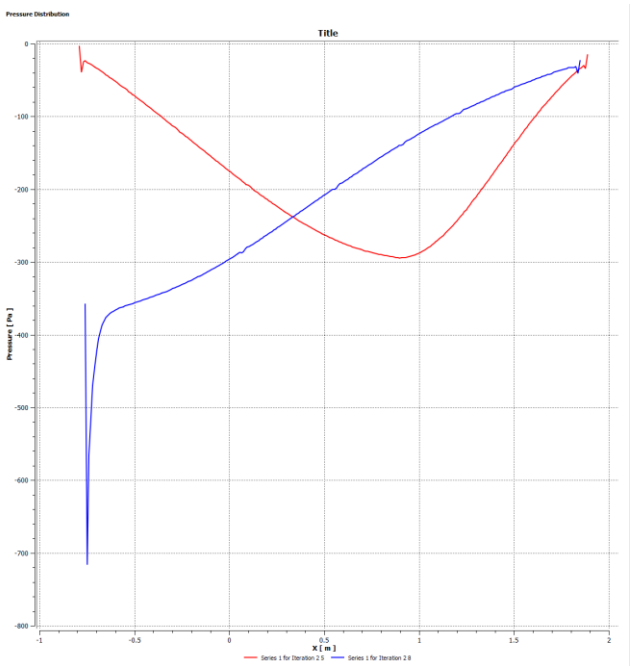

Figure 160: Example pressure distributions generated by an undertray

The only remaining variable geometry parameter, the diffuser entrance location, was then iterated upon in order to find the optimum combination of lift coefficient and center of pressure location. Generally it was found that the center of pressure moved with the diffuser entrance, so in order to move the center of pressure beneath the center of gravity, the diffuser entrance should be moved towards the rear of the car. Moving the diffuser entrance rewards was also accompanied by reduction in lift coefficient since the ride height would have to be raised to satisfy the desired value of hr/dtheta. Therefore, the diffuser entrance was moved as far forwards to maximize lift while still keeping the center of pressure within the acceptable range of 100mm, following the process outlined below.

Given the inherent errors introduced by the two dimensional CFD simulations, the center of pressure had to be predicted given a three dimensional case. A significant reduction in pressure was expected since cross flow from the sides of the car would occur. In order to simulate a reduction in pressure, the ride height was increased by 20mm, while the rest of the geometry remained fixed. This resulted in a pressure contour of similar shape but lower magnitude. With this ride height shift, the diffuser entrance was moved rearwards until the center of pressure was within 100 mm of the center of gravity in order to meet the design parameter. This occurred with the diffuser entrance 125 mm behind the center of gravity. The ride height was then lowered until hr/dtheta approached 0.7, which occurred at a ride of roughly 55 mm with a diffuser angle of 14.2 degrees.

The width of the under tray was maximized to the greatest width allowed by the front wheels at maximum steer. The FSAE rules also allow for extension in the area between front and rear wheels. The width in this zone was increased to the wheel centerline in order to minimize cross flow in this area directly around the pressure peak. 7 Vertical strakes were also added to prevent cross flow, since more efficient sliding skirts are banned in the FSAE rules. 5 internal strakes were used in order to best interface with the minimum required rear jack bar width.

Instrumentation

Pressure instrumentation was integrated into the undertray assembly in order to verify performance as well as provide live approximate downforce values. Twenty differential pressure transducers were supported by the electronics system on the car. These sensors were distributed across the under tray surface in order to best understand the undertray pressure field. The lower surface of the undertray was split into 6 channels by the vertical strakes. Instrumentation was placed in the inner two channels on one half of the car since it was assumed that the pressure would be mirrored about the vehicle centerline. Ten sensors were placed in each channel, with one sensor at the expected pressure peak location. Five sensors were evenly placed behind the pressure peak, and four in front. Since the sensors were differential sensors, the reference ports were all connected and passed to a single static pressure probe mounted at the front of the car.

Manufacturing

The undertray was manufactured using an aluminum honeycomb core fiberglass layup. First, the strake profiles were water jetted from a single sheet of fiberglass. The lower surface of the under tray was then created as a two layer thick flexible flat plate. Once cured, the flat plate was supported from underneath to form the basic curve of the undertray. The strakes were then tacked on in place in order to form an undertray "skeleton" that would support the rest of the structure. The pressure sensors were glued onto the lower skin and wired to a single connector at the center of the car by the electronics box. The pressure ports were passed through holes to the lower surface and the reference ports linked together with a connection for the static probe.

Quarter inch aluminum honeycomb was then trimmed around the sensors to fill the entire undertray surface. A final layer of fiberglass was vacuumed over the top in order to seal the sensors and improve the rigidity of the undertray. Sealing the bag to the side of the undertray was attempted first, but a vacuum was not achieved due to complex sealing geometry that caused excessive leaks. To overcome this problem, the entire undertray was placed in a vacuum bag, with extra care taken to ensure enough bagging material was folded around each of the strakes to avoid excessive stretching and possible bag punctures. Extra breather fabric was also laid around any sharp edges to avoid bag punctures. The weight of the undertray at the completion of vacuum bagging was around 11 kilograms, well within the desired weight specification.

System integration/assembly

The undertray was mounted with bolts to mounting tabs parallel to the ground plane, except in the rear where the jackbar structure was integrated as the mounting point. The jackbar spanned the width of two strakes and passed though the upper surface to mount in four places to the rear bulkhead. Once the jackbar was bolted in place, the gaps in the undertray were sealed with fiberglass.

Future Recommendations

The 2016 Formula MQP Team focused the majority of their work on the basic design and implementation of various critical systems on the 2016 FSAE vehicle. While the frame was the starting point of this project, the designs needed to be created from the ground up with all analysis and validation to confirm the designs were sound. Due to the numerous areas of design and manufacturing, analysis of components and systems needed to be somewhat limited in scope to allow the project to stay within the allotted timeline.

Future WPI FSAE teams should begin with consulting all designs and understand in detail and verify all design decisions and calculations to create a basis for which to formulate the next iteration of a FSAE vehicle. Several areas of work can be changed from the 2016 car to improve workflow and save time, along with including a strong validation set with the next vehicle iteration.

Initially, a well-organized and properly fixtured CAD model must be created to allow a solid foundation for all designs to be based off of. This includes using proper file management and naming standards. All previous revisions of parts and subassemblies must be archived to allow for part comparison and prototyping review. The CAD model should contain all components in a rigid orientation for aerodynamic and bodywork design, as well as a properly constrained configuration to allow for motion analysis and collision detection under various dynamic conditions.

The frame design needs to be modified in several ways. The changes the 2016 team made to allow the frame to meet the SES requirements must be taken into account when the next iteration is in the design process. The FSAE rules must be carefully consulted for every system to ensure the vehicle is always in compliance with the rules. A study of ergonomics on the 2016 vehicle should be completed to reveal potential visibility and aesthetic concerns, such as the front roll hoop being potentially higher than necessary. The 2015 team designed the roll hoop to be higher than necessary to be able to package drivers over 6 feet tall comfortably, yet this could be reduced based on the next team's design intent.

The suspension and steering systems should be analyzed in depth. The calculations for the 2016 vehicle prove the system will work reliably while not giving the exact mathematical equations that govern the system. These equations are critical when interfacing with sensors to properly map the real time suspension position for force and motion diagnostics. Simulation software, such as Adams Car can be used to predict the dynamics forces and kinematic variables at different loadings. Other software such as MathCad and Solidworks Simulation can be used to predict and graph motion equations and resultant forces the system could experience in worst case scenarios.

The engine systems should also be analyzed in depth to fully understand the methods to building a proper base tune. Programs such as WAVE and Lotus Simulation allow engine models to be created and analyzed. More advanced features of the engine tune such as ignition timing maps, decel cut, and transient throttle maps need to be refined to boost engine performance while reducing fuel economy.

A future team should start by understanding the designed sensor integration and how that can affect the testing and tuning stage. For validation of all systems, sensors need to be integrated early on in the design process along with the methods of obtaining and transmitting data. Even a well-designed system may not function as needed, and proper sensor integration can help a team decipher the complex vehicle dynamics problem by isolating certain components and subsystems.

Lastly, and most importantly, the team must work cohesively between each subgroup to achieve the same goal. Teamwork is critical to an FSAE vehicle design. The team must also become familiar with all FSAE rules and have design meetings to ensure from early stages through the final manufacturing and assembly stages that all components adhere to the current rule set.

Bibliography

"Ackermann Steering Geometry." Wikipedia. Wikimedia Foundation, n.d. Web. 26 Apr. 2016.

Dahlberg, H. (2014). Aerodynamic Development of Formula Student Race Car. KTH Royal Institute of Technology.

Gearvalves. N.p., n.d. Web.

Hammond, A., Flay, R. (2014). Aerodynamic Design of a Formula SAE Race Car. The University of Aukland.

Merkel, J. (2013). Development of Multi-Element Active Aerodynamics for the Formula SAE Car. The University of Texas at Arlington.

Milliken, William F., and Douglas L. Milliken. *Race Car Vehicle Dynamics*. Warrendale, PA, U.S.A.: SAE International, 1995. Print.

Ruhrmann, A., Zhang, X. Influence of Diffuser Angle on a Bluff body in Ground Effect, ASME J. Fluids Eng. 125, pp. 332-338.

"Universal Joint." Wikipedia. Wikimedia Foundation, n.d. Web. 26 Apr. 2016.